Titre: Title:	New improved formulas for calculating gravity and magnetic anomalies based on a cylinder model
Auteur: Author:	Yong Jun Su
Date:	2010
Type:	Mémoire ou thèse / Dissertation or Thesis
Référence: Citation:	Su, Y. J. (2010). New improved formulas for calculating gravity and magnetic anomalies based on a cylinder model [Mémoire de maîtrise, École Polytechnique de Montréal]. PolyPublie. https://publications.polymtl.ca/314/

UNIVERSITÉ DE MONTRÉAL

NEW IMPROVED FORMULAS FOR CALCULATING GRAVITY AND MAGNETIC ANOMALIES BASED ON A CYLINDER MODEL

YONG JUN SU

DÉPARTEMENT DES GÉNIES CIVIL, GÉOLOGIQUE ET DES MINES

ÉCOLE POLYTECHNIQUE DE MONTRÉAL

MÉMOIRE PRÉSENTÉ EN VUE DE L'OBTENTION

DU DIPLÔME DE MAÎTRISE ÈS SCIENCES APPLIQUÉES

(GÉNIE MINÉRAL)

MARS 2010

UNIVERSITÉ DE MONTRÉAL

ECOLE POLYTECHNIQUE DE MONTRÉAL

UNIVERSITÉ DU QUÉBEC EN ATIBITI-TÉMISCAMINGUE

Ce mémoire intitulé:

NEW IMPROVED FORMULAS FOR CALCULATING GRAVITY AND MAGNETIC ANOMALIES BASED ON A CYLINDER MODEL

présenté par: SU Yong Jun
en vue de l'obtention du diplôme de: Maîtrise ès sciences appliquées
a été dûment accepté par le jury d'examen constitué de:

M. AUBERTIN Michel, Ph.D., président
Mme CHENG Li Zhen, Ph.D., membre et directrice de recherche
M. CHOUTEAU Michel, Ph.D., membre et codirecteur de recherche
M. KEATING Pierre, Ph.D., membre

ACKNOWLEDGEMENTS

I would like to express my deepest gratitude to my supervisor Professor Li_Zhen CHENG (Université du Québec en Abitibi-Témiscamingue) and my co-supervisor professor Michel Chouteau (École Polytechnique à Montréal) for giving me invaluable guidance and patience during my master's program as well as financial support, I also wish to express my thanks to Professor Xuben WANG (ChengDu University of Technology) for his guidance. It is your mentoring and instructions that have provided for my insights into the way I approach my study and process this program. Without your persistent inspiration and encouragement, my efforts could not have turned this rewarding, and the study could not have been this fruitful. I am very grateful for this opportunities I was given. I would thank to KEGS who awarded me "2008 KEGS Foundation Award", financial support from Québec and China Scholarship Council for the Québec Bursary Granting Exemption from Differential Tuition Fees.

I would also like to extend a special thank to friends in China for their help, Shuquan GAO, Qinglong HU, Chengping WU, Xuelin SHEN, Zhikun LIU etc. In addition, I would like to thank my colleagues: Nacim Foudil-Bey and Mahdi Brakni, they have provided much insight, advice and friendship over the years as we discussed problems related to my research. All of the above proved to be valuable mentors as I pursued my Master's degree.

Last but not least, I would like to express my greatest respect and love to my family, my parents, my wife and elder sister. Their love and unflagging support lend me the very power and confidence in the course of my thesis writing. I also want to say thank you to my friends: Denis Bois, Louise Labbé, Thomas Genty, Caroline Fournier, Yilmaz Erol, Monique Fay, Weidan DING, Huaitong XU, Yiqin ZHOU, Yun ZHANG and Park Young-In and the other students in Canada.

RÉSUMÉ

Nous avons développé deux nouvelles formules pour calculer les anomalies de gravité et de magnétisme basées sur un modèle de cylindre librement orienté dans l'espace. Comparé à la méthode conventionnelle, notre nouveau développement considère des facteurs multiples qui ont un impact sur les observations géophysiques - certains ont été ignorés dans les études précédentes - comme l'angle d'inclinaison, l'orientation par rapport au nord, la grandeur, la profondeur et les propriétés physiques d'un cylindre. Nous pouvons utiliser ces nouvelles formules pour calculer l'anomalie des trois composantes du champ magnétique aussi bien que l'anomalie gravitationnelle.

En outre, basé sur une série de modélisations directes en utilisant ces nouvelles formules, deux systèmes de régression linéaire multiples (un pour la gravité et un autre pour le magnétisme) ont été développés pour estimer les paramètres du cylindre à partir de la gravité observée et des données de magnétisme.

Mots clés: Calcul direct, calcul inverse, régression linéaire multiple, interprétation conjointe, gravité et magnétisme.

ABSTRACT

We have developed two new formulas for the calculation of gravity and magnetic anomalies over a cylinder model freely oriented in space. Compared with the conventional method, our new development considers multiple factors that have impact on geophysical observations (some neglected in previous studies) such as the dip angle, the strike direction, the size, top depth and the physical properties of a cylinder. We can use these new formulas to calculate the anomaly of the three components of magnetic field as well as its gravitational anomaly.

Furthermore, based on a series of forward modeling by using these new formulas, two multiple linear regression systems (one for gravity and another for magnetism) have been developed in order to estimate the cylinder's parameters from observed gravity and magnetic data.

Keywords: Forward problem, Inverse problem, Multiple Linear Regression, Joint interpretations, gravity and magnetism.

CONDENSÉ EN FRANÇAIS

INTRODUCTION

L'interprétation d'observations géophysiques peut être réalisée de deux façons : par une modélisation/simulation directe ou par des calculs inverses. La modélisation directe est fondée sur un modèle géologique plausible pour reproduire la réponse géophysique en imposant des propriétés physiques au modèle géologique. Par exemple, dans le cas sismique, la modélisation directe produit un sismogramme synthétique. Dans le cas des données gravimétriques, la procédure de calcul direct du champ de gravité est basée sur une distribution de densité sous la surface du sol. Afin de choisir une méthode mathématique appropriée, il est aussi important de savoir combien de paramètres du modèle concerné devraient être utilisés et d'identifier lesquels sont les plus significatifs pour influencer la variation de champ géophysique.

L'objectif de recherche dans le cadre de ce mémoire est de faire l'amélioration du calcul dans l'interprétation des données gravimétriques et magnétiques, causées par une structure cylindrique d'orientation quelconque, afin de valoriser les observations pour l'exploration minérale.

Ce mémoire est composé de cinq parties:

1. L'introduction présente la problématique, une revue des travaux antérieurs et les différentes parties du mémoire.
2. La deuxième partie illustre la théorie fondamentale de régression linéaire multiple, qui est la méthode essentielle utilisée dans nos développements.
3. La troisième partie se compose d'une série de modélisations directes, pour choisir les facteurs les plus significatifs qui peuvent influencer les variations des champs magnétiques et gravimétriques.
4. Dans la quatrième partie du mémoire, nous avons développé deux nouvelles formules mathématiques, dans lesquelles plus de paramètres sont considérés, afin de calculer la réponse gravimétrique et la réponse magnétique d'un cylindre. En nous basant sur ces nouvelles relations fonctionnelles et linéaires, nous pouvons estimer simultanément la densité, la susceptibilité magnétique, la profondeur, l'azimut, l'inclinaison et le rayon d'un cylindre.

5. Une conclusion permet de faire le point sur les résultats les plus significatifs des travaux présentés et de discuter de pistes de recherche possibles pour le futur.

BASE THÉORIQUE

La méthode mathématique fondamentale que nous avons utilisée dans nos développements est la régression linéaire multiple. On exprime les valeurs d'observation comme une variable dépendante (y_i), qui dépend d'une série de variables ($x_0, x_1, ..., x_{m-1}$) explicatives. Elles ont une relation linéaire comme suit :

$y_i = a_0 x_0 + a_1 x_1 + ... + a_{m-1} x_{m-1} + a_m + \varepsilon_i$ pour i=0, 1, 2…m

$a_0, a_1 ..., a_{m-1}, a_m$ sont les paramètres à estimer.

Nous supposons que les distributions de la densité et de la susceptibilité magnétique à l'intérieur de la terre sont, d'une façon linéaire, rattachées aux observations gravimétriques et magnétiques. La distribution de ces propriétés physiques est aussi une question de position et de géométrie. Ces facteurs représentent les variables explicatives, et l'observation géophysique est la variable endogène.

Dans notre développement, nous avons d'abord développé des algorithmes, afin de modéliser la réponse géophysique de plusieurs corps ayant une géométrie simple, qui représentent certaines situations géologiques. Le but de cet exercice est d'étudier la relation entre les paramètres du corps causatif et l'anomalie géophysique, pour voir comment les paramètres affectent la variation d'une anomalie géophysique et, ensuite, nous considérons les paramètres les plus significatifs dans le nouveau développement de ce mémoire.

MODÉLISATION DIRECTE

Dans le chapitre II, les modélisations directes sont fondées sur des modèles simplifiés, qui sont pourtant représentatifs de la géométrie des corps minéralisés. Ce sont les modèles de dipôle, de plaque mince, de prisme, de cube ou de sphère.

Pour résumer des caractéristiques d'une anomalie magnétique en fonction du changement des paramètres de modèle et de la différence de direction de magnétisation, il y a trois formes d'anomalies fondamentales sur un profil : 1) aucune valeur négative (peu importe symétrique ou

asymétrique); 2) une anomalie composée d'un pic négatif et d'un autre positif; 3) l'anomalie le long du profil est symétrique ou asymétrique et elle est négative. L'amplitude et la forme d'anomalie sont affectées surtout par l'inclinaison du champ magnétique terrestre, par le pendage de la structure géologique et par le contraste de densité ou de susceptibilité magnétique du corps. L'amplitude de l'anomalie décroît rapidement avec l'augmentation de la profondeur sous la surface. Une anomalie négative de gravimétrie signifie qu'il y a une déficience de masse. Cependant, l'anomalie négative ou positive dans le champ magnétique dépend de multiples facteurs, soit le pendage de la structure géologique, la direction et l'intensité de la magnétisation, l'extension du corps, etc.

Sur un profil d'une image bidimensionnelle ou d'une image tridimensionnelle, l'apparence d'une anomalie géophysique apporte certaines informations qualitatives de la source. Cependant, l'exploration minière a besoin de plus de précision sur la géométrie et la nature de la source. À cette fin, nous cherchons un lien quantitatif entre l'anomalie gravimétrique ou magnétique et un corps cylindrique, en le mettant dans une situation plus proche de la réalité que les développements précédents ont considéré.

NOUVELLES FORMULES DE CALCUL

Les modèles physiques simples, comme la plaque, le prisme et la sphère, sont utiles pour l'interprétion rapide sur le terrain en l'exploration minérale. Par la méthode conventionnelle (Figure 3.5), on calcule l'anomalie géophysique le long d'un profil passant par la projection à la surface du corps incliné; dans ce cas, le corps est incliné dans le plan du profil. Nous avons démontré dans le chapitre II que les variations de la forme d'anomalie, surtout magnétique, ont des implications complexes. Afin d'améliorer la méthode de calcul, nous avons choisi le modèle du cylindre qui peut être représentatif d'une structure de cheminée kimberlitique ou d'une intrusion. En considérant des facteurs multiples, comme le pendage, l'orientation par rapport au nord, la longueur, la profondeur et la propriété physique d'un cylindre, nous avons développé de nouvelles formules mathématiques pour les méthodes gravimétriques et magnétiques. Dans ce nouveau développement, le cylindre est librement orienté dans l'espace.

Nouvelle formule pour la méthode gravimétrique

Un cylindre est sous le plan XOY (Figure 3.1) : α est le pendage, θ est son orientation par

rapport au nord, $r_{cylinder}$ est le rayon. L'attraction gravitationnelle sur le point P d'un élément dl du cylindre est donnée par :

$$\Delta g_r = G \cdot \rho \cdot s \cdot dl / r^2$$

ρ est la densité de l'élément dl, $s = \pi . r_{cylinder}^{\ 2}$ est l'aire de la section droite, r est la distance entre l'élément dl et le point P. En l'exploration minière, ce qu'on cherche est le corps minéralisé, qui a une valeur économique, en métaux de base (nickel, cuivre, zinc, argent et or). Ces derniers ont une propriété physique différente par rapport aux roches encaissantes; donc, c'est l'excès de masse du corps minéralisé qui provoque une anomalie dans le champ gravitationnel. La densité ρ ici est effectivement le contraste de densité entre le cylindre et son environnement.

La contribution d'élément dl à l'anomalie gravitationnelle est donné par :

$$\Delta g^{'} = G \cdot \rho \cdot s \cdot dl . \sin \angle 4 / r^2$$

La contribution totale de cylindre est :

$$\Delta g = G \cdot \rho \cdot s \cdot (H / \sin \alpha + l) \sin \alpha / \{(H / \sin \alpha + l)^2 + (x^2 + y^2) - 2(H / \sin \alpha + l) \cdot \sqrt{x^2 + y^2}$$

$$\cdot \cos \angle 2 . \cos \alpha \} \cdot \int_0^L \frac{(H / \sin \alpha + l) dl}{\left\{(H / \sin \alpha + l)^2 + (x^2 + y^2) - 2(H / \sin \alpha + l) \cdot \sqrt{x^2 + y^2} \cdot \cos \angle 2 \cdot \cos \alpha\right\}^{\frac{3}{2}}}$$

Cette équation est résolue numériquement. La solution détaillée est présentée à l'annexe 4. Les calculs directs de la réponse gravimétrique du cylindre, dans le chapitre suivant, en fonction de la variation de ses paramètres, sont basés sur cette formule.

À partir de cette équation, en supposant qu'il n'y a pas de variation de l'attraction gravitationnelle le long de l'axe des y, nous pouvons obtenir le formule conventionnelle donnée dans Telford (1976):

$$\Delta g = G \cdot \rho \cdot s \cdot \sin \alpha \int_0^L \frac{(H / \sin \alpha + l) dl}{\left\{(H / \sin \alpha + l)^2 + x^2 - 2(H / \sin \alpha + l) x \cdot \cos \alpha\right\}^{\frac{3}{2}}}$$

$G : 6.67 * 10^{-8} cm^3 / g.s^2$ est la constante gravitationnelle universelle.

La solution est:

$$\Delta g = G \cdot \rho \cdot s \cdot \sin\alpha \left[\frac{\cos\alpha((H/\sin\alpha + l)) + x}{x \cdot \sin^2\alpha \cdot \left\{(H/\sin\alpha + l)^2 + 2x(H/\sin\alpha + l)\cos\alpha + x^2\right\}^{\frac{1}{2}}} \right]_L^0$$

$$= \frac{G \cdot \rho \cdot s}{x \cdot \sin\alpha} \left[\frac{H\cot\alpha + x}{(H^2/\sin^2\alpha + 2xH\cot\alpha + x^2)^{\frac{1}{2}}} - \frac{x + H\cot\alpha + L\cos\alpha}{\left\{(H/\sin\alpha + L)^2 + 2x(L\cos\alpha + H\cot\alpha) + x^2\right\}^{\frac{1}{2}}} \right]$$

Lorsque le cylindre est vertical, la solution est devenue :

$$\Delta g = 6.67 * 10^{-8} \cdot \rho \cdot s \left[\frac{1}{(H^2 + x^2)^{\frac{1}{2}}} - \frac{1}{\left\{(H+L)^2 + x^2\right\}^{\frac{1}{2}}} \right]$$

<u>Nouvelle formule pour la méthode magnétique</u>

L'anomalie magnétique ne dépend pas seulement des paramètres de cylindre, mais aussi de la variation d'inclinaison (*I*) et de déclinaison (*D*) du champ magnétique terrestre. La figure 3.2 démontre (chapitre III) qu'il y a plus de paramètres à considérer pour le champ magnétique que le champ gravitationnel. Cependant, les variations de déclinaison et d'inclination du champ magnétique terrestre sont fonction de position géographique (longitude, latitude) du levé ; c'est pour cette raison que nous considérons, dans une région d'étude spécifique, ces deux paramètres comme constants. Les expressions pour les trois composants du champ magnétique sont :

$$\Delta X = kM_x \cdot s \left(\frac{x - H\sin\theta/\tan\alpha}{r_1^3} - \frac{x - (H/\sin\alpha + L)\cos\alpha \cdot \sin\theta}{r_2^3} \right)$$

$$\Delta Y = kM_y \cdot s \left(\frac{H\cos\theta/\tan\alpha - y}{r_1^3} - \frac{(H/\sin\alpha + L)\cos\alpha \cdot \cos\theta - y}{r_2^3} \right)$$

$$\Delta Z = kM_z \cdot s \left(\frac{H}{r_1^3} - \frac{H + L\sin\alpha}{r_2^3} \right)$$

où: $s = \pi \cdot r_{cylinder}^{\ 2}$

$$r_1 = AP = \left\{(x - H\sin\theta/\tan\alpha)^2 + (y - H\cos\theta/\tan\alpha)^2 + H^2\right\}^{\frac{1}{2}}$$

$$r_2 = CP = \left\{(x - (H/\sin\alpha + L)\cos\alpha \cdot \sin\theta)^2 + (y - (H/\sin\alpha + L)\cos\alpha \cdot \cos\theta)^2 + ((H/\sin\alpha + L)\sin\alpha)^2\right\}^{\frac{1}{2}}$$

$$\begin{cases} M_x = M\cos I \cdot \sin D \\ M_y = M\cos I \cdot \cos D \\ M_z = M\sin I \end{cases}$$

Le champ total magnétique est donc :

$$\Delta T = \Delta X\cos I \cdot \sin D + \Delta Y\cos I \cdot \cos D + \Delta Z\sin I$$

Veuillez noter que cette nouvelle formule est basée sur le modèle de tige cylindrique magnétique; il est valide seulement lorsque le rayon de cylindre est très petit par rapport à la distance d'observation.

APPLICATION DE LA MÉTHODE DE RÉGRESSION LINÉAIRE MULTIPLE

En nous basant sur les deux nouvelles formules que nous avons développées, par les modélisations directes, nous pouvons reproduire un grand nombre d'anomalies gravimétriques et magnétiques en variant les 6 ou les 9 paramètres du cylindre respectivement. Nous choisissons ensuite 8 attributs (α_i, i=1, 8) déterminés sur les anomalies gravimétriques du cylindre, qui représentent significativement des changements de forme d'anomalie en fonction de la variation de la profondeur, de l'extension en profondeur, du pendage, de l'orientation, du rayon et de la densité résiduelle de cylindre. Nous appliquons ces attributs aux anomalies provenant de 34 modèles, afin de développer le système de régression linéaire avec multiples variables de cylindre. Ultimement, nous utilisons ce système pour estimer l'occurrence de modèle du cylindre à partir de l'anomalie de gravité.

Système de régression pour la méthode gravimétrique

Un des algorithmes développés dans ce mémoire permet de calculer les anomalies gravimétriques en variant les paramètres de cylindre. La fonction suivante entre le maximum d'anomalie et les paramètres est un des exemples de la relation linéaire établie, qui est utile pour faire une simulation rapide de la réponse de gravité d'un corps cylindrique sur le terrain :

$$y_{\max i} = -0.01684592\times H - 0.00008811848\times L + 0.003451422\times\alpha - 0.00140625\times\theta$$

$$+ 0.08508292\times r_{cylinder} + 2.48574\times\rho - 1.060923 \qquad (\rho \neq 0)$$

À partir des 8 attributs d'anomalie gravimétrique, les équations suivantes nous offrent un outil d'estimation des paramètres de source cylindrique:

$$\rho = 2.889256 * \alpha_1 + 122.1366 * \alpha_2 + 112.6437 * \alpha_4 - 177.3349 * \alpha_6$$
$$- 35.04415 * \alpha_7 - 25.98408 * \alpha_8 + 77.181$$

$$H = \text{-}55.90585 * \alpha_1 + 2212.613 * \alpha_2 + 1655.03 * \alpha_4 - 857.7549 * \alpha_5 - 3250.931 * \alpha_6$$
$$- 464.0917 * \alpha_7 + 94.85623 * \alpha_8 + 671.3411$$

$$L = \text{-}6506.249 * \alpha_2 \text{ - } 5982.137 * \alpha_4 + 8508.451 * \alpha_6 + 2523.032 * \alpha_7$$
$$+ 2042.171 * \alpha_8 - 4575.77$$

$$\alpha = 1043.717 * \alpha_2 + 739.3492 * \alpha_4 \text{ - } 214.7961 * \alpha_5 - 1996.947 * \alpha_6$$
$$- 20.27874 * \alpha_7 + 262.3575 * \alpha_8 + 541.4631$$

$$\theta = -53.37571 * \alpha_2 + 1462.129 * \alpha_4 \text{ - } 1078.221 * \alpha_6 + 955.4258 * \alpha_7$$
$$- 1369.722 * \alpha_8 + 788.5574$$

$$r_{cylinder} = -290.9525 * \alpha_2 \text{ - } 248.3274 * \alpha_4 + 213.8204 * \alpha_6 + 206.6426 * \alpha_7$$
$$+ 167.5164 * \alpha_8 - 221.8726$$

En nous basant sur les modèles synthétiques, nous avons estimé les paramètres du modèle à partir de l'anomalie calculée. L'erreur de prédiction est de moins de 15% de la valeur réelle (Tableau 3.6).

Système de régression pour la méthode magnétique

Parallèlement au développement de la méthode gravimétrique, nous utilisons la nouvelle formule pour calculer les réponses magnétiques des 34 modèles. Nous avons d'abord établi des relations linéaires entre l'anomalie magnétique et les 9 paramètres choisis. Les deux équations suivantes sont utiles pour faire une simulation rapide de la réponse magnétique d'un corps cylindrique sur le terrain :

$$y_{\max i} = -0.8495511 \times H - 0.05466737 \times L + 0.2417084 \times \alpha - 0.2057476 \times \theta$$
$$+ 2.767968 \times r + 6.613053 \times \mu + 76.01499$$

$$y_{\min i} = 0.004370969 \times H - 0.001963786 \times L + 0.3242243 \times \alpha + 0.01333939 \times \theta$$
$$- 0.1613043 \times r - 0.5365263 \times k - 14.07616$$

Selon la variation significative de la forme d'anomalie en fonction des 9 paramètres, nous avons sélectionné 13 attributs d'anomalie (β_i, i = 1, …13), afin d'estimer les paramètres de cylindre à partir d'observation du champ magnétique :

$$H = 17.0251 * \beta_1 - 363.3289 * \beta_2 - 26.56787 * \beta_3 + 609.533 * \beta_4$$
$$+ 578.9358 * \beta_6 + 344.1536 * \beta_8 + 7802.103 * \beta_9$$
$$- 6364.752 * \beta_{10} - 2471.2 * \beta_{12} - 2374.77$$

$$L = -1249.16 * \beta_1 + 432.4964 * \beta_2 - 399.2165 * \beta_4 + 28.97969 * \beta_5$$
$$- 1164.122 * \beta_6 + 767.3705 * \beta_8 - 13744.46 * \beta_9 + 10822.2 * \beta_{10}$$
$$+ 5145.374 * \beta_{12} + 2682.55$$

$$\alpha = 58.66501 * \beta_1 - 132.7803 * \beta_2 - 6.843981 * \beta_3 + 78.43094 * \beta_4$$
$$+ 223.3361 * \beta_6 + 80.26672 * \beta_8 + 2061.873 * \beta_9$$
$$- 1680.958 * \beta_{10} - 675.9877 * \beta_{12} - 603.0068$$

$$\theta = -1207.091 * \beta_1 + 579.23 * \beta_2 + 221.94 * \beta_3 - 1965.463 * \beta_4$$
$$- 23.28669 * \beta_5 + 552.4362 * \beta_8 - 1629.684 * \beta_9$$
$$+ 4353.063 * \beta_{10} - 947.8782 * \beta_{12} + 767.0967$$

$$r_{cylinder} = 158.0792 * \beta_1 - 41.57005 * \beta_2 + 165.7851 * \beta_4 + 5.707602 * \beta_5$$
$$- 17.38298 * \beta_6 - 117.0736 * \beta_8 + 242.4679 * \beta_9$$
$$- 400.1155 * \beta_{10} + 74.04848 * \beta_{12} - 140.8824$$

$$k = 19.45921 * \beta_1 - 13.97551 * \beta_2 + 5.205135 * \beta_4 - 1.820279 * \beta_5$$
$$+ 53.28494 * \beta_6 + 5.480995 * \beta_8 + 349.4315 * \beta_9$$

$$-279.7742 * \beta_{10} - 128.7827 * \beta_{12} - 103.3701$$

En nous basant sur des modèles synthétiques, nous avons estimé les paramètres du modèle à partir de l'anomalie calculée. L'erreur de prédiction est de moins de 10% de la valeur réelle pour la profondeur, la longueur et le pendage du modèle (Tableau 3.12), de moins de 16% pour l'azimut et de 18% pour la susceptibilité magnétique.

A la fin de ce mémoire, nous avons démontré certains avantages à combiner les deux méthodes (gravimétrie et magnétisme) pour faire une interprétation conjointe. Cette dernière permet d'améliorer l'incertitude dans l'interprétation d'une seule méthode.

Une étude de cas a été réalisée par appliquer les nouvelles méthodes développées aux données réelles.

CONCLUSIONS

Afin d'améliorer la méthode de calcul et la rendre plus réaliste, nous avons développé deux nouvelles formules pour le calcul d'anomalie gravimétrique et d'anomalie magnétique. Ces calculs sont basés sur un modèle de cylindre, qui est librement orienté dans l'espace.

Basées sur les nouvelles formules développées dans ce mémoire et 34 modèles de cylindre établis de manière à couvrir les cas des structures les plus fréquemment rencontrées en exploration minérale, une série de modélisations ont été effectuées afin d'identifier les paramètres qui donnent le plus grand impact sur la variation d'anomalies gravimétriques et magnétiques, et ainsi de sélectionner les attributs d'anomalies qui sont les plus significatifs pour caractériser la variation des paramètres de cylindre. Pour établir une relation linéaire entre la réponse géophysique et la présence de structure cylindrique, nous pouvons faire soit un calcul direct, soit un calcul inverse. Le calcul direct nous permet de faire une simulation rapide de la réponse géophysique sur le terrain selon la méthode utilisée. Quant au calcul inverse, il nous permet d'estimer simultanément la densité ou la susceptibilité magnétique, la profondeur au toit, la longueur, le pendage, l'azimut et le rayon du cylindre à partir des attributs d'anomalie gravimétrique et magnétique. Des tests sur des modèles synthétiques ont prouvé la validité de cette approche. Si nous appliquons les deux nouvelles méthodes d’interprétation simultanément pour une interprétation conjointe, on peut réduire l'ambiguïté dans l'estimation des paramètres de la structure.

Nous avons appliqué la nouvelle méthode d'interprétation aux données réelles dans une région de la ceinture verte d'Abitibi (Québec, Canada). Nous avons estimé la géométrie et les propriétés physiques de trois intrusions à partir de données gravimétriques et magnétiques. Malheureusement, il n'y a aucun renseignement géologique disponible pour confirmer la validité de notre prédiction.

TABLE OF CONTENTS

LIST OF TABLES

LIST OF FIGURES

SYMBOLS AND ABBREVIATIONS

Abbreviation or Symbol	Definition
$a_0, a_1 ..., a_{m-1}, a_m$	Regression coefficients
Cr	Credibility
d	Density
$d^{'}$	Predicted density
D	Magnetic declination
dl	Infinitesimal length
d_v	Element of volume integral
F	Total magnetic field of the earth
G	Universal gravitation constant
$Gra - Cr$	Credibility of predicted gravity value
$Gra - p.v$	Predicted gravity value
H	Top depth of the cylinder
$H - profile$	Anomaly profile of H_{xy}
$H_{\max}$	Maximum value of H_{xy}
$H_{\min}$	Minimum value of H_{xy}
H_{xy}	Horizontal field
$H^{'}$	Predicted top depth of the cylinder
I	Magnetic inclination
k	Magnetic susceptibility
$k^{'}$	Predicted Magnetic susceptibility
l	Element of the integral
L	Length of the cylinder or thick plate
$L^{'}$	Predicted length of the cylinder
m	Pole strength

M	Total intensity of magnetization
M_x	X axis' component of M
M_y	Y axis' component of M
M_z	Z axis' component of M
$Mag-p.v$	Credibility of predicted magnetic value
$Mag-Cr$	Predicted magnetic value
P	Observation point
q	Sum of square residuals
r, r_1, r_2	Distance between element and observation point
r_3	Coefficient of total correlation
$r_{cylinder}$	Radius of cylinder
$r_{cylinder}'$	Predicted radius of cylinder
s	Cross-section area
s_1	Mean standard deviation
u	Regression sum of square
U	Magnetic potential
V	Volume
v_j	Partial correlation coefficient
$x_0, x_1, ..., x_{m-1}$	Independent variable
$x_{\max i}$	Corresponding coordinate of $y_{\max i}$
$x_{\min i}$	Corresponding coordinate of $y_{\min i}$
y_i	Dependent variable
y_{ex}	Extremum of gravity anomaly
$y_{\max i}$	Maximum value of gravity or magnetic anomalies
$y_{\min i}$	Minimum value of magnetic anomalies

$Z-profile$	Anomaly profile of ΔZ
2-D, 3-D	Two dimensional, three dimensional
π	Circumference ratio (PI)
Δg	Gravity anomaly
ΔT	Magnetic anomaly
ΔX	X axis' component of ΔT
ΔY	Y axis' component of ΔT
ΔZ	Vertical component of ΔT
α	Dip angle
α'	Predicted dip angle
$\alpha_1, \alpha_2, \alpha_3, \alpha_4, \alpha_5, \alpha_6, \alpha_7, \alpha_8$	Attributes computed from gravity anomaly
$\beta_1, \beta_2, \beta_3, \beta_4, \beta_5, \beta_6, \beta_7, \beta_8,$ $\beta_9, \beta_{10}, \beta_{11}, \beta_{12}, \beta_{13}$	Attributes computed from magnetic anomaly
θ	Strike angle
θ'	Predicted strike angle
ε_i	Minimizing error
ξ_1, ξ_2	Range of integration along X axis
η_1, η_2	Range of integration along Y axis
ζ_1, ζ_2	Range of integration along Z axis

LIST OF APPENDICES

INTRODUCTION

Geophysics is the application of physical principles to study the interior structure of the earth. Our knowledge of the earth's interior is mainly based on the interpretation of measurements made at the surface, rather than direct sampling of the material in the earth. The interpretation of geophysical observation can be performed in two ways: forward modeling and inverse estimation. The forward modeling is based on a plausible geological model to reproduce geophysical response by imposing physical properties on the geological model. For example, in the seismic case, forward modeling is producing a synthetic seismogram. In the case of gravity data, the forward modeling procedure computes the gravity field from an assumed subsurface density distribution. In addition to the choice of an appropriate mathematical method, it is also important to know how many model parameters should be used and which parameters are the most significant to influence the variation of geophysical field.

The inversion can be defined as a procedure for obtaining subsurface models that may adequately describe an observed data set. The nature and the occurrence of underground structures are estimated or interpreted according to variations in geophysical data sets; and by minimizing the difference between the observed and the calculated responses. Very often there is no unique solution for inverse problems due to equivalence of response from different sources, e.g. an infinite number of solutions satisfy the data within prescribed error bounds (Cary and Chapman, 1988). These values, in turn, should produce a model response satisfying the observed data within prescribed error bounds. Tarantola (1987) is one of the earliest proponents of this inversion philosophy based on the classic work of the British clergyman and statistician Thomas Bayes (1763). The literature refers to the approach as "Bayesian Inversion". Excellent discussions can be found in papers by Duijndam (1988a, 1988b) and by Gouveia and Scales (1997, 1998). The broader implications of Bayesian inversion have been discussed in an incisive essay by Scales and Snieder (1997).

The (general) nonlinear problem is typically solved by an iterative application of a given optimization algorithm (Wang 2007). The problem is that in order for convergence to the "correct" subsurface model to take place, the initial modeling must be "close" to the true solution. There has therefore been much recent interest in the development of so-called "global optimization" algorithms, which, in theory at least, can produce models whose responses fit the

observed data well. Among such methods, genetic algorithms and simulated annealing (Smith, Scales, and Fischer, 1992; Sen and Stoffa, 1995; Yao, et al, 2003; Shi, et al., 2007), Marquardt inversion (Chakravarthi and Sundararajan, 2005), as well as Monte Carlo search (Cary and Chapman, 1988; Wang, 2007), more recently, there has been growing interest in the use of artificial neural networks to solve inverse problems (Calderon-Macias, Sen and Stoffa, 1998, Shi, et al., 2004). Multiple linear regression has been a common computer tool for petroleum geologists (Wendt, Sakurai, & Neson, 1986), application of multiple regression to predict shear wave velocity (Eskandari, Rezaee & Mohammadnia, 2004), the use of multiple linear regressions for trap quality evaluation in western China (Shi, et al., 2004), and develop a rapid and efficient detection and classification of airborne time-domain electromagnetic anomalies (Claprood, et al., 2008). However, the application of multiple linear regressions for joint geophysical interpretation of gravity and magnetic has not appeared in the literature. The purpose of this thesis is to make improvements in the calculation for gravity and magnetic field data interpretation for mineral exploration. Since the resolution of geophysical methods is under the influence of multiple factors, such as the source occurrence as well as its nature, we choose the multiple linear regression method to make links between the variations in gravity and magnetic field and the changes of source's parameters.

The content of this thesis contains the following chapters:

- The introduction exclusively introduces background and the theory of forward and inverse problems, overviewing the main achievements.
- The first chapter illustrates the basic theory of multiple linear regression.
- The second chapter consists of a series of forward modeling for selecting the most significant factors that can make influence on the variations of the magnetic and gravity fields.
- In the third chapter, we developed new mathematical formulas in which more model parameters are considered, in order to calculate the gravity and magnetic response over a cylinder model. We then build the relationship between gravity and magnetic anomalies and the cylinder’s parameters up to estimate simultaneously the density, the magnetic susceptibility, the top depth, the dip extent, the dip angle, the strike angle and the radius of cylinder.
- The conclusion presents a discussion and the conclusion.

CHAPTER I BASIC THEORY OF MULTIPLE LINEAR REGRESSION

The basic mathematical method that we used in our developments is the multiple linear regression. It aims to model the relationship between two or more explanatory variables and a response variable by fitting a linear equation to observed data (Yale University: http://www.stat.yale.edu/Courses/1997-98/101/linmult.htm). We assume that the density and the susceptibility distributions inside the earth are linearly related to the gravity and the magnetic observations. The distribution of these physical properties is a question of position and geometry of the source bodies. Thus multiple variables have effects on geophysical observations.

The multiple linear regression examines if there is a linear relationship between a dependent variable (y_i) and related variables $x_0, x_1, ..., x_{m-1}$ as follow.

$$y_i = a_0 x_0 + a_1 x_1 + ... + a_{m-1} x_{m-1} + a_m + \varepsilon_i \quad \text{For i=0, 1, 2…m.} \tag{1-1}$$

Or

$$\begin{cases} y_0 = a_0 x_{00} + a_1 x_{10} + ... + a_{m-1} x_{m-1,0} + a_m + \varepsilon_0 \\ y_1 = a_0 x_{01} + a_1 x_{11} + ... + a_{m-1} x_{m-1,1} + a_m + \varepsilon_1 \\ \qquad ..... \\ y_i = a_0 x_{0i} + a_1 x_{1i} + ... + a_{m-1} x_{m-1,i} + a_m + \varepsilon_i \end{cases} \tag{1-2}$$

Once coefficients $a_0, a_1 ..., a_{m-1}, a_m$ are determined a linear relationship is established. Based on the least-squares method, the best-fitting line for the observed data is calculated by minimizing the sum of squared error from each data point to the line. If a point lies on the fitted line exactly, then the sum of squared error is zero.

$$q = \sum_{0}^{n-1} \left[y_i - (a_0 x_{0i} + a_1 x_{1i} + ... + a_{m-1} x_{m-1.i} + a_m) \right]^2 \tag{1-3}$$

In order to get the minimum of the objective function (1-3), we need calculating partial derivatives of the sum of squared errors related to the coefficients. By setting the first derivative equal to zero, the coefficients can be determined by the following operations:

$$(cc^T)\begin{bmatrix} a_0 \\ a_1 \\ a_2 \\ \vdots \\ a_{m-1} \\ a_m \end{bmatrix} = c\begin{bmatrix} y_0 \\ y_1 \\ y_2 \\ \vdots \\ y_{n-2} \\ y_{n-1} \end{bmatrix}$$

$$c = \begin{bmatrix} x_{00} & x_{01} & x_{02} & \cdots & x_{0,n-1} \\ x_{10} & x_{11} & x_{12} & \cdots & x_{1,n-1} \\ \vdots & \vdots & \vdots & \vdots & \vdots \\ x_{m-1,0} & x_{m-1,1} & x_{m-1,2} & \cdots & x_{m-1,n-1} \\ 1 & 1 & 1 & \cdots & 1 \end{bmatrix} \qquad (1\text{-}4)$$

From the previous equations, in order to determine the coefficients $a_0, a_1 ..., a_{m-1}, a_m$ we must know the elements of matrix c (direct problem); in the case of a linear relation we can determine the unknown variables which are the elements of matrix c. In our work, we first developed some algorithms for modeling geophysical several simple geometries that representative of geological bodies (chapter II). These developments are then used to determine coefficients $a_0, a_1 ..., a_{m-1}, a_m$ in order to build the linear relationship between the geophysical responses and the parameters of the anomaly source. Forward modeling is used to determine the most significant parameters for the inversion development (chapter III).

For the multiple linear regressions, detail calculations are as below:

(1). calculate the sum of square residuals:

$$q = \sum_{0}^{n-1} \left[y_i - (a_0 x_{0i} + a_1 x_{1i} + ... + a_{m-1} x_{m-1.i} + a_m) \right]^2$$

(2). calculate the mean standard deviation: $s_1 = \sqrt{q/n}$

(3). calculate the coefficient of total correlation: $r_3 = \sqrt{1 - q/t}$

Where $t = \sum_{i=0}^{n-1} (y_i - \bar{y})^2$ $\bar{y} = \sum_{i=0}^{n-1} y_i / n$

When $r_1 \approx 1$ indicates relative error $q/t \approx 0$, the regression is good.

(4). calculate the partial correlation coefficient: $v_j = \sqrt{1 - q / q_j}$, $j = 0,1,...,m-1$.

Where $q_j = \sum_{i=0}^{n-1} [\vec{y} - (a_m + \sum_{\substack{k=0 \\ k \neq j}}^{m-1} a_k x_{ki})]^2$

When the bigger the value of v_j, the more notable to y, shows the corresponding x_j has most significant attribute to y.

(5). calculate the sum of squares of the regression:

$$u = \sum_{0}^{n-1} \left[\overline{y_i} - (a_0 x_{0i} + a_1 x_{1i} + ... + a_{m-1} x_{m-1.i} + a_m)\right]^2$$

It may be expected that for prediction purposes, the regression equations should include as many independent variables as possible, so that the regression equation will fit the data better. Nevertheless, in order to simplify the regression equations, and due to the difficulties in obtaining information on a large number of independent variables, the equations should include as few independent variables as possible. Furthermore, including too many independent variables would not be more effective, as their number should be restricted. Therefore, it is essential to determine the number of variables to be used in the regression equations. The compromise between the above-mentioned extremes (i.e., the number of independent variables in the equation) is usually called selecting the “best” regression equation.

CHAPTER II FORWARD MODELING

2.1 2-D modeling

In preparation for solving inverse problems, we need to find the most important parameters that characterize the target and which may have a major impact on the geophysical observations. If we can build a relationship between the observations and those significant parameters, we should be able to quantify the target from the data. In this chapter, we developed a series of algorithms to perform direct calculations of several simple models in order to characterize the variability of gravity and magnetic anomalies as a function of the source occurrence.

It is very often assumed that simple bodies are homogeneous magnetized or has a density and is located in a non-magnetic or homogeneous medium. In practice many common geological features can be approximated in this fashion. Modeling is particularly useful for the analysis of the characteristics of geophysical responses over known sources.

2.1.1 The dipole model

The magnetic anomaly of a dipping rod can be obtained from the field of two poles separated by a distance L. Following Telford et al., (1976) and assuming that the vertical field is positive downward, the strength of vertical component of the magnetic field from a para magnetized rod is:

$$\Delta Z = kF\left\{\left(\frac{1}{r_1{}^2}\right)\left(\frac{z}{r_1}\right)-\left(\frac{1}{r_2{}^2}\right)\left(\frac{z+L\sin\partial}{r_2}\right)\right\}$$

$$= kF\left\{\left(\frac{z}{r_1{}^3}\right)-\left(\frac{z+L\sin\partial}{r_2{}^3}\right)\right\} \qquad (2\text{-}1)$$

Similarly the horizontal component is the given by

$$H_{xy} = kF\left\{\left(\frac{x}{r_1{}^3}\right)-\left(\frac{x+L\sin\partial}{r_2{}^3}\right)\right\} \qquad (2\text{-}2)$$

Where k is the magnetic susceptibility of material, F is the total magnetic field of the earth, ∂ is the dip angle of the dipole and r is the distance between the rod and the observation point. The

above expressions are valid only under one or both of the following conditions (i) the intrinsic field of the rod is very much larger than the external field; (ii) the rod is oriented along the external field direction. The first assumption is quite possible for magnetite rich rocks, but the second highly unlikely due to arbitrary orientation of anomaly source. When the rod is vertical and vertically magnetized, then $\partial = \pi/2$, $F = Z_0$, and we have:

$$\Delta Z = kZ_0 \left(\frac{z}{r_1^3} - \frac{z+L}{r_2^3} \right) \tag{2-3}$$

$$H_{xy} = kZ_0 x \left(\frac{1}{r_1^3} - \frac{1}{r_2^3} \right) \tag{2-4}$$

In the second case, if the rod is horizontal and horizontally magnetized, we have $\partial = \pi$, $F = H_0$ (H_0 is the horizontal component of the total field) and

$$\Delta Z = kH_0 z \left(\frac{1}{r_1^3} - \frac{1}{r_2^3} \right) \tag{2-5}$$

$$H_{xy} = kH_0 \left(\frac{x}{r_1^3} - \frac{x-L}{r_2^3} \right) \tag{2-6}$$

Equation (2-1) to (2-6) can be used to simulate thin sheet likely magnetic body, such as some contact metamorphic rocks in aureoles or ore body. Figure 2.1 to Figure 2.3 show some anomalies for the vertical (ΔZ) and horizontal (H_{xy}) component in case where the magnetization is along the thin sheet plane.

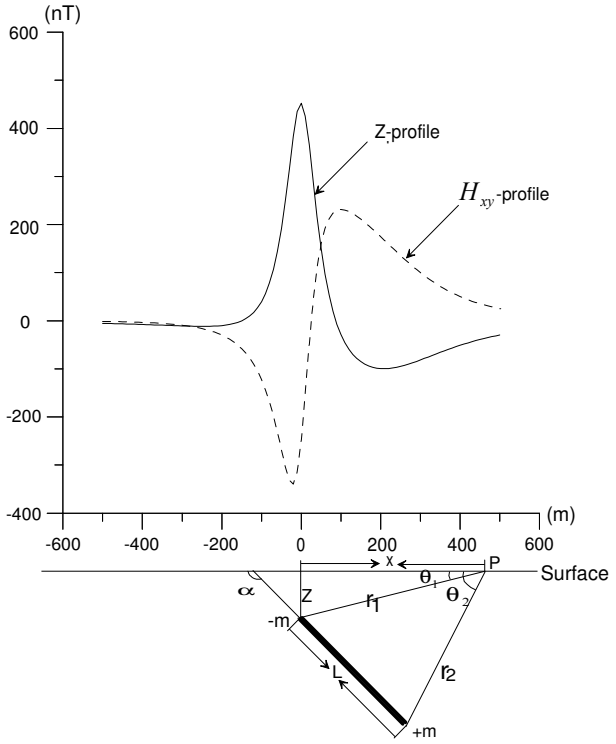

Figure 2.1: Dipping dipole magnetized along its axis, ΔZ and H_{xy}, $\partial = 135^{\circ}$

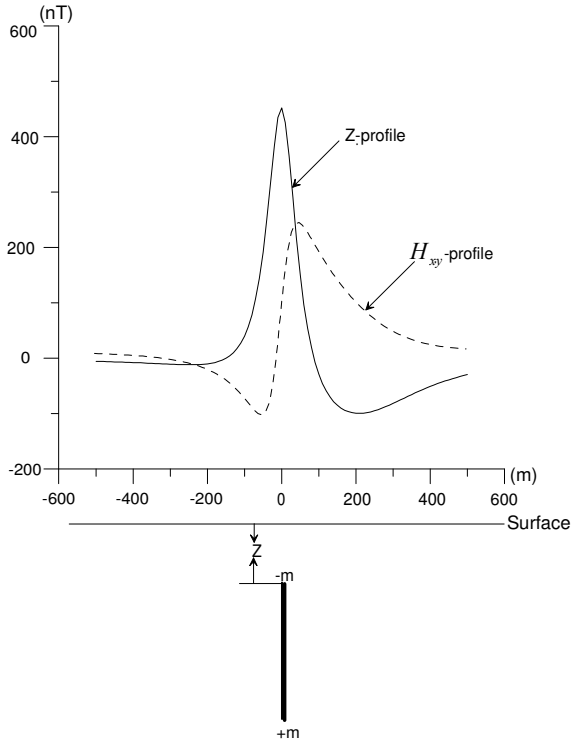

Figure 2.2: Vertical dipole magnetized along its axis ΔZ and H_{xy} profiles

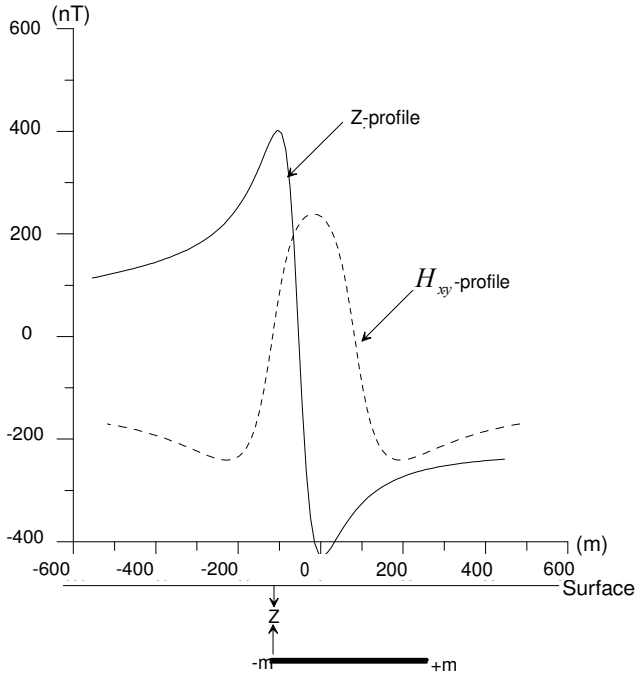

Figure 2.3: Horizontal dipole magnetized along its axis ΔZ and H_{xy} profiles

From Figure 2.1 to Figure 2.3, the vertical-component profiles are somewhat sharper and the maxima slightly smaller, due to the effect of the N-seeking pole at finite depth. To interpret magnetic anomalies, we can use the same trial-and-error method for interpreting observed magnetic anomalies.

2.1.2 The thick plate model

Magnetic and gravity anomalies caused by igneous intrusions in the form of dikes are common features in regions favourable to mineral exploration. Considering the huge difference between the length and the thickness of the dikes; such structures may often be simulated by a thick plate, which is illustrated in Figure 2.4.

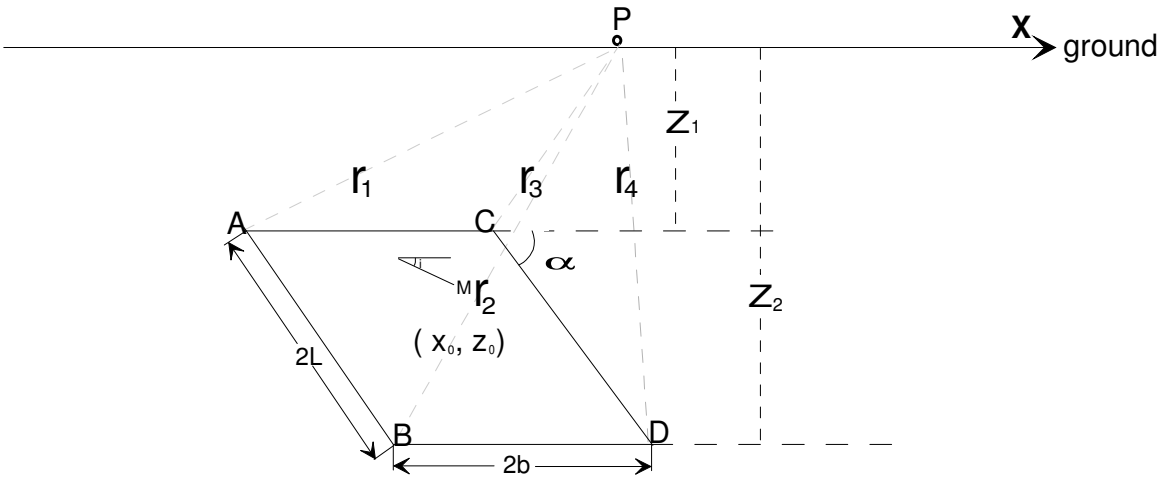

Figure 2.4: Geometry relation of dipping thick plate

A, B, C, and D are the endpoint of the thick plate model, the observation point is P, r_1, r_2, r_3 and r_4 are the distance between A, B, C, D and P respectively, φ_1, φ_2, φ_3 and φ_4 are the angle between r_1, r_2, r_3, r_4 and X-axis respectively, those angles taken clockwise-count from the positive X-axis.

The relationships between parameters are as follow:

$$r_1^2 = (x_K - x_0 + b + l\cos\alpha)^2 + (z_0 - z_k - l\sin\alpha)^2$$

$$r_2^2 = (x_K - x_0 + b - l\cos\alpha)^2 + (z_0 - z_k + l\sin\alpha)^2$$

$$r_3^2 = (x_K - x_0 - b + l\cos\alpha)^2 + (z_0 - z_k - l\sin\alpha)^2$$

$$r_4^2 = (x_K - x_0 + b - l\cos\alpha)^2 + (z_0 - z_k + l\sin\alpha)^2$$

$$\varphi_1 = \pi - \arctan\frac{z_0 - z_k - l\sin\alpha}{x_K - x_0 + b - l\cos\alpha}$$

$$\varphi_2 = \pi - \arctan\frac{z_0 - z_k + l\sin\alpha}{x_K - x_0 + b - l\cos\alpha}$$

$$\varphi_3 = \pi - \arctan\frac{z_0 - z_k - l\sin\alpha}{x_K - x_0 - b + l\cos\alpha}$$

$$\varphi_4 = \pi - \arctan\frac{z_0 - z_k - l\sin\alpha}{x_K - x_0 + b - l\cos\alpha} \tag{2-7}$$

The component-x along strike and the component-z of magnetic field and gravity anomaly Δg are given by Zhang and Pan (2000) as follow:

$$\Delta X = 2M\sin\alpha\left[\ln\frac{r_2 r_3}{r_1 r_4}\cos(\alpha - I) - \sin(\alpha - I)(\varphi_1 - \varphi_2 - \varphi_3 + \varphi_4)\right] \tag{2-8}$$

$$\Delta Z = 2M\sin\alpha\left[\sin(\alpha - I)\ln\frac{r_2 r_3}{r_1 r_4} + \cos(\alpha - I)(\varphi_1 - \varphi_2 - \varphi_3 + \varphi_4)\right] \tag{2-9}$$

$$\begin{aligned}\Delta g = 2G.d.\{&[Z_1(\varphi_2 - \varphi_4) - Z_2(\varphi_1 - \varphi_3)] \\ &+ x_k[\sin^2\alpha\ln\frac{r_2 r_3}{r_1 r_4} + \cos\alpha\sin\alpha(\varphi_1 - \varphi_2 - \varphi_3 + \varphi_4)] \\ &+ 2b[\sin^2\alpha\ln\frac{r_4}{r_3} + \cos\alpha\sin\alpha(\varphi_3 - \varphi_4)]\}\end{aligned} \tag{2-10}$$

Making use of the equation (2-8) and equation (2-9); and varying parameters we obtain the models shown in Figure 2.5 and Figure 2.6.

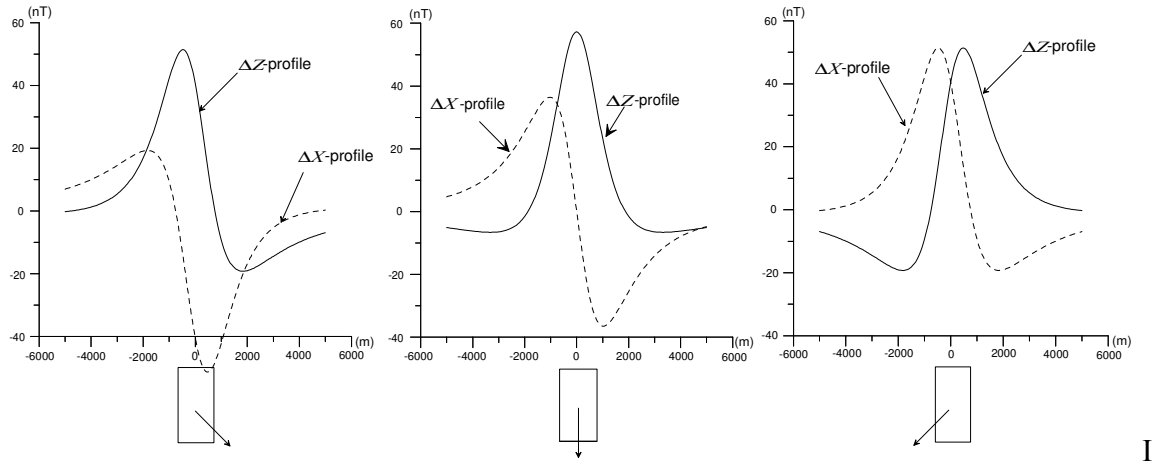

I

Inclination= 45^0 90^0 135^0

Figure 2.5: Magnetic anomaly profiles (ΔX , ΔZ) of a thick plate

Note: The inducing magnetic field strength is 52000nT with three inclination angles 45^0 , 90^0 and 135^0 respectively. The vertical thick plate (L=2b) is buried at depth of 500m.

Figure 2.5 shows three profiles for a vertical thick plate buried deeply and with an inducing magnetic field having different inclination of magnetization 45^0 , 90^0 and 135^0 . When the thick plate has a vertical magnetization (90^0), it produces a symmetric anomaly in the component-z, when the thick plate has an inclined magnetization, the anomalies are asymmetric, and the thick plate is located between the maximum value and the minimum value of the anomaly.

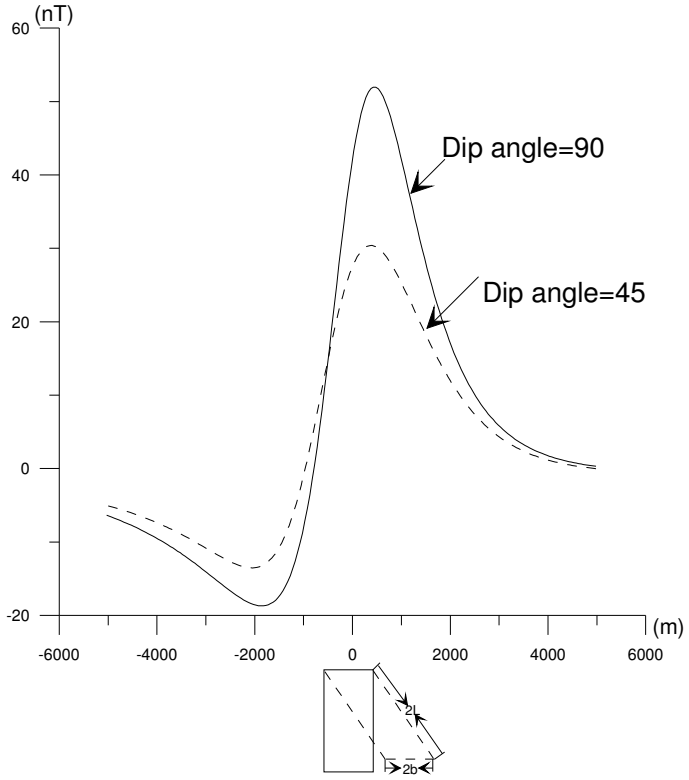

Figure 2.6: Magnetic anomaly of a dipping thick plate on the ΔZ profile, the inclination of magnetization is 135^0 . The dip angles of the thick plate are 45^0 and 90^0 .

In the case of an inclined magnetization, the anomaly profile has a negative minimum and is asymmetric; the position of the thick plate lies between the maximum value and the minimum value; the negative value lies in the piercing direction of the intensity of magnetic field. Those characteristics tell us that the dip angle of thick plate impacts on the shape of the anomaly.

Based on the Equation (2-10), the gravity anomaly over a dipping thick plate is shown in Figure

2.7. The dip of thick plate ($45^0, 90^0$ and 135^0) has much less effect on the shape of the anomaly than for the magnetic field anomaly.

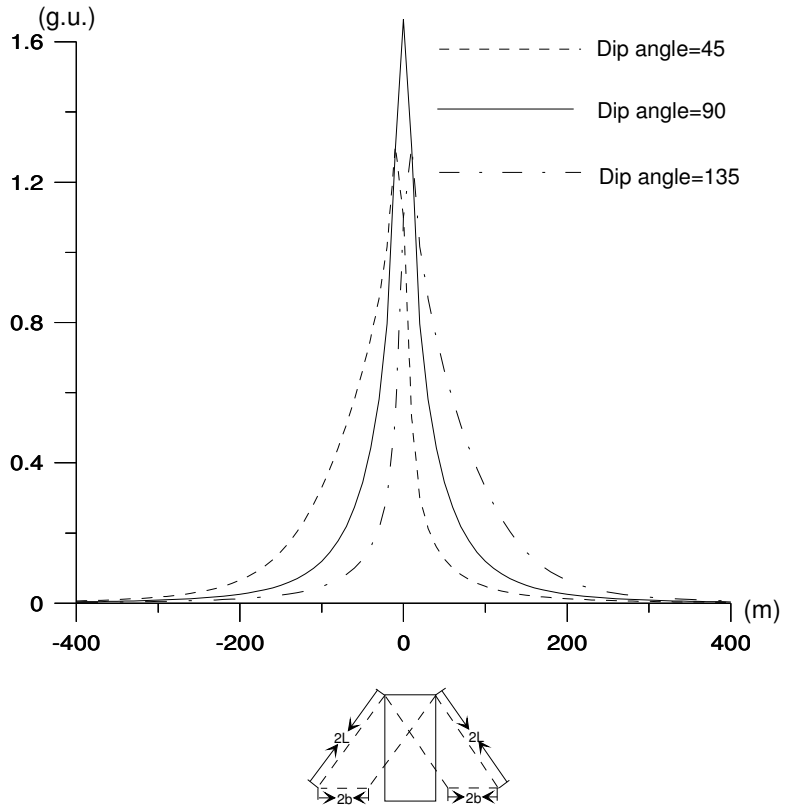

Figure 2.7: Gravity anomaly profiles of a thick at different dip angles. The Earth's magnetic field is vertical down (90^0).

When the dip is 90^0, the anomaly profile is symmetric; when the dip is 45^0 or 135^0, the anomaly profile is asymmetric; and the steep slope side indicates the direction of inclination.

2.2 3-D modeling

2.2.1 Rectangular prism

Compared with a plate model, the rectangular prism model has limited strike extent (Figure 2.8). An irregular body can be subdivided into a number of vertical prisms. We assume that each prism has constant magnetic susceptibility or density. The magnetic or gravity anomaly of the body at any point can be approximated by summing the effects of all the prisms. The magnetic potential of a prism of dimensions limited by $\xi_1 < x < \xi_2$, $\eta_1 < y < \eta_2$ and $\zeta_1 < z < \zeta_2$ is:

$$U = \iiint_V \frac{\overrightarrow{R} \cdot \overrightarrow{M} dv}{R^3} = -\iiint_v (\overrightarrow{M} \cdot grad_k \frac{1}{R}) d_v \tag{2-11}$$

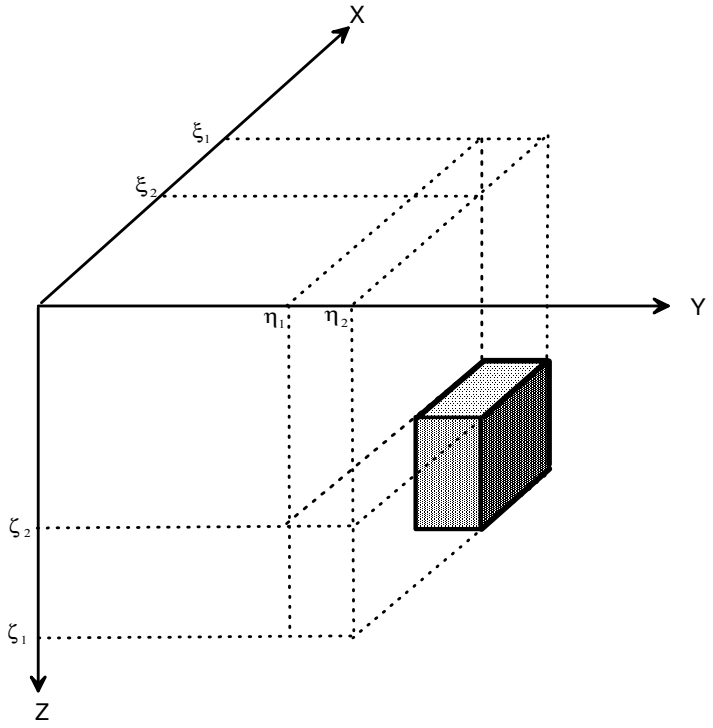

Figure 2.8: Rectangular prism model

Three components of magnetic field are given,

$$\Delta X = -\frac{\partial U}{\partial x}, \quad \Delta y = -\frac{\partial U}{\partial y}, \quad \Delta z = -\frac{\partial U}{\partial z} \tag{2-12}$$

This can be written further form (given by Zhang and Pan 2000):

$$\Delta X = \left\{ -M_x \arctan \frac{(y-y_k)(z-z_k)}{(x-x_k)R} + M_y \ln[R+(z-z_k)] + M_z \ln[R+(y-y_k)] \right\} \Big|_{\xi_2}^{\xi_1} \Big|_{\eta_2}^{\eta_1} \Big|_{\zeta_2}^{\zeta_1}$$

(2-13)

$$\Delta Y = \left\{ M_x \ln[R+(z-z_k)] - M_y \arctan \frac{(x-x_k)(z-z_k)}{(y-y_k)R} + M_z \ln[R+(x-x_k)] \right\} \Big|_{\xi_2}^{\xi_1} \Big|_{\eta_2}^{\eta_1} \Big|_{\zeta_2}^{\zeta_1}$$

(2-14)

$$\Delta Z = \left\{ M_x \ln\left[R + (y - z_k)\right] - M_y \ln\left[R + (x - x_k)\right] - M_z \arctan \frac{(x - x_k)(y - y_k)}{(z - z_k)R} \right\} \Bigg|_{\xi_2}^{\xi_1} \Bigg|_{\eta_2}^{\eta_1} \Bigg|_{\zeta_2}^{\zeta_1}$$

(2-15)

The horizontal field is given:

$$H_{xy} = \Delta X \sin D + \Delta Y \cos I \tag{2-16}$$

The total-field anomaly is ΔT,

$$\Delta T = \Delta X \cos I \cos D + \Delta Y \cos I \sin D + \Delta Z \sin I \tag{2-17}$$

For the same source, the gravity anomaly can be calculated (Nagy, 1996):

$$\Delta g = G.d.\left\{ (x - x_k) \ln\left[R + (y - z_k)\right] + (y - y_k) \ln\left[R + (x - x_k)\right] - (z - z_k) \arctan \frac{(x - x_k)(y - y_k)}{(z - z_k)R} \right\}$$
$$\Bigg|_{\xi_2}^{\xi_1} \Bigg|_{\eta_2}^{\eta_1} \Bigg|_{\zeta_2}^{\zeta_1}$$

(2-18)

Equations (2-13) to (2-18) are often used as basic equations to calculate magnetic and gravity anomalies for a geological body of arbitrary shape.

In order to look at the anomaly variations with different magnetization inclinations and with different dip angles for the prism, we used MAGPRISM (Hjelt, 1972a) from the University of Oulu, Finland to characterize the magnetic anomaly and GRAPRISM (Hjelt, 1972b) for the gravity anomaly (Figure 2.9 to Figure 2.23).

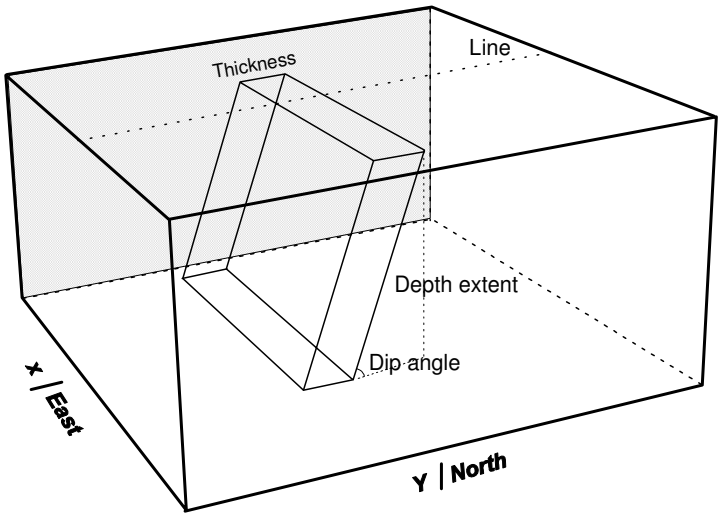

Figure 2.9: Parameters of a dipping prism model

As show in Figure 2.9, the xyz-position of the prism is defined by the centre of the top of the prism. In addition, the top and bottom faces of the prism are horizontal.

The dip angle is measured from the horizontal plane and the depth extent means the vertical height of the prism (not along the dip). The strike angle is taken counter-clockwise from the positive x-axis.

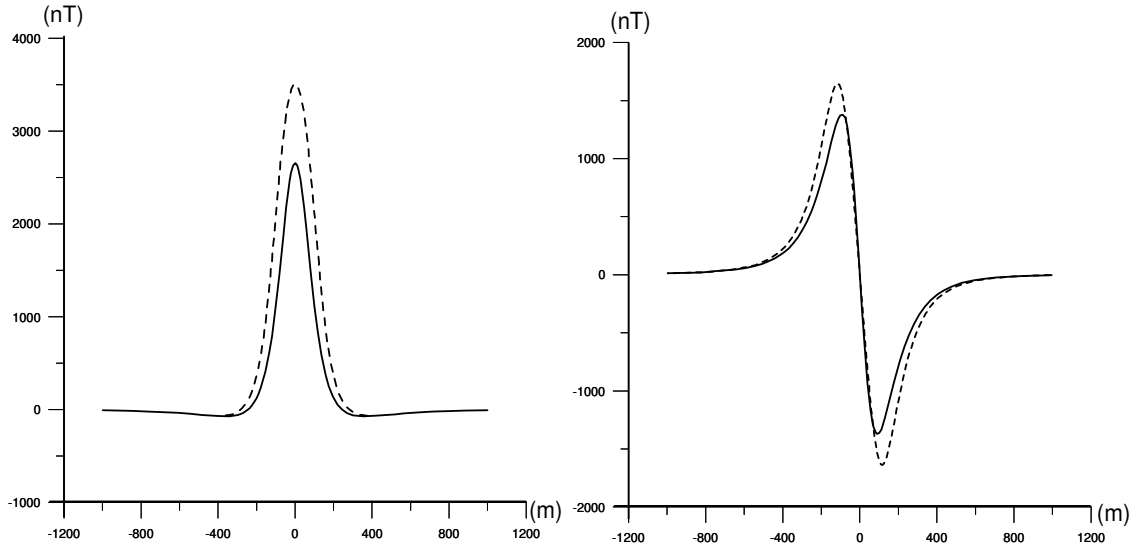

(a) (b)

Figure 2.10: Magnetic anomaly profiles (total anomaly ΔT on the left panel, horizontal anomaly H_{xy} on the right panel) of a vertical prism with vertical magnetization.

Note: The strength of inducing magnetic field is 52000nT, declination 10^0 and inclination 90^0. The prism (thickness=100m, Length=400m, Height=200m) is buried at a depth of 100m (dashed line) and 150m (solid line).

When the prism has a vertical magnetization, $\Delta T = \Delta Z$ show in (a), its maximum value corresponds to the origin. This profile characteristic can be used to confirm that magnetization is in the same direction as dipping direction. However, the profile curve H_{xy} has a one-side negative anomaly, the magnetic profile curve H_{xy} is asymmetric, and the body lies between $H_{\max}$ and $H_{\min}$. It seems that increasing the depth of burial makes more impact on the vertical component than on the horizontal component.

Figure 2.11 shows perspective views of the magnetic anomaly of a prism at various depths. We see again that the amplitude of anomaly drops quickly with increasing depth. The map grid is coarser, the image is less smooth.

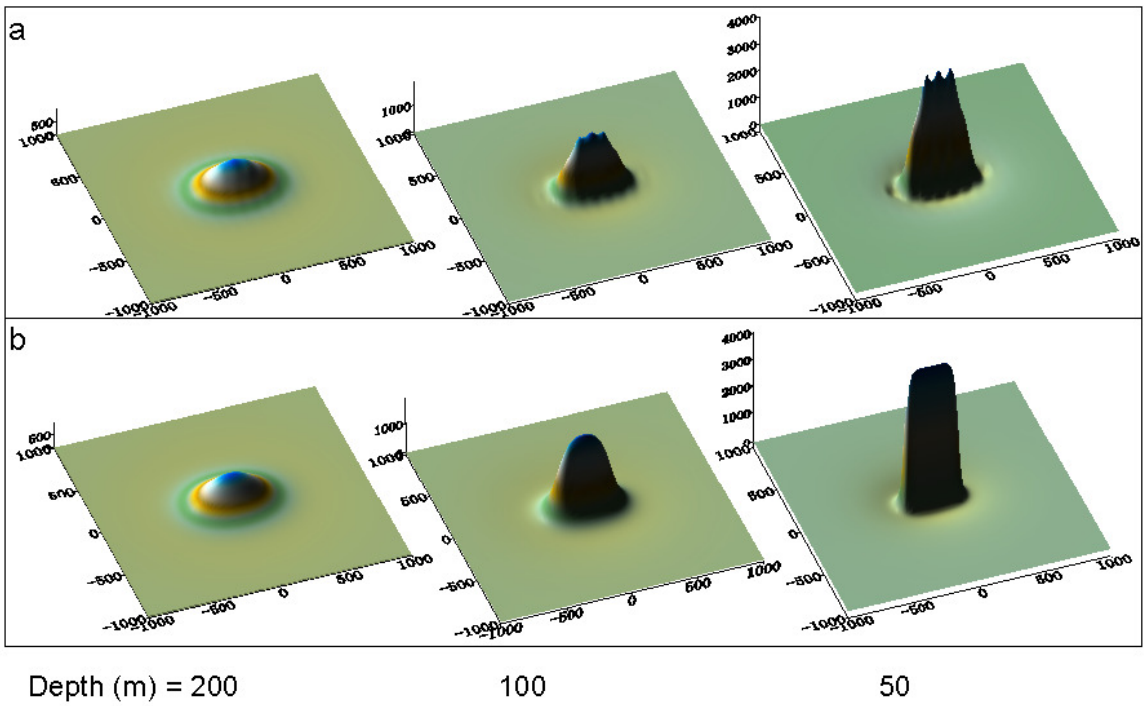

Figure 2.11: Magnetic anomaly over a prism in an inducing field with different sampling grid.

Note: The magnetic field strength is 52000nT, with an inclination of 90^0. The vertical prism (100m×400m×200m) is buried at 200m, 100m and 50m of depth; (a) sampling grid is 100m×10m. (b) Sampling grid is 10m×10m.

In Figure 2.12 and Figure 2.13 we show more complexity in the magnetic field that the anomaly shape varies with inclination and declination of the inducing magnetic field; and it is also in function of the dip angle of magnetic body, the strike direction of the body related to the inducing magnetic field direction.

Inclination= 90^0

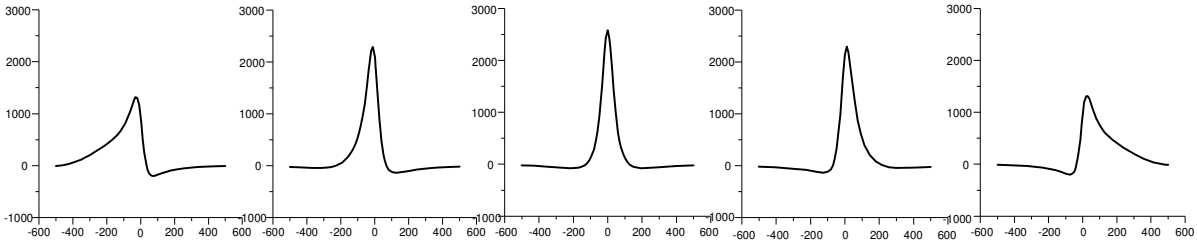

Inclination= 60^0

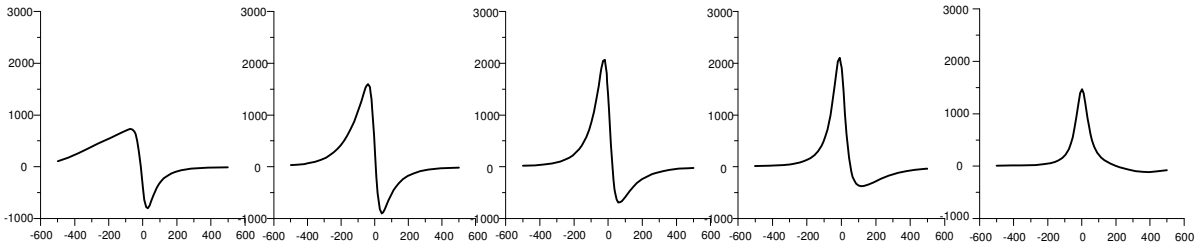

Inclination= 30^0

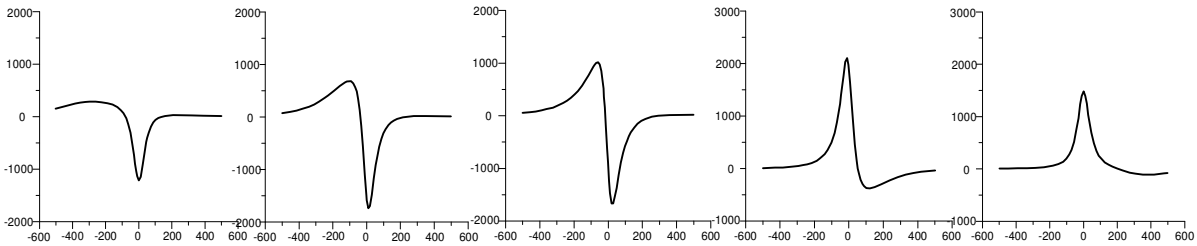

Dip angle= 30^0 60^0 90^0 120^0 150^0

Figure 2.12: Total-field magnetic anomaly (ΔT) profiles over a prism (50m×400m×200m) at different inducing field and for various dips of the prism.

Inclination= 0^0 , declination = 10^0 , dip angle= 0^0

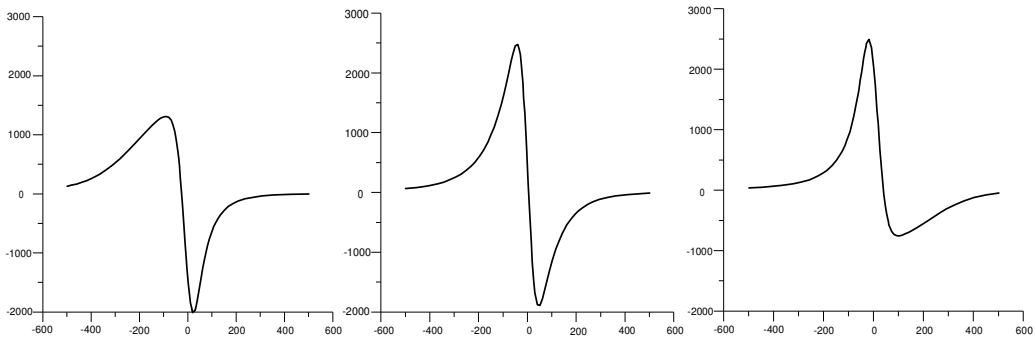

Strike angle= 45^0 90^0 135^0

Inclination= 45^0 , declination = 10^0 , dip angle = 45^0

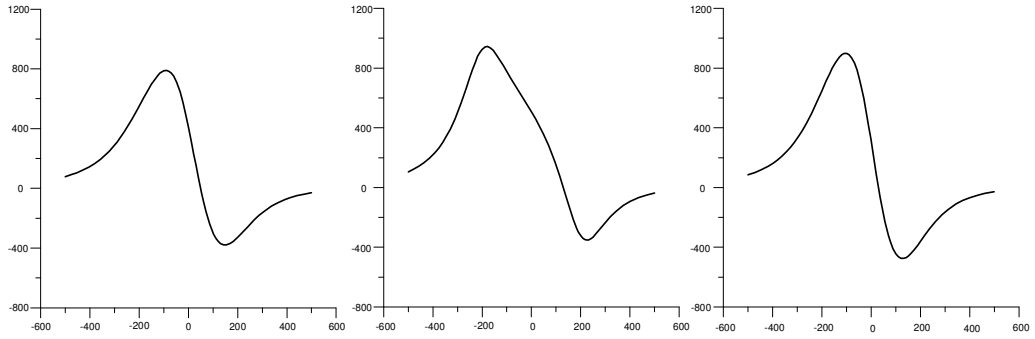

Strike angle= 45^0 90^0 135^0

Inclination= 90^0 , declination = 10^0 , dip angle = 90^0

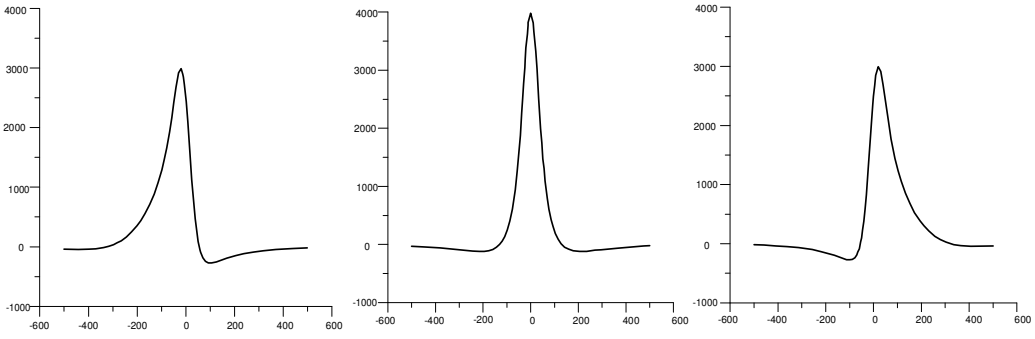

Strike angle= 45^0 90^0 135^0

Figure 2.13: Total-field magnetic anomaly (ΔT) profiles over a prism (50m×400m×200m) at different inclinations of inducing magnetic field, dip angles and strike angles of the prism.

Based on above tests, we saw that the inclination and the declination of the inducing magnetic field, as well as the dip angle and the strike angle of the prism influence the shape of the magnetic anomaly. Even if the geomagnetic field inclination and the declination vary with latitude and longitude, when the survey region is small enough we can consider them as constant. Therefore, the most of the variability in anomaly shape is due to changes in the dip and of the strike angles relative to the direction of declination. The importance of these two parameters is considered in the further development.

The magnetic anomaly contour maps often better demonstrate the magnetic source distribution. Figure 2.14 shows the anomaly map of a vertical prism caused by vertical magnetization. With the increasing distance from the center of the prism, the magnetic anomaly profile becomes smaller.

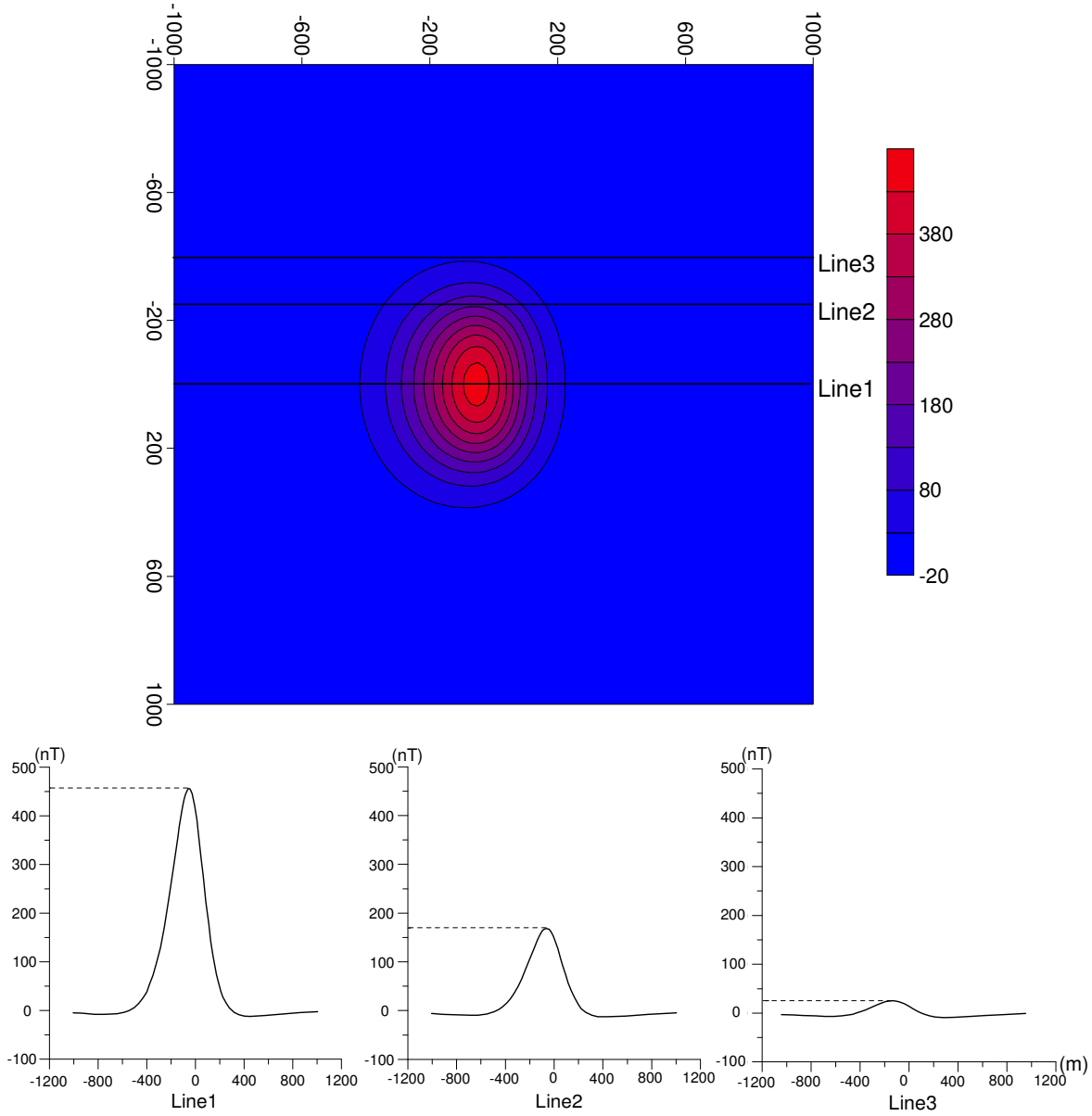

Figure 2.14: Magnetic anomaly map and profiles caused by a magnetic prism.

Note: The magnetic field strength is 52000nT, declination of 0^0 and inclination 90^0, the prism is 50m×400m×200m and buried at a depth of 1000m; dip angle is 45^0; sampling grid is 10m×10m.

In the case of inclined magnetization (Figure 2.15), the anomaly is asymmetric.

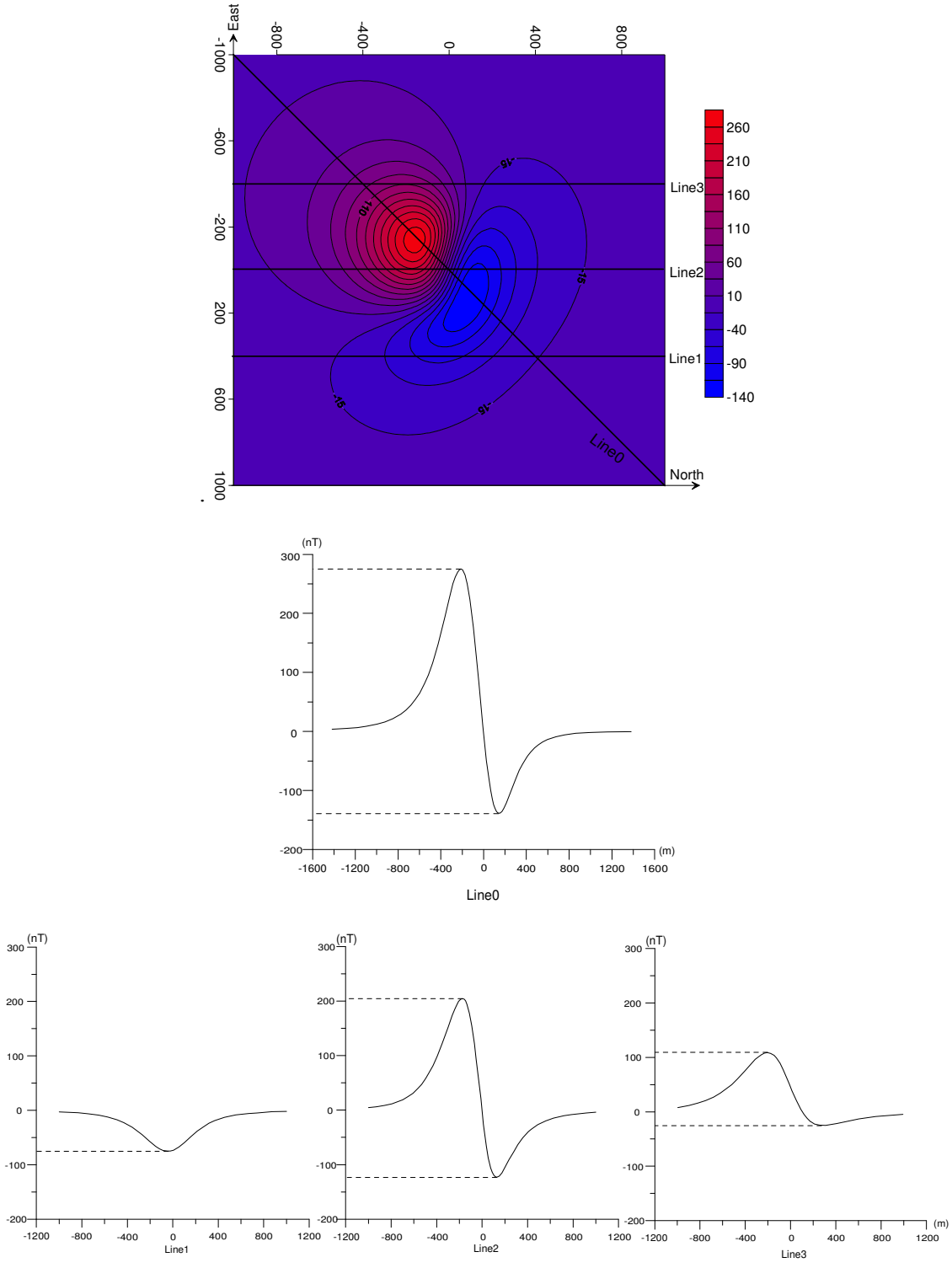

Figure 2.15: Magnetic anomaly map and profiles caused by a magnetized prism.

Note: The magnetic field strength is 52000nT, with declination 45^0 and inclination 45^0. The prism is 50m×400m×200m and is located at a depth of 1000m.

The anomaly shape is much simpler for the gravity than for the magnetic method. From Figure 2.16, we can see that the tendency of the anomaly on the profile is the same to the three-dimensional maps' trend, namely same to the prism's inclination. The gravity anomaly is the strongest when the dip angle is 90^0 .

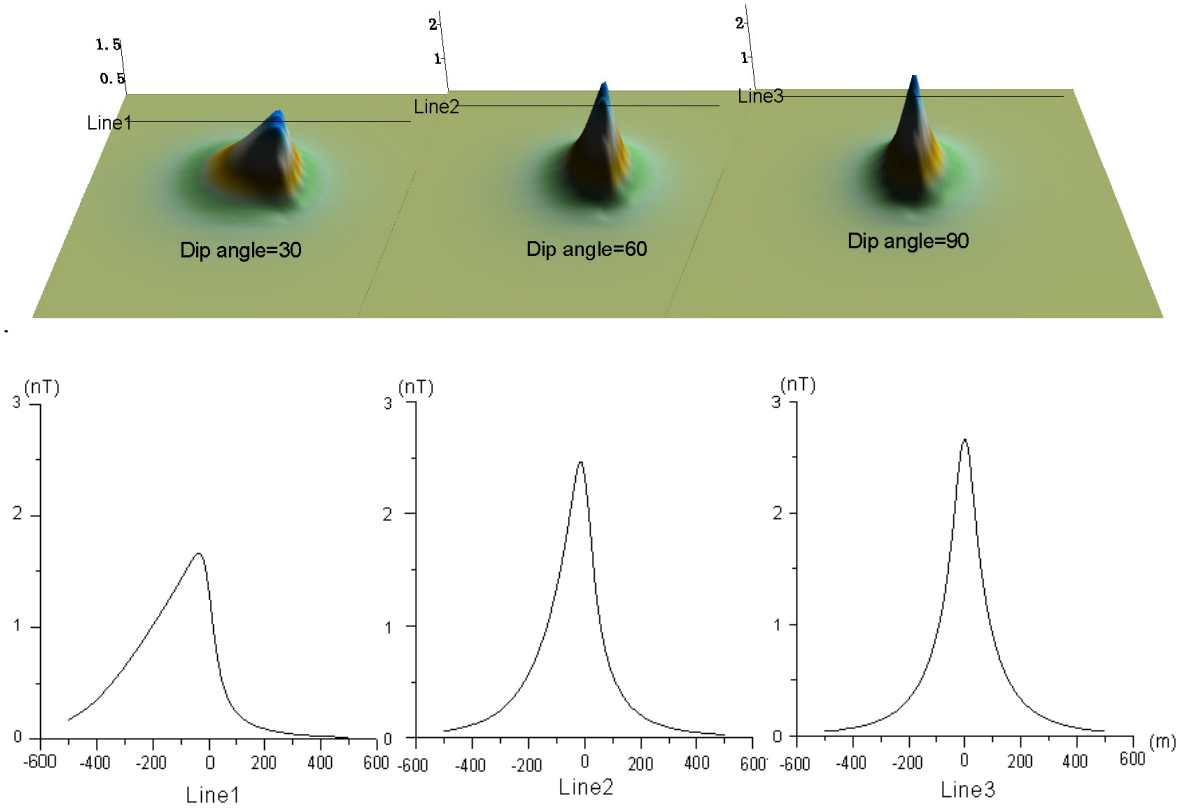

Figure 2.16: Three-dimensional gravity anomaly maps and corresponding profiles over a prism(50m×400m×200m) at different dip angles.

Figure 2.17 shows that amplitude and width of the gravity anomaly increase with the increasing thickness of the prism.

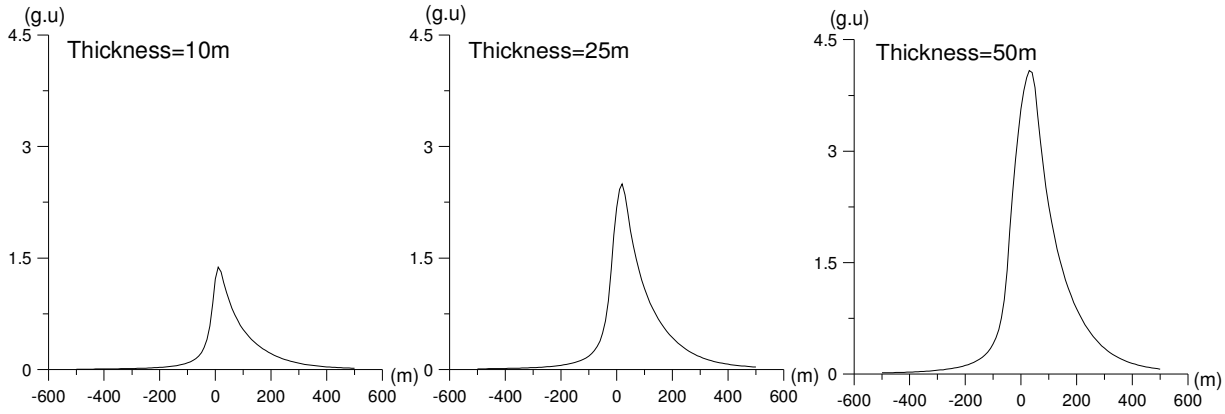

Figure 2.17: Gravity anomaly profiles for a prism (the dip angle 45^0) with different thickness.

Note: the length of the prism is 200m, depth extent (vertical height) is 100m; and depth to top 10m, the thickness is 10m, 25m and 50m, respectively.

2.2.2 The cube

When the geologic source produces closed anomaly contours roughly of circular shape, we can approximate the source by a cube or a sphere. From modeling tests we can see that variations in the inclination of inducing magnetic field make visible impact on the shape of magnetic anomaly over such body with limited depth extension.

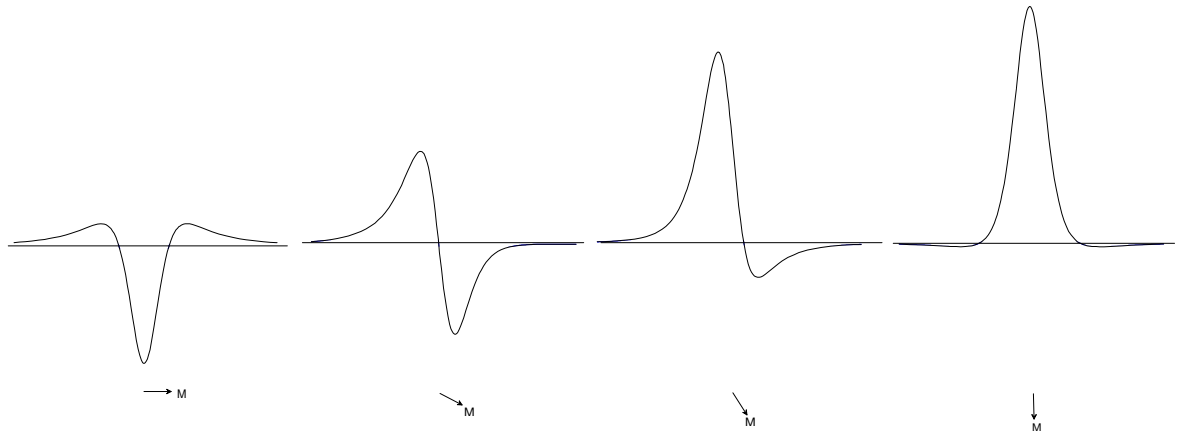

Inclination= 0^0 30^0 60^0 90^0

Figure 2.18: Total-field profiles for magnetic cube in an inducing field with strength 52000nT, the response for different inclinations.

With increasing inclination, the positive anomaly become obvious and the maximum value of magnetic anomaly also gradually increase and the negative anomaly characteristics become less obvious.

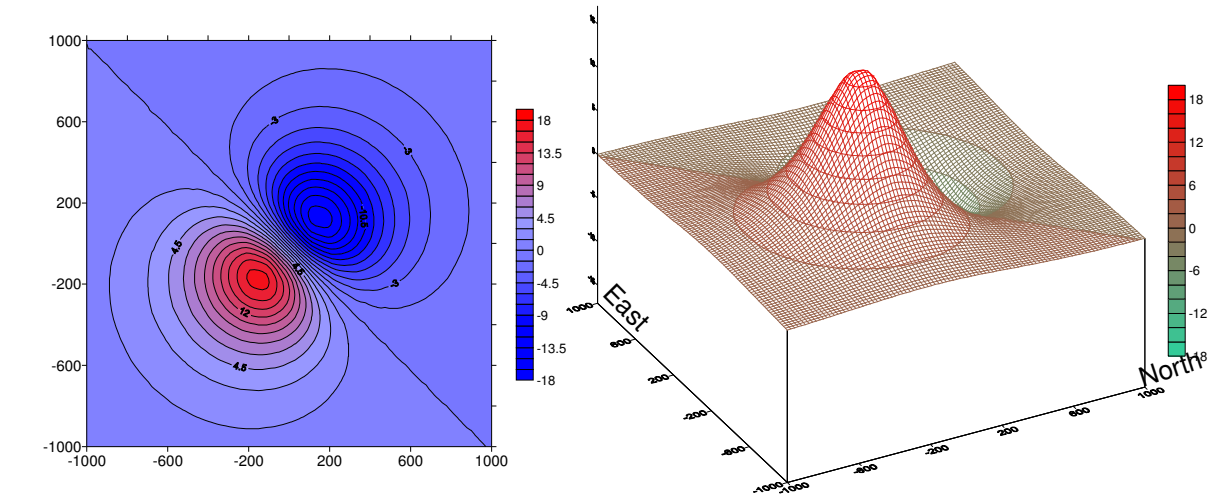

(a)

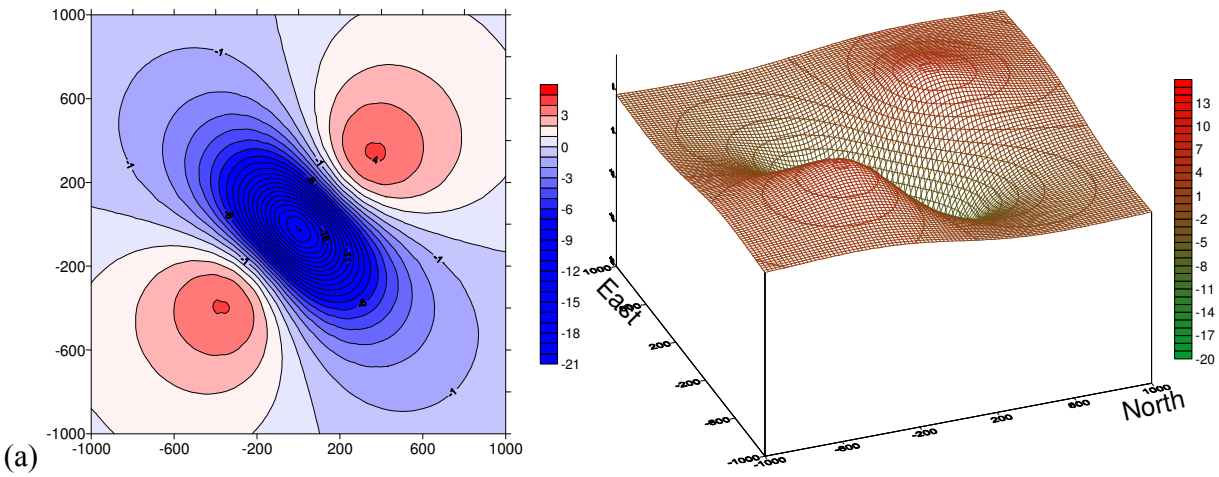

(a)

(b)

Figure 2.19: Magnetic anomaly maps of a cube (Horizontal magnetization)

Note: Magnetic anomaly maps for magnetic cube in an inducing field with strength 52000nT and inclination= 0^0 (horizontal magnetization). (a) Magnetic anomaly ΔZ map and three-dimensional ΔZ map. (b) Total magnetic anomaly ΔT map and three-dimensional ΔT map.

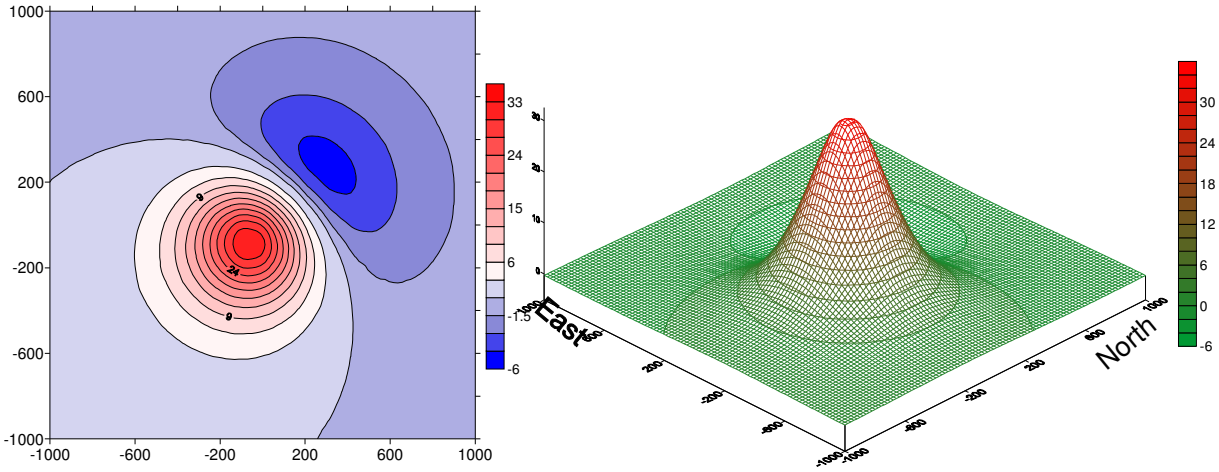

(a)

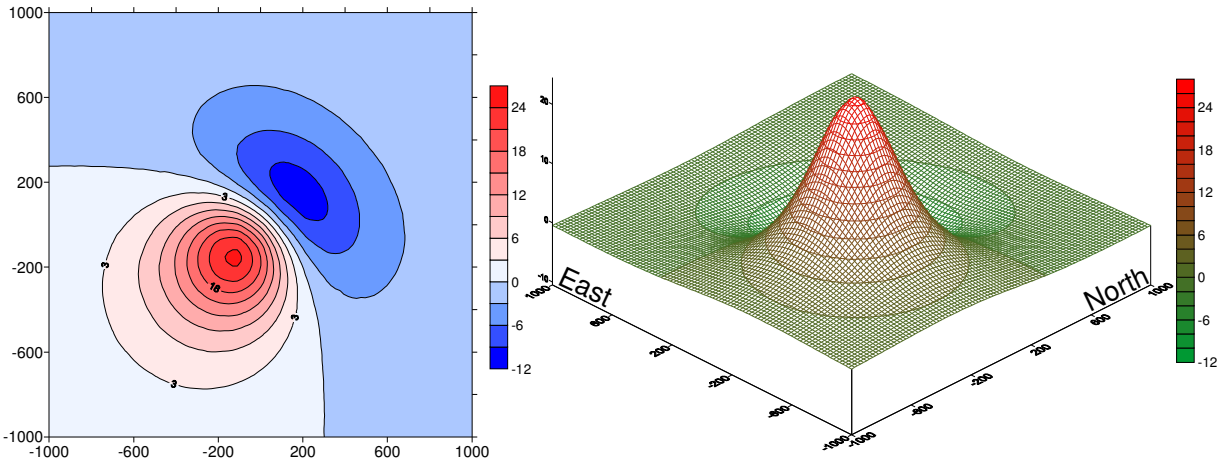

(b)

Figure 2.20: Magnetic anomaly maps of a cube (inclined magnetization)

Note: Magnetic anomaly maps for magnetic cube in an inducing field with strength 52000nT and $0^0 <$ inclination$< 90^0$ (inclined magnetization). (a) Magnetic anomaly ΔZ map and three-dimensional ΔZ map. (b) Magnetic anomaly ΔT map and three-dimensional ΔT map.

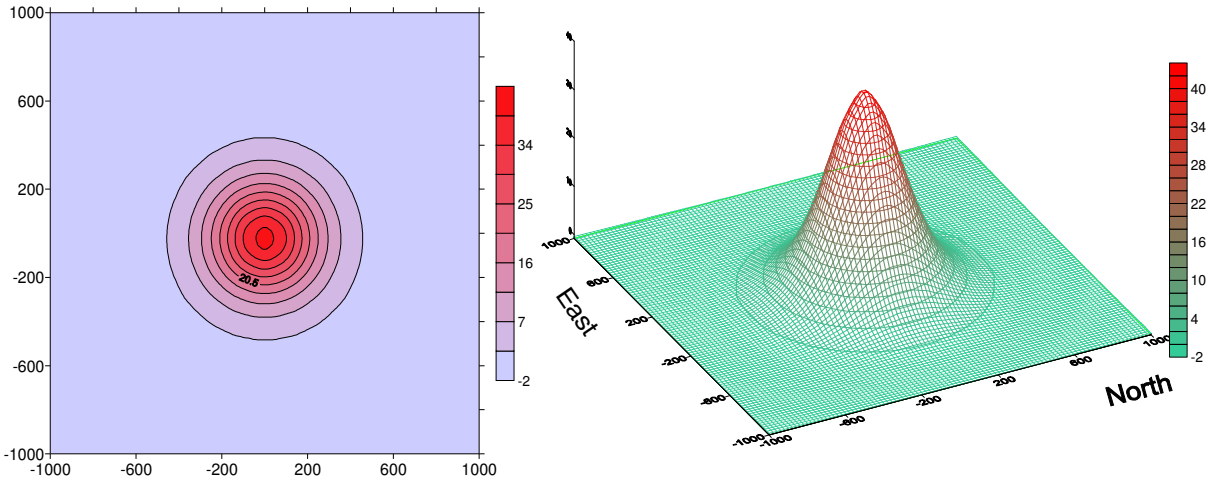

Figure 2.21: Magnetic anomaly maps of a cube (vertical magnetization)

Note: The total magnetic anomaly maps for magnetic cube in an inducing field with strength 52000nT and inclination= 90^0 (vertical magnetization), left is the total anomaly contour map, right is corresponding three-dimensional map.

From Figure 2.19 and Figure 2.20, it can be seen that the magnetic anomaly contour maps of the cube are of isometric shape, when the cube is vertically magnetized, $\Delta Z = \Delta T$, having strong positive anomaly show in Figure 2.21.

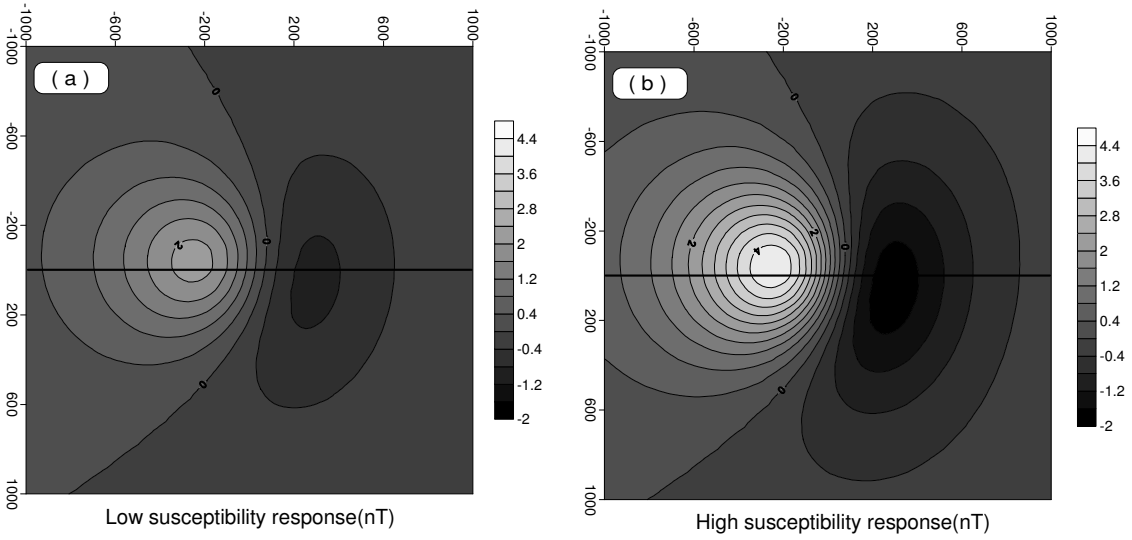

Figure 2.22: Anomaly map over a cube with two susceptibilities (0.5 SI and 1 SI) in a same inducing magnetic field.

From Figure 2.22, it can be seen that the magnetic anomaly is directly proportional to the

susceptibility of its source. The higher susceptibility is, the magnetic response is stronger and anomaly contours are denser.

Figure 2.23 shows four types presentation of a total field of magnetic anomaly: (a) the profile; (b) the vector map; (c) the color anomaly map; and (d) the three-dimensional map.

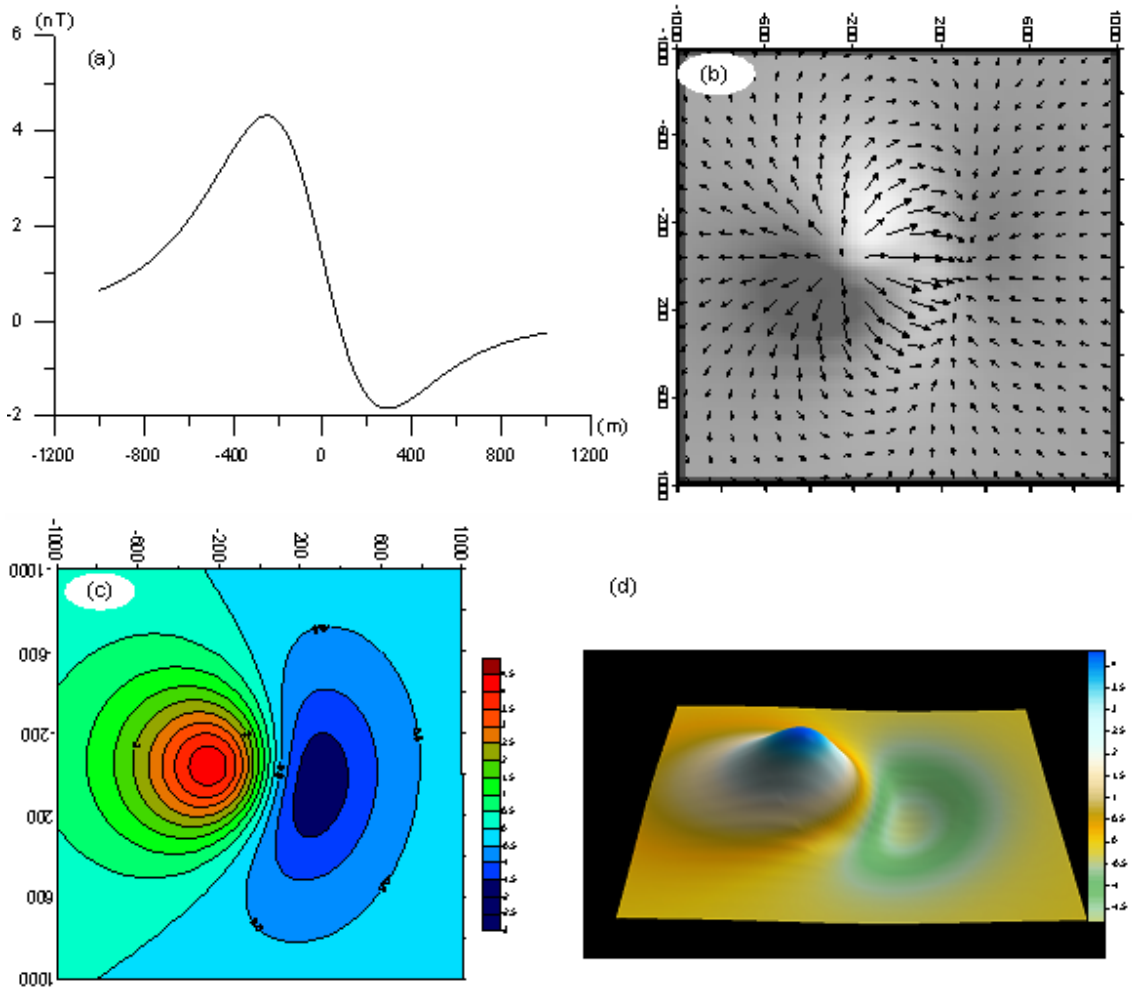

Figure 2.23: ΔT maps and profiles for magnetic cube in an inducing field with strength 52000nT and inclination 45^0.

Summarizing the forward modeling assessments, the characteristics of magnetic anomaly on profiles or on maps, may help us interpret observation qualitatively and then choose the right physical model in order to perform the quantitative interpretation.

2.3 Summary

The magnetic profile, depending on magnetization directions and the physical parameters of the geological bodies, has three basic shapes: no negative anomaly on both sides of the curve, one side has the negative anomaly and both sides have the negative anomaly. The anomaly profiles shown that variations of the amplitude and the form of profile are affected mostly by the inclination of the inducing magnetic field and the dip of the geological body; the depth of geological body impacts on the amplitude of anomaly, the amplitude drops quickly with increasing depth. There is no horizontal component when the body has a vertical magnetization, the vertical component is the equal to the total field anomaly, and its maximum value corresponds to the location of the body. High susceptibility bodies produce stronger magnetic anomalies.

The form of magnetic anomaly contour map for a single body can be roughly divided into three types, long belt shape, isometric shape and ellipse shape. Generally, the magnetic anomaly map of the spheroid is of isometric shape, the magnetic anomaly contour map of two-dimensional plate and the horizontal cylinder show long belt shape, the magnetic anomaly contour map of finite horizontal cylinder and the plate is the ellipse shape.

The 3-D anomaly map is useful to show the spatial distribution of the anomaly source.

Gravity anomaly is very straightforward. The high residual density produces stronger gravitational anomaly. The dip angle of the geological body has much less effect on gravitational anomaly than the magnetic; the asymmetry of anomaly profile can reflect the dip angle of the geological body. The amplitude of gravitational anomaly attenuates quickly with the increasing burial depth.

Magnetic anomaly is a function of latitude as we see from the Figure 2.18; due to this effect the magnetic anomaly changes its shape, plus the variations from different source occurrences it makes difficulty to the interpretation of magnetic data. However, from forward modeling exercises, it is possible to characterize anomaly variations by finding out a correlation between anomaly shape and several main factors such as dip and strike direction, geometry and depth of geological body. As we mentioned in the chapter II that we need optimize the number of independent variables to be used in order to ensure efficient calculation. Therefore, we have chosen 9 key parameters for magnetic field and 6 parameters for gravity field in our new development in the next chapter.

CHAPTER III NEW DEVELOPMENT FOR FORWARD AND INVERSE MODELING

3.1 New gravity and magnetic formulas

Simple physical models, such as plate, prism and sphere, are useful to make quick interpretation in the field for mineral exploration. Conventional methods calculate the geophysical anomaly along a profile passing over the top centre of an inclined body, assuming that body dip lies within the profile plane. As we see from forward modeling exercises the variations in shape of magnetic anomaly have complex implications. In order to improve the method of calculation, we have chosen the cylinder model which can be representative of a kimberlitic pipe structure. Considering multiple factors, such as the dip angle, strike direction, size, top depth and physical property of a cylinder, we developed new mathematic formulas for gravity and magnetic methods, by letting the cylinder freely oriented in the space.

3.1.1 New formula for the gravity method

A cylinder is under the surface XOY (Figure 3.1). It has a dip angle α, a strike angle θ and the radius $r_{cylinder}$. The gravitational attraction on the point P from an element dl of the cylinder is given by $\Delta g_r = G \cdot \rho \cdot s \cdot dl / r^2$.

ρ is the density of the element dl, $s = \pi . r_{cylinder}^{\ 2}$ is the cross-sectional area of dl, r is the distance between the element dl and the point P. Since the field observations estimate the variations of gravitational acceleration, the gravity anomaly is only dependent on the density difference (usually referred to as density contrast or residual density) between the objective body and the surrounding rocks. The present development aims to localize the residual density; therefore ρ is indeed the density contrast between the cylinder and its environment.

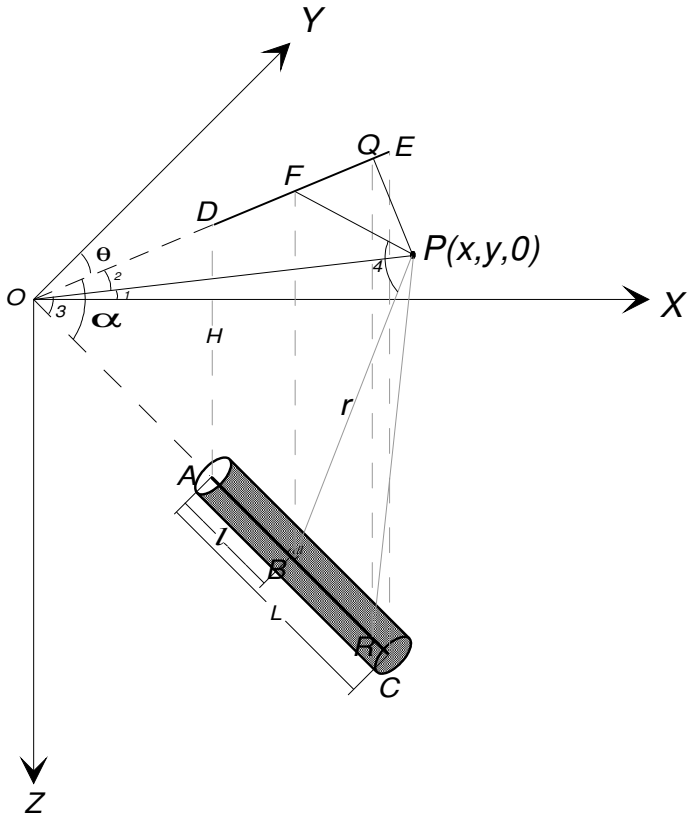

Figure 3.1: Geometrical parameters of the cylinder model

We defined that the dip angle (α) of the cylinder varies between $0^0 \le \alpha \le 90^0$, and that the depth extent means the length of the cylinder along the dip direction (L). The strike angle (θ) is taken counter-clockwise from the positive y-axis ($0^0 \le \theta < 360^0$), D, F, Q, E indicate the projected position of A, B, R and C on the surface XOY along the strike direction of the cylinder. H is the top depth of the cylinder. $\angle 1$ is the angle between OP and axes-X, $\angle 2$ is between OE and OP, $\angle 3$ between OP and OC, and $\angle 4$ is between FP and PB (Figure 3.1).

The geometrical relationships between above parameters are as follow:

$$\Delta ODA : OD = H / \tan\alpha, OA = H / \sin\alpha$$

$$\Delta OQP : OP = \sqrt{X^2 + Y^2}, PQ = \sin\angle 2.OP, OQ = \cos\angle 2.OP$$

$$\Delta OQR : QR = \tan\alpha.OQ = \tan\alpha.\cos\angle 2.OP, OR = OQ / \cos\alpha = \cos\angle 2.OP / \cos\alpha$$

$$\Delta QPR : PR = \sqrt{QP^2 + QR^2} = \sqrt{(X^2 + Y^2)(\sin^2\angle 2 + \tan^2\angle\alpha.\cos^2\angle 2)}$$

$$\Delta OPR : \cos\angle 3 = (OP^2 + OP^2 - PR^2)/2.OP.OR$$

$$\Delta OPB : r^2 = OB^2 + OP^2 - 2.OB.OP.\cos\angle 3$$

$$\Delta OFB : FB = (H/\sin\alpha + l)\sin\alpha$$

$$\Delta PFB : \sin\angle 4 = (H/\sin\alpha + l)\sin\alpha / r$$

$$\angle 1 = \arctan y/x, \angle 2 = 90 - \theta - \angle 1 \tag{3-1}$$

The vertical component is $\Delta g' = G \cdot \rho \cdot s \cdot dl.\sin\angle 4 / r^2, s = \pi \cdot r_{cylinder}{}^2$ and then the total effect of the cylinder is

$$\Delta g = G \cdot \rho \cdot s \cdot (H/\sin\alpha + l)\sin\alpha / \{(H/\sin\alpha + l)^2 + (x^2 + y^2) - 2(H/\sin\alpha + l) \cdot \sqrt{x^2 + y^2}$$

$$\cdot \cos\angle 2.\cos\alpha\} \cdot \int_0^L \frac{(H/\sin\alpha + l)dl}{\left\{(H/\sin\alpha + l)^2 + (x^2 + y^2) - 2(H/\sin\alpha + l) \cdot \sqrt{x^2 + y^2} \cdot \cos\angle 2 \cdot \cos\alpha\right\}^{\frac{3}{2}}} \tag{3-2}$$

Where ρ is the residual density, we call it the density in following text.

This can be written further form with equations (3-1),

$$\Delta g = G \cdot \rho \cdot s \cdot \sin\angle 4 \cdot \int_0^L \frac{(H/\sin\alpha + l)dl}{\left\{(H/\sin\alpha + l)^2 + (x^2 + y^2) - 2(H/\sin\alpha + l) \cdot \sqrt{x^2 + y^2} \cdot \cos\angle 2 \cdot \cos\alpha\right\}^{\frac{3}{2}}} \tag{3-3}$$

This integral was solved with MATLAB, and the result of the integration is the C program presented in APPENDIX 4. This program was used to compute the forward models presented in the next section.

From equation (3-3) we can find out the solution of conventional method along the x axis by taking y = 0 (Telford et al., 1976, equation. 2.41a).

$$\Delta g = G \cdot \rho \cdot s \cdot \sin\alpha \int_0^L \frac{(H/\sin\alpha + l)dl}{\left\{(H/\sin\alpha + l)^2 + x^2 - 2(H/\sin\alpha + l)x \cdot \cos\alpha\right\}^{\frac{3}{2}}} \tag{3-4}$$

Thus

$$\Delta g = G \cdot \rho \cdot s \cdot \sin\alpha \left[\frac{\cos\alpha((H/\sin\alpha + l)) + x}{x \cdot \sin^2\alpha \cdot \left\{(H/\sin\alpha + l)^2 + 2x(H/\sin\alpha + l)\cos\alpha + x^2\right\}^{\frac{1}{2}}} \right]_L^0$$

$$= \frac{G \cdot \rho \cdot s}{x \cdot \sin\alpha} \left[\frac{H\cot\alpha + x}{(H^2/\sin^2\alpha + 2xH\cot\alpha + x^2)^{\frac{1}{2}}} - \frac{x + H\cot\alpha + L\cos\alpha}{\left\{(H/\sin\alpha + L)^2 + 2x(L\cos\alpha + H\cot\alpha) + x^2\right\}^{\frac{1}{2}}} \right]$$

(3-5)

G : $6.67 * 10^{-8} cm^3 / g.s^2$, Universal gravitation constant.

ρ : The residual density, unit in g / cm^3.

When the cylinder is vertical, the equation (3-3) can be simplified to (Telford et al., 1976, equation. 2.41c).

$$\Delta g = 6.67 * 10^{-8} \cdot \rho \cdot s \left[\frac{1}{(H^2 + x^2)^{\frac{1}{2}}} - \frac{1}{\left\{(H + L)^2 + x^2\right\}^{\frac{1}{2}}} \right] \quad (3\text{-}6)$$

3.1.2 New formula for the magnetic method

The model geometry is shown in Figure 3.2, the cylinder having a dip angle α, a strike angle θ and the radius $r_{cylinder}$, the observation point is at P.

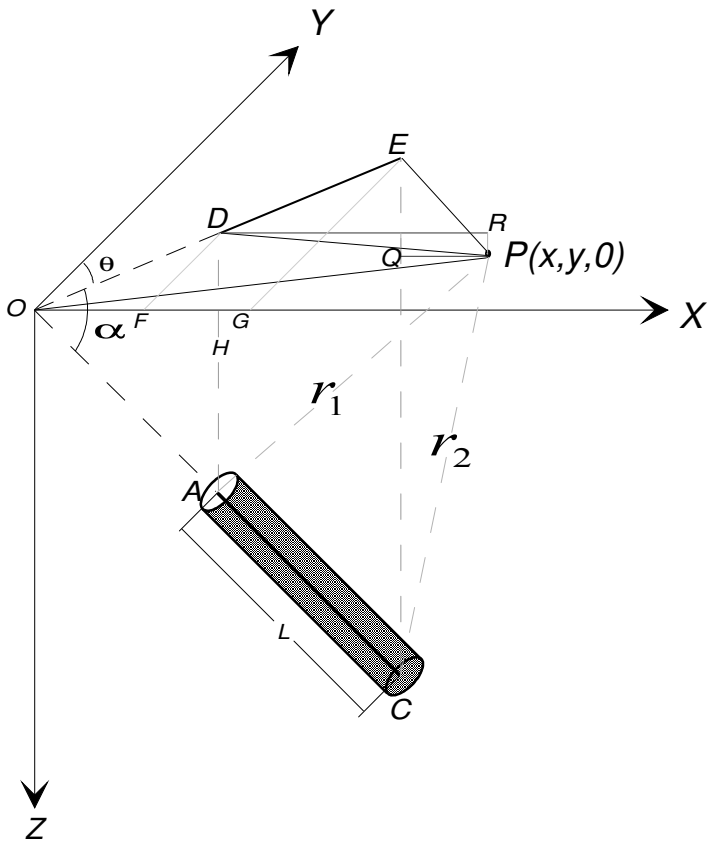

Figure 3.2: Geometrical parameters of the magnetic cylinder model

As show in Figure 3.2, the dip angle (α) is made by the inclination of cylinder with the horizontal plane ($0^0 \le \alpha < 90^0$) and, depth extent means the length of the cylinder along the dip direction (L). The strike angle (θ) is taken counter-clockwise from the positive y-axis ($0^0 \le \theta < 360^0$), $r_{cylinder}$ is the radius of the cylinder, r_1 and r_2 are the distance from P to A and to C of cylinder, respectively. D and E are the projection of A and C onto horizontal plane. The declination angle and the inclination angle as well as the normal magnetic field strength are considered as constant in a given region.

The geometrical relationships of above parameters are as follows:

$D : (H.\sin\theta / \tan\alpha, H.\cos\theta / \tan\alpha)$

$E : ((H / \sin\alpha + L).\cos\alpha.\sin\theta, (H / \sin\alpha + L).\cos\alpha.\cos\theta)$

$Q : ((H / \sin\alpha + L).\cos\alpha.\sin\theta, y)$

$R : (H.\sin\theta / \tan\alpha, y)$

The magnetic potential at P is given by $U = m/r$, where m is the pole strength. If the body is magnetized by induction only (and assuming the magnetization is uniform) we can write the pole strength m in the form $m = k.M.s$, where k represents the susceptibility and M is the Earth's field strength and s is the cross-section area. Thus the three components of magnetic field of cylinder are:

$$\Delta X = -\partial U/\partial x, \Delta Y = -\partial U/\partial y, \ \Delta Z = -\partial U/\partial z \tag{3-7}$$

$$\Delta X = k.M_x \cdot s\left(\frac{\overrightarrow{RP}}{r_1^3} - \frac{\overrightarrow{QP}}{r_2^3}\right) = kM_x \cdot s\left(\frac{x - H\sin\theta/\tan\alpha}{r_1^3} - \frac{x - (H/\sin\alpha + L)\cos\alpha\cdot\sin\theta}{r_2^3}\right) \tag{3-8}$$

$$\Delta Y = kM_y \cdot s\left(\frac{\overrightarrow{RD}}{r_1^3} - \frac{\overrightarrow{QE}}{r_2^3}\right) = kM_y \cdot s\left(\frac{H\cos\theta/\tan\alpha - y}{r_1^3} - \frac{(H/\sin\alpha + L)\cos\alpha\cdot\cos\theta - y}{r_2^3}\right) \tag{3-9}$$

$$\Delta Z = kM_z \cdot s\left(\frac{AD}{r_1^3} - \frac{CE}{r_2^3}\right) = kM_z \cdot s\left(\frac{H}{r_1^3} - \frac{H + L\sin\alpha}{r_2^3}\right) \tag{3-10}$$

(Telford et al., 1976, equation 3.30a)

Where

$$s = \pi \cdot r_{cylinder}^{\ 2} \tag{3-11}$$

$$r_1 = AP = \left\{(x - H\sin\theta/\tan\alpha)^2 + (y - H\cos\theta/\tan\alpha)^2 + H^2\right\}^{\frac{1}{2}} \tag{3-12}$$

$$r_2 = CP = \left\{(x - (H/\sin\alpha + L)\cos\alpha\cdot\sin\theta)^2 + (y - (H/\sin\alpha + L)\cos\alpha\cdot\cos\theta)^2 + ((H/\sin\alpha + L)\sin\alpha)^2\right\}^{\frac{1}{2}} \tag{3-13}$$

$$\begin{cases} M_x = M\cos I\cdot\sin D \\ M_y = M\cos I\cdot\cos D \\ M_z = M\sin I \end{cases} \tag{3-14}$$

I: the magnetic inclination.

D: the magnetic declination

Thus the total magnetic response of the cylinder is:

$$\Delta T = \Delta X \cos I \cdot \sin D + \Delta Y \cos I \cdot \cos D + \Delta Z \sin I \qquad (3\text{-}15)$$

3.2 Application of multiple linear regression method

The interpretation of a single type of geophysical data is inherently non-unique. The use of various datasets that contain complementary information may improve the interpretation. We developed in this chapter two systems of regression for the joint interpretations of gravity data and magnetic data based on the cylinder model. Figure 3.3 summarizes the working flow chart of multiple linear regressions to the forward modelling of a cylinder. We choose 6 and 9 physical parameters to correspondingly describe the gravity and magnetic models. Based on forward modeling results, we select the most significant attributes from anomalies which were in turn used in the determination of the major parameters of cylinder (dip, depth, physical properties etc.) for data inversion. Figure 3.4 shows the working flow of the inverse problem.

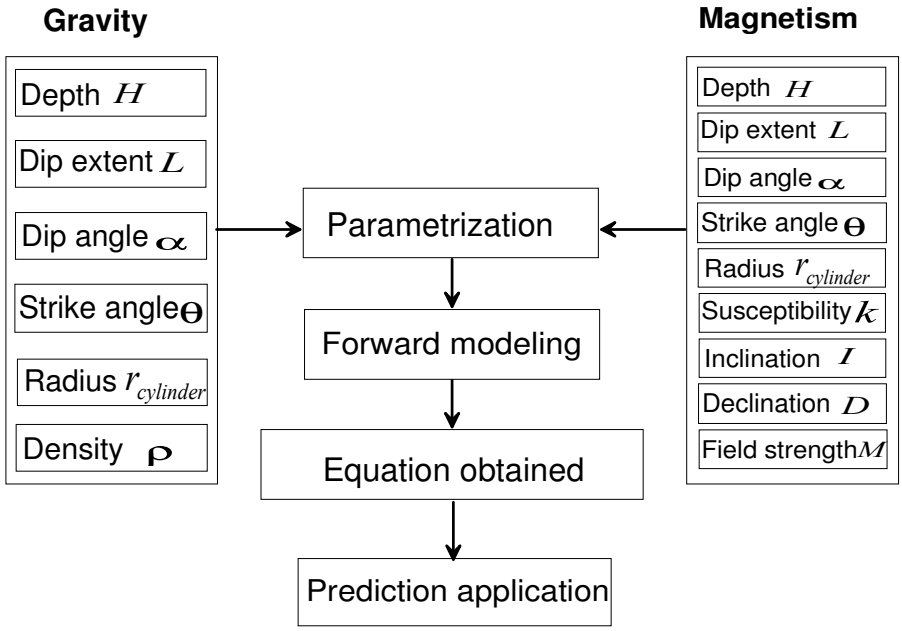

Figure 3.3: Flow chart for the forward problem of cylinder

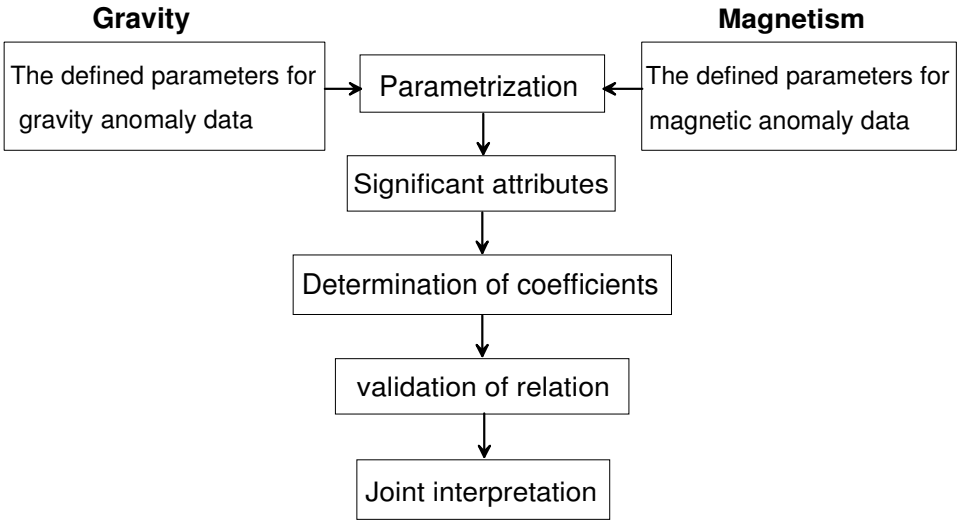

Figure 3.4: Flow chart for the inverse problem of cylinder

3.2.1 Gravity forward modeling

Telford et al. (1976) presents a formula for the computation of the gravity anomaly of a dipping cylinder with a small radius, also called a dipping rod, along a profile over the axis of the cylinder. Our result, presented in Appendix 4, is more general as it allows the computation of the gravity anomaly at any point above the cylinder. This is illustrated in figures 3.5 and 3.6. Compare the conventional consideration (left) with the new calculation of gravity anomaly (right), the new model is more realistic.

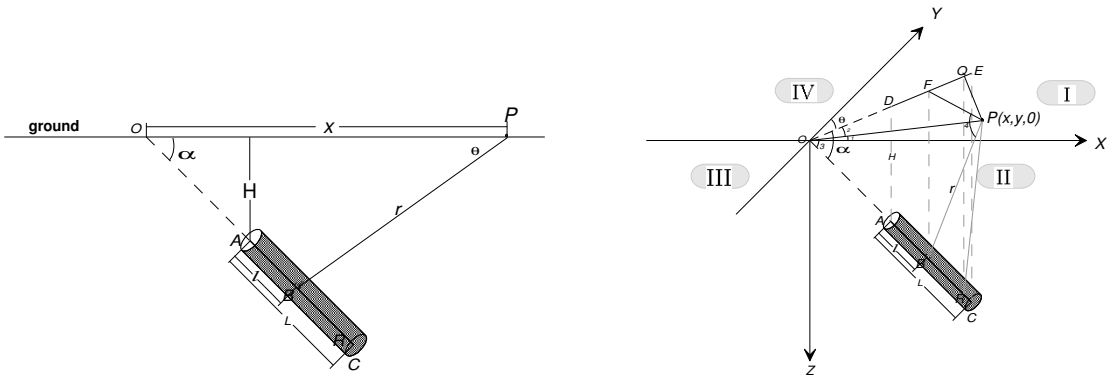

(a) (b)

Figure 3.5: Comparison between conventional consideration - profile (a) and our new development (b) for calculating the gravity anomaly over a cylinder.

This new method allows us to calculate the gravity anomaly of a cylinder in full space and better

localizing its occurrences (Figure 3.6).

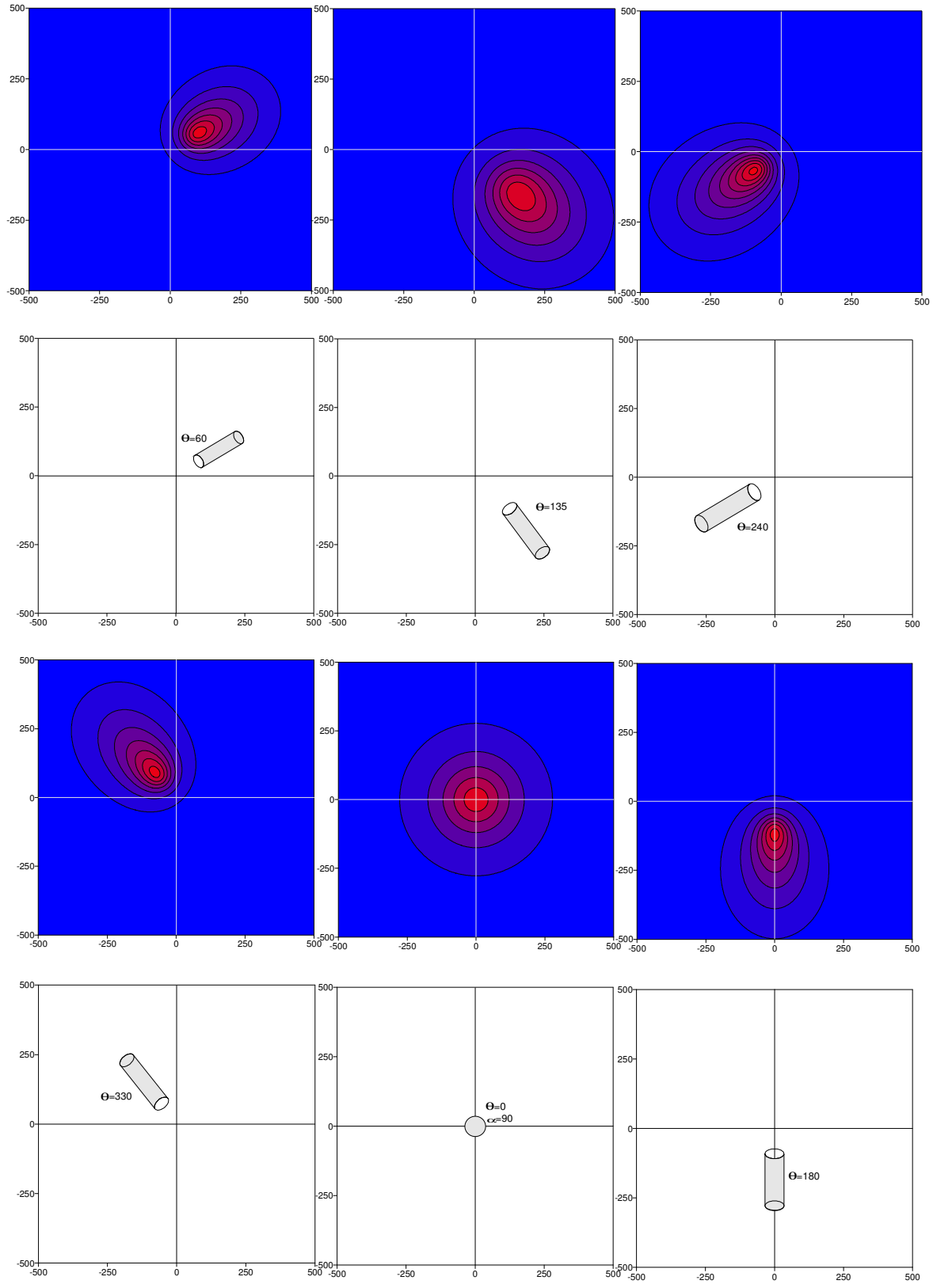

Figure 3.6: Contour maps of the gravity anomaly over a cylinder are shown on the upper panel and the position of cylinder is indicated on the lower panel.

Based on the new formula, we performed a series of forward modeling by varying the density, depth, dip extent, dip angle, strike angle, and radius of cylinder. These parameters are cited in the Table 3.1.

Table 3.1: Initial parameters of the cylinder

Depth (H) **(m)**	**Dip Extent** (L) **(m)**	**Radius** ($r_{cylinder}$)**(m)**	**Dip angle** (α) (^{0})	**Strike angle** (θ) (^{0})
20	100	10	0	0, 30, 60, 90
50	200	20	15	
100	300	30	30	120, 150, 180
150	400	40	45	
200	500	50	60	210, 240, 270
300			75	
			90	300, 330

We used 34 models (shown in Table 3.2) to develop a regression equation that gives the linear relationship between the maximum gravity anomaly and cylinder parameters, as described by the following equation. This formula could be useful, for example, to make a quick interpretation of the gravity anomaly over a kimberlite in the field.

$$y_{\max i} = -0.01684592 \times H - 0.00008811848 \times L + 0.003451422 \times \alpha - 0.00140625 \times \theta$$

$$+ 0.08508292 \times r_{cylinder} + 2.48574 \times \rho - 1.060923 \qquad (\rho \neq 0) \qquad (3\text{-}16)$$

Table 3.2: Parameters of the 34 models and corresponding maximum values of gravity anomaly

NO.	Depth (m)	Dip Extent (m)	Dip angle (^{0})	Strike angle (^{0})	Radius (m)	Density g/cm^3	Maximum (g.u)
1	100	500	45	300	50	0.2	1.061996
2	50	300	45	330	20	1	1.140039
3	150	500	75	270	50	0.6	1.693291
4	50	200	30	270	20	0.3	1.039530
5	100	300	60	330	30	0.4	0.514741
6	20	200	45	60	20	0.22	1.015856
7	50	500	60	30	50	0.55	4.842146
8	100	400	30	60	40	1	3.398846
9	50	400	45	60	30	0.2	0.814438
10	100	500	60	90	50	0.3	1.599207
11	200	400	75	60	40	0.5	0.572983
12	20	100	60	60	10	0.66	0.635366
13	50	200	30	120	20	0.48	0.815723
14	100	300	45	150	50	0.85	2.570188
15	100	400	60	90	40	0.25	0.820607
16	50	300	60	120	40	0.7	4.435195
17	100	500	75	120	50	0.3	1.343621
18	200	500	75	120	40	0.42	0.515883
19	20	100	45	120	10	0.34	0.360961
20	150	400	60	210	40	0.5	0.737628
21	200	300	75	210	40	0.3	0.294363
22	50	300	60	270	40	0.25	1.751224
23	100	300	30	270	20	0.66	1.081782
24	100	200	45	240	30	0.4	0.603792
25	50	500	60	240	50	0.5	5.240250
26	100	200	45	270	30	0.9	1.845415
27	50	300	30	120	20	0.34	0.624328
28	200	400	75	60	40	0.6	0.687579
29	100	400	30	60	40	0.2	0.679769
30	50	200	30	120	20	0.39	0.662775
31	100	500	75	120	50	0.6	2.687242
32	150	400	60	210	40	0.38	0.560597
33	100	400	45	240	30	0.3	0.550219
34	50	300	45	330	20	0.84	0.957632

3.2.2 Gravity inverse problem

We select 8 attributes from the gravity anomaly representing variations of anomaly shape due to the variation caused by depth, dip extent, dip angle, strike angle, radius of cylinder and density. The attributes were selected by considering previous studies (Zhang and Pan, 2000) and (Claprood et al., 2008) and are shown in Table 3.3.

Table 3.3: Attributes computed from the gravity anomaly

NO.	**symbol**	**Attribute**
1	α_1	$\log(\lvert y_{ex} \rvert)$
2	α_2	$\log(\lvert x_{ex} - x_1 \rvert)$
3	α_3	$(y_{ex} - y_1)/(x_{ex} - x_1)$
4	α_4	$\log(\lvert x_2 - x_{ex} \rvert)$
5	α_5	$(y_{ex} - y_2)/(x_{ex} - x_2)$
6	α_6	$\log(\lvert x_2 - x_1 \rvert)$
7	α_7	$\log(\lvert x_{ex} - x_3 \rvert)$
8	α_8	$\log(\lvert x_4 - x_{ex} \rvert)$

Note: y_{ex} is the extremum value of the gravity anomaly ($y_{\max i}$ or $y_{\min i}$) the values of gravity anomaly y_1 , y_2 , y_3 , y_4 and y_{ex} are corresponding coordinate x_1 , x_2 , x_3 , x_4 and x_{ex} , respectively. $y_1 = y_2 = 0.5 y_{\max i}$, $y_3 = y_4 = 0.25 y_{\max i}$.

We used above anomaly attributes from 34 selected models to develop the regression system (Table 3.4). Ultimately we use this system to estimate the occurrence of cylinder models from the gravity anomaly.

Table 3.4: 8 attributes from the modelled gravity anomalies

NO.	α_1	α_2	α_3	α_4	α_5	α_6	α_7	α_8
1	1.0261229	2.3117539	0.0259023	2.1238516	-0.0399247	2.5289167	2.5658478	2.3502480
2	0.0569197	2.0211893	0.0054288	1.9190781	-0.0068677	2.2741578	2.2855573	2.1643529
3	0.8307916	2.3283796	0.0158994	2.2695129	-0.0182074	2.6009729	2.5774918	2.5078559
4	0.4561698	2.0413927	0.0519765	1.7708520	-0.0969053	2.2278867	2.2479733	1.9637878
5	0.7115885	2.1818436	0.0169323	2.1238516	-0.0193512	2.4548449	2.4183013	2.3598355
6	1.0068322	1.4623980	0.1751476	1.6812412	-0.1058183	1.8864907	1.6989700	1.9912261
7	0.9860679	1.8920946	0.0620788	1.9731279	-0.0515122	2.2355284	2.1643529	2.2787536
8	0.5313315	2.1731863	0.0114055	2.3541084	-0.0075196	2.5740313	2.3820170	2.5751878
9	0.9108582	1.8388491	0.0590173	2.0681859	-0.0348051	2.2695129	2.0791812	2.3560259
10	0.9820562	2.0934217	0.0386905	2.2430380	-0.0274150	2.4756712	2.3304138	2.5105450
11	0.7581414	2.3636120	0.0124022	2.3979400	-0.0114597	2.6821451	2.5888317	2.6294096
12	0.8030236	1.4149733	0.1221857	1.5563025	-0.0882452	1.7923917	1.6532125	1.8195439
13	0.9115428	1.8750613	0.0543815	2.0606978	-0.0354662	2.2787536	2.0827854	2.2741578
14	1.0463613	2.1760913	0.0171346	2.2405492	-0.0147712	2.5105450	2.4082400	2.4756712
15	0.5161955	2.0791812	0.0136768	2.2174839	-0.0099468	2.4548449	2.3096302	2.4683473
16	0.9479428	1.8195439	0.0671999	1.9590414	-0.0487384	2.1958997	2.0644580	2.2355284
17	0.9733749	2.1238516	0.0353585	2.1875207	-0.0305368	2.4578819	2.3765770	2.4548449
18	0.7125513	2.3802112	0.0107476	2.4216039	-0.0097705	2.7024305	2.6127839	2.6589648
19	0.5574600	1.4149733	0.0694155	1.6127839	-0.0440196	1.8260748	1.6434527	1.8692317
20	0.8678375	2.3424227	0.0167643	2.2922561	-0.0188170	2.6190933	2.5774918	2.5237465
21	0.4620717	2.3692159	0.0062898	2.3541084	-0.0065125	2.6627578	2.5910646	2.5751878
22	0.8454019	1.9637878	0.0380701	1.7923917	-0.0564911	2.1875207	2.2405492	2.0413927
23	1.0719372	2.2648178	0.0293963	2.0569049	-0.0474466	2.4742163	2.4623980	2.2504200
24	0.8834554	2.1613680	0.0208204	2.0791812	-0.0251580	2.4232459	2.3820170	2.2922561
25	1.0203820	2.0000000	0.0524025	1.8325089	-0.0770625	2.2253093	2.3096302	2.0934217
26	0.7432154	2.1461280	0.0197723	2.0293838	-0.0258703	2.3926970	2.3579348	2.2355284
27	0.7954130	1.8920946	0.0400210	2.1335389	-0.0229532	2.3304138	2.1038037	2.3747483
28	0.8373226	2.3654880	0.0148185	2.3979400	-0.0137516	2.6830470	2.5899496	2.6294096
29	1.0628105	2.1731863	0.0387788	2.3541084	-0.0255665	2.5740313	2.3838154	2.5751878
30	0.8213661	1.8692317	0.0447821	2.0492180	-0.0295882	2.2695129	2.0827854	2.2741578
31	1.0313669	2.1238516	0.0404097	2.1875207	-0.0348993	2.4578819	2.3765770	2.4548449
32	0.4476211	2.3424227	0.0063704	2.2922561	-0.0071505	2.6190933	2.5774918	2.5237465
33	0.7585167	2.2741578	0.0146335	2.1139434	-0.0211623	2.5024271	2.5185139	2.3384565
34	0.6801688	2.0170333	0.0230200	1.9190781	-0.0288443	2.2718416	2.2855573	2.1643529

Before the determination of the coefficients of the linear relationship, it is necessary to ensure that the independent variables do not correlate with each other. We use also the stepwise regression to determine the most significant attributes to the physical parameters of cylinder. Table 3.5 presents the criteria of four estimated coefficients for selecting the most significant attributes. The coefficient of total correlation r_3 expresses the linear relation between explanatory variables (parameters of model) and dependent variables (observations). The coefficient of total correlation r_3 is equal to 1.0 for a perfect linear relation and zero in the absence of linear relation. In the course of stepwise regression, we first analyse the values of q, s_1, u, and r_3, and then decide the most significant attributes.

Table 3.5: Using estimated coefficients for selecting the "best" regression equation

	q	s_1	u	r_3
ρ	43.80818	1.135111	43.37446	0.7053457
H	43.78061	1.134753	43.40204	0.7055699
L	51689.22	38.99066	432134.3	0.9450741
α	2286.392	8.200415	5926.108	0.8494682
θ	78568.14	48.07107	222058.3	0.8594486
R	1426.295	6.47687	3811.941	0.8530619

The following equations are the final equations of regression obtained to estimate the density, the depth, the dip extent, the dip angle, the strike angle and the radius of cylinder, respectively. Namely we obtain the system of regression for the gravity anomaly interpretation.

$$\rho = 2.889256 * \alpha_1 + 122.1366 * \alpha_2 + 112.6437 * \alpha_4 - 177.3349 * \alpha_6 - 35.04415 * \alpha_7 - 25.98408 * \alpha_8 + 77.181$$

$$H = \text{-}55.90585 * \alpha_1 + 2212.613 * \alpha_2 + 1655.03 * \alpha_4 - 857.7549 * \alpha_5 - 3250.931 * \alpha_6 - 464.0917 * \alpha_7 + 94.85623 * \alpha_8 + 671.3411$$

$$L = \text{-}6506.249 * \alpha_2 \text{ - } 5982.137 * \alpha_4 + 8508.451 * \alpha_6 + 2523.032 * \alpha_7 + 2042.171 * \alpha_8 - 4575.77$$

$$\alpha = 1043.717 * \alpha_2 + 739.3492 * \alpha_4 \text{ - } 214.7961 * \alpha_5 - 1996.947 * \alpha_6$$

$$-20.27874*\alpha_7+262.3575*\alpha_8+541.4631$$

$$\theta=-53.37571*\alpha_2+1462.129*\alpha_4-1078.221*\alpha_6+955.4258*\alpha_7$$
$$-1369.722*\alpha_8+788.5574$$

$$r_{cylinder}=-290.9525*\alpha_2-248.3274*\alpha_4+213.8204*\alpha_6+206.6426*\alpha_7$$
$$+167.5164*\alpha_8-221.8726 \qquad (3\text{-}17)$$

We used the above equations to predict the physical parameters (initial model parameters in the Table 3.2) using the gravitational attributes in Table 3.4; the predicted results are shown in the Table 3.6. By comparing the predicted results with the initial model parameters, it can be seen that the system of regression for the determination of the density, the depth, the dip extent, the strike angle and the radius of cylinder yields consistent results.

Table 3.6: Gravity prediction for random model

No.	d	d'	Cr(%)	H	H'	Cr(%)	L	L'	Cr(%)	α	α'	Cr(%)	θ	θ'	Cr(%)	R	R'	Cr(%)
1	2.0	2.28	85.91	100	89.07	89.07	500	468.7	93.74	45	47.6	94.26	300	276.1	92.02	50	42.8	85.52
2	1.0	0.76	75.70	50	63.74	72.51	300	329.7	90.08	45	51.5	85.63	330	253.7	76.88	20	24.6	76.91
3	2.4	2.87	80.23	150	134.52	89.68	500	453.5	90.70	75	65.2	86.91	270	205.7	76.19	50	46.0	91.93
4	3.3	4.16	74.09	50	43.22	86.44	200	186.9	93.45	30	22.9	76.16	270	324.6	79.78	20	14.3	71.45
5	4.0	3.56	89.08	100	111.76	88.24	300	331.0	89.66	60	61.0	98.34	330	288.8	87.51	30	35.8	80.55
6	2.2	2.26	97.10	20	18.41	92.07	200	256.1	71.91	45	54.3	79.37	60	50.5	84.09	20	23.2	84.23
7	1.1	1.29	82.91	50	56.59	86.81	500	445.5	89.10	60	75.9	73.51	30	38.8	70.80	50	44.6	89.23
8	1.0	1.26	73.80	100	123.41	76.59	400	372.2	93.06	30	38.9	70.38	60	67.8	87.09	40	35.2	88.09
9	2.0	1.83	91.27	50	42.36	84.71	400	455.3	86.17	45	41.2	91.44	60	46.7	77.88	30	39.1	69.63
10	1.8	1.44	80.08	100	92.55	92.55	500	456.5	91.31	60	58.3	97.16	90	74.9	83.22	50	43.5	87.01
11	5.0	4.48	89.67	200	165.69	82.84	400	423.5	94.13	75	65.0	86.70	60	68.4	85.96	40	43.9	90.29
12	6.6	5.56	84.25	20	18.94	94.71	100	85.5	85.45	60	52.4	87.39	60	83.2	61.32	10	9.6	96.42
13	4.8	4.77	99.35	50	51.14	97.73	200	185.0	92.53	30	33.5	88.19	120	119.5	99.55	20	19.4	97.20
14	1.7	1.47	86.43	100	122.85	77.15	300	355.4	81.52	45	59.7	67.43	150	151.4	99.09	50	37.7	75.53
15	1.0	1.00	99.57	100	103.15	96.85	400	386.3	96.56	60	51.7	86.21	90	98.7	90.34	40	38.2	95.44
16	1.4	1.58	87.04	50	43.60	87.19	300	324.3	91.90	60	59.0	98.30	120	98.5	82.11	40	32.9	82.16
17	2.1	2.46	82.69	100	102.28	97.72	500	442.0	88.41	75	69.7	92.87	120	131.7	90.27	50	44.8	89.68
18	4.2	3.84	91.44	200	168.42	84.21	500	467.3	93.46	75	66.2	88.32	120	142.7	81.11	40	47.4	81.46
19	3.4	3.29	96.80	20	23.93	80.36	100	71.0	71.01	45	30.7	68.14	120	112.1	93.41	10	9.1	91.25
20	5.0	3.63	72.65	150	144.29	96.19	400	412.7	96.83	60	64.8	92.05	210	196.9	93.77	40	42.8	93.08
21	3.0	3.16	94.54	200	174.32	87.16	300	379.2	73.61	75	61.9	82.46	210	181.4	86.36	40	40.4	99.07
22	1.0	1.09	91.00	50	36.43	72.85	300	359.3	80.24	60	50.2	83.69	270	290.4	92.46	40	34.4	85.89
23	6.6	4.95	75.01	100	96.80	96.80	300	244.3	81.42	30	35.9	80.49	270	277.6	97.20	20	23.2	83.78
24	4.0	4.86	78.45	100	106.79	93.21	200	233.0	83.48	45	53.9	80.10	240	236.5	98.55	30	27.3	91.03
25	1.0	0.86	86.33	50	40.83	81.67	500	485.7	97.15	60	58.9	98.13	240	301.1	74.55	50	44.9	89.85
26	2.7	3.02	88.23	100	98.47	98.47	200	193.6	96.78	45	48.0	93.35	270	252.2	93.39	30	23.1	77.00
27	3.4	3.21	94.34	50	36.98	73.96	300	336.5	87.84	30	25.3	84.30	120	111.7	93.05	20	28.6	56.82
28	6.0	5.74	95.71	200	163.92	81.96	400	421.7	94.56	75	65.7	87.53	60	58.4	97.37	40	43.8	90.60
29	3.4	3.93	84.28	100	108.35	91.65	400	376.8	94.19	30	42.7	57.58	60	79.5	67.56	40	35.6	89.02
30	3.9	4.14	93.79	50	49.28	98.56	200	213.0	93.48	30	36.2	79.46	120	112.9	94.13	20	22.0	89.94
31	2.4	3.03	73.70	100	102.78	97.22	500	442.0	88.41	75	70.6	94.12	120	131.7	90.27	50	44.8	89.68
32	1.9	2.42	72.73	150	157.77	94.82	400	412.7	96.83	60	62.3	96.22	210	196.9	93.77	40	42.8	93.08
33	3.0	3.14	95.26	100	96.33	96.33	400	403.8	99.08	45	47.8	93.89	240	243.1	98.72	30	32.7	90.88
34	4.2	3.46	82.40	50	56.08	87.83	300	337.1	87.64	45	56.5	74.50	330	256.4	77.70	20	25.3	73.34

Note: d : Density, H : Depth to the top of the cylinder, L : Length of the cylinder, α : Dip angle, θ :Strike angle, R : Radius of cylinder, $d^{'}$: Predicted d , $H^{'}$: Predicted H , $L^{'}$: Predicted L , $\alpha^{'}$: Predicted α , $\theta^{'}$: Predicted θ , $R^{'}$: Predicted R , Cr : Credibility.

3.2.3 Magnetic forward modeling

Parallel to the development of gravity method, we used Equation (3-8) to Equation (3-15) to calculate magnetic anomalies of a cylinder by varying its parameters. From the Figure 3.7 and the Figure 3.8, we show that the new magnetic formula can calculate the magnetic anomaly of a cylinder in arbitrary spatial position.

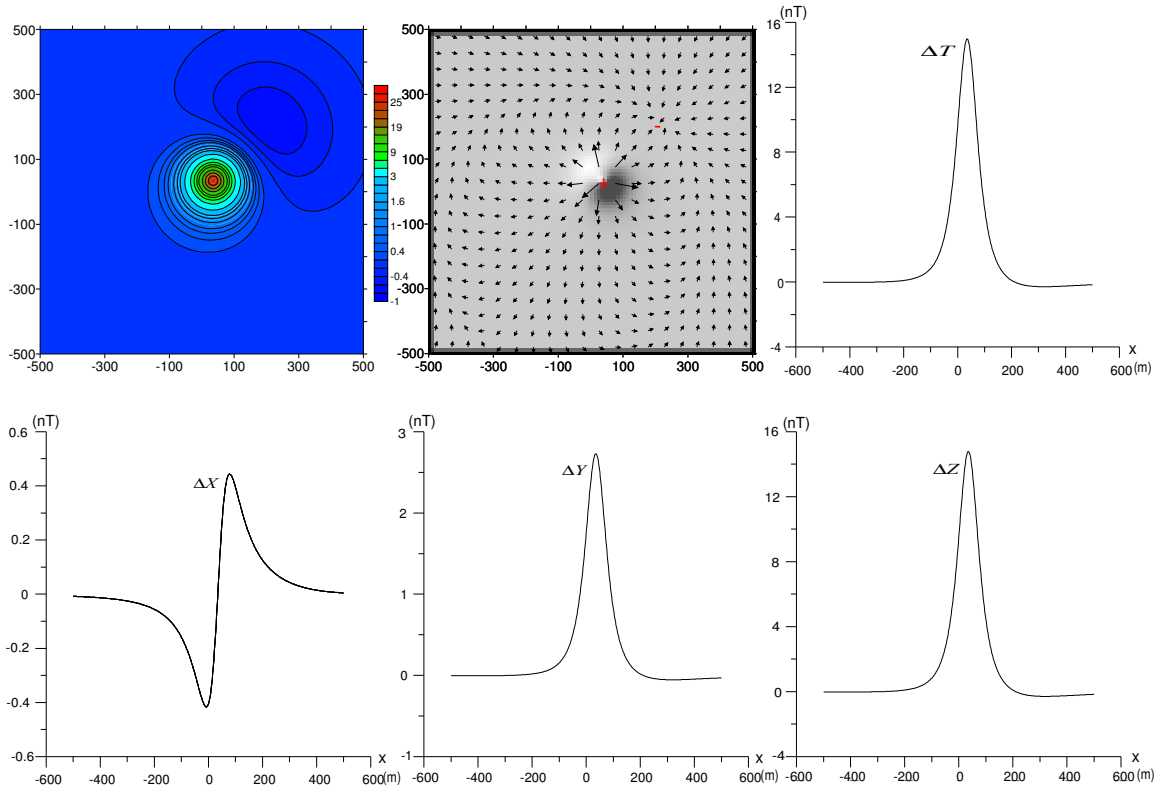

Figure 3.7: Magnetic anomaly map is on the upper left panel, vector map in the middle and anomaly profiles over a cylinder are on the right and lower panels

Note: The top depth of cylinder is 50m, dip extent 300m, dip angle 45^{0}, radius of cylinder 20m and magnetic susceptibility is 1.0, strike 45^{0}. The magnetic field strength is 57000nT, the magnetic inclination is 75^{0} and the magnetic declination is 13^{0}.

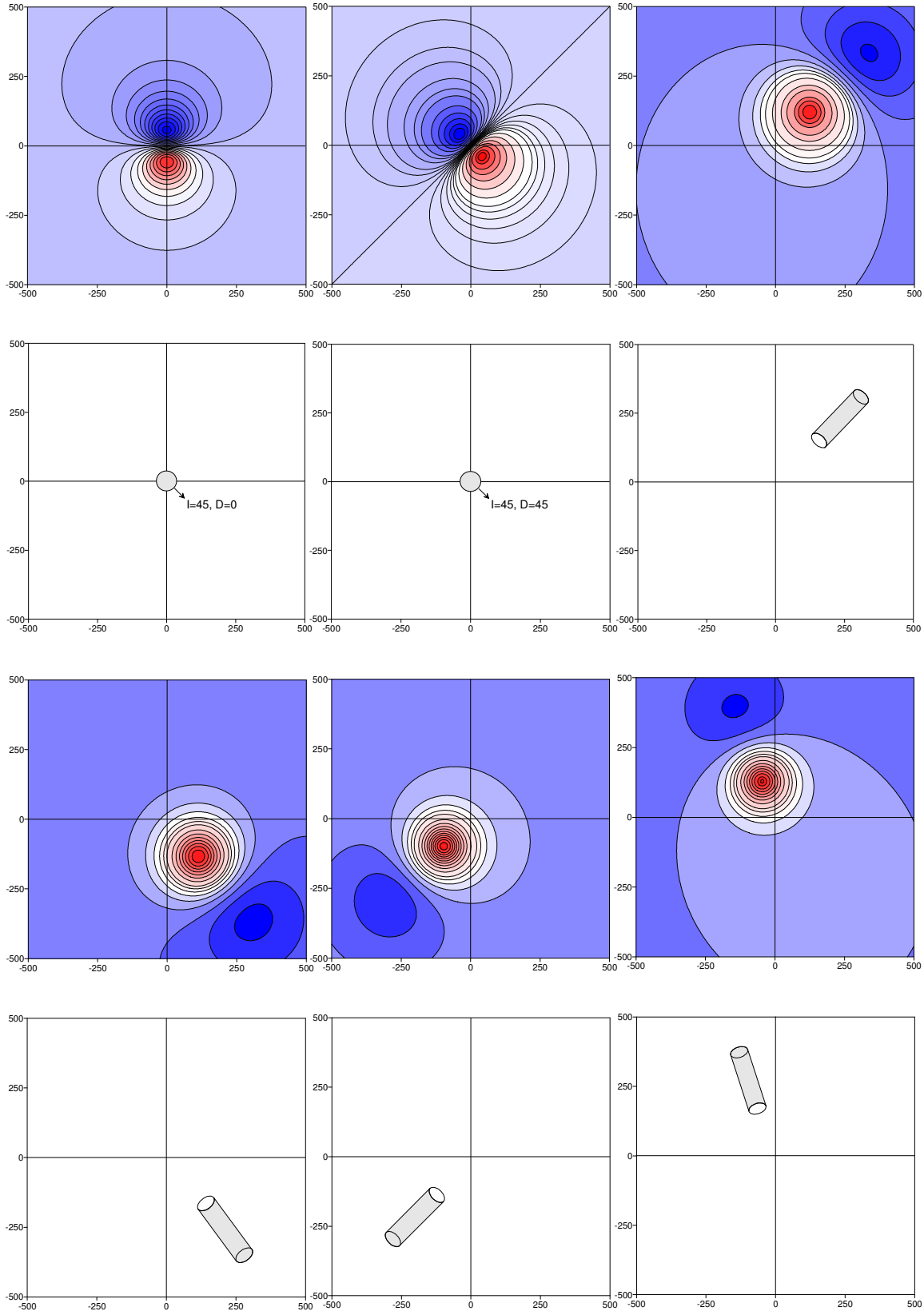
I=45, D=0
I=45, D=45

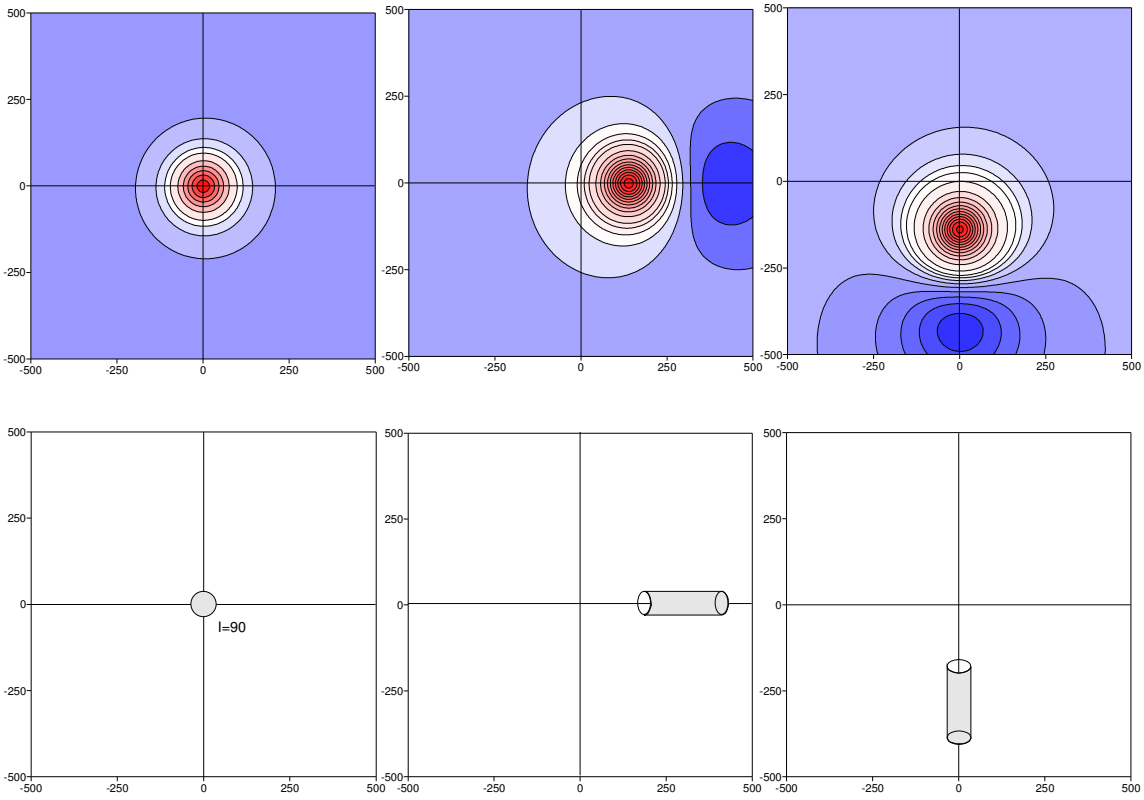

Figure 3.8: Contour maps of the magnetic anomaly for a cylinder at arbitrary spatial position with different modeling parameters.

We performed a series of forward modeling by varying the susceptibility, the depth, the dip extent, the dip angle, the strike angle, and the radius of the cylinder. These parameters are listed in Table 3.7. Corresponding to the forward modeling of gravity method, the 34 models and the peak values of magnetic anomaly are shown in the Table 3.8.

Table 3.7: Initial parameters of the cylinder

Parameters	**Range of values**
Depth H (m)	50, 100, 150, 200, 300, 400
Dip extent L (m)	100, 200, 300, 400, 500
Dip angle α (^{0})	0, 30, 45, 60, 90
Strike angle θ (^{0})	30, 60, 90, 120, 150, 180, 210, 240, 270,300, 330, 360
Radius $r_{cylinder}$ (m)	10, 20, 30, 40, 50
Susceptibility k ($10^{-5} SI$)	Random
Magnetic inclination I (^{0})	Random($-90 \le I \le 90$), Abitibi region: $I = 75$
Magnetic declination D (^{0})	Random($-180 \le D \le 180$), Abitibi region: $D = 13$
Field strength M (nT)	Random, Abitibi region: $M = 57500$

Table 3.8: Parameters of 34 models and corresponding maximum and minimum values of magnetic anomaly

NO.	Depth (m)	Dip extent (m)	Dip angle (^{0})	Strike angle (^{0})	Radius (m)	Susceptibility ($10^{-5} SI$)	$y_{\max i}$ (nT)	$y_{\min i}$ (nT)
1	100	500	15	300	50	6.7	30.76587	-4.206106
2	50	300	45	330	20	3	35.821859	-0.531507
3	150	500	75	270	50	1.2	21.284654	-0.334562
4	150	200	30	270	20	4	9.64004	-2.147682
5	100	300	60	330	30	3.6	37.439225	-0.687285
6	20	100	45	60	20	1	120.722606	-3.659948
7	200	500	60	30	50	2	14.103539	-0.289361
8	100	400	30	60	40	2.7	31.435155	-2.338184
9	50	400	45	60	30	1.7	75.30358	-1.234651
10	100	500	15	90	50	3	124.507083	-22.961653
11	200	400	75	60	40	10.6	62.325844	-1.286156
12	20	100	60	60	10	3.7	136.976909	-2.300527
13	50	200	60	120	20	5	112.339811	-2.403625
14	100	300	45	150	50	7	108.718271	-2.928806
15	100	400	30	90	40	4.4	114.960335	-10.962256
16	50	300	60	120	40	2.4	220.278269	-2.977227
17	100	500	15	90	50	6.2	257.314639	-47.454084
18	200	500	75	120	40	15	89.523073	-1.597258
19	20	100	45	120	10	2	56.383249	-1.708739
20	150	400	60	210	40	11.4	86.212349	-1.725094
21	200	300	75	210	40	5.4	25.663442	-0.550096
22	50	300	30	270	40	0.4	42.526671	-2.431203
23	100	300	15	270	20	13.1	84.317184	-25.079531
24	100	200	45	240	30	12	48.694686	-3.368604
25	50	500	60	240	50	0.8	116.196326	-0.796287
26	100	200	30	270	30	8.4	113.756757	-20.427172
27	50	300	30	120	20	9.4	100.170037	-4.771408
28	200	400	75	60	40	12.8	75.261396	-1.553094
29	100	400	30	60	40	6.8	79.170021	-5.888761
30	50	200	30	120	20	4.1	42.413886	-3.15316
31	100	500	75	120	50	3	118.54366	-1.137287
32	150	400	60	210	40	11	83.187355	-1.664564
33	100	400	45	240	30	7	70.110228	-2.746297
34	50	300	45	330	20	3.6	42.986231	-0.637808

Based on these 34 models, we developed the regression system to find the predicted magnetic anomaly. The multiple linear regression for the prediction of the maximum value $y_{\max i}$ and the minimum value $y_{\min i}$ of magnetic anomaly of cylinder is described by the following equations.

They can be used in the field to estimate quickly the magnetic anomaly for a cylindrical body.

$$y_{\max i} = -0.8495511 \times H - 0.05466737 \times L + 0.2417084 \times \alpha - 0.2057476 \times \theta + 2.767968 \times r + 6.613053 \times \mu + 76.01499 \quad (3\text{-}18)$$

$$y_{\min i} = 0.004370969 \times H - 0.001963786 \times L + 0.3242243 \times \alpha + 0.01333939 \times \theta - 0.1613043 \times r - 0.5365263 \times k - 14.07616 \quad (3\text{-}19)$$

3.2.4 Magnetic inverse problem

13 attributes were selected from the magnetic anomaly representing the variation of different occurrences of a cylinder (Table 3.9). And then based on the 34 models we developed the regression system in order to estimate the parameters of the cylinder from these attributes (Table 3.10).

Table 3.9: Definition of attributes of the magnetic anomaly

NO.	symbol	Attribute
1	β_1	$\log(\lvert y_{\max i} \rvert)$
2	β_2	$\log(\lvert y_{\min i} \rvert)$
3	β_3	$(y_{\max i} - y_{\min i})/(x_{\max i} - x_{\min i})$
4	β_4	$\log(\lvert x_{\max i} - x_1 \rvert)$
5	β_5	$(y_{\max i} - y_1)/(x_{\max i} - x_1)$
6	β_6	$\log(\lvert x_2 - x_{\max i} \rvert)$
7	β_7	$(y_{\max i} - y_2)/(x_{\max i} - x_2)$
8	β_8	$\log(\lvert y_{\max i} - y_{\min i} \rvert)$
9	β_9	$\log(\lvert x_{\max i} - x_{\min i} \rvert)$
10	β_{10}	$\log(\lvert x_0 - x_{\max i} \rvert)$
11	β_{11}	$(y_{\max i} - y_0)/(x_{\max i} - x_0)$
12	β_{12}	$\log(\lvert x_{\min i} - x_0 \rvert)$
13	β_{13}	$(y_0 - y_{\min i})/(x_0 - x_{\min i})$

Note: the values of magnetic anomaly y_0 y_1 , y_2 , $y_{\min i}$ and $y_{\max i}$ are corresponding coordinates x_0 $x_1, x_2, x_{\min i}$ and $x_{\max i}$, respectively. $y_0 = 0$, $y_1 = y_2 = 0.5 y_{\max i}$.

Table 3.10: Attributes from the modelled magnetic anomalies.

No.	β_1	β_2	β_3	β_4	β_5	β_6	β_7	β_8	β_9	β_{10}	β_{11}	β_{12}	β_{13}
1	1.488	0.624	0.065	2.158	0.107	2.190	0.049	1.544	2.731	2.500	0.097	2.346	0.019
2	1.554	-0.274	0.119	1.699	0.358	1.690	0.092	1.561	2.486	2.290	0.184	2.045	0.005
3	1.328	-0.476	0.036	2.037	0.098	2.045	0.027	1.335	2.780	2.599	0.054	2.312	0.002
4	0.984	0.332	0.045	1.934	0.056	2.025	0.031	1.071	2.422	2.196	0.061	2.029	0.020
5	1.573	-0.163	0.094	1.903	0.234	1.908	0.070	1.581	2.606	2.430	0.139	2.130	0.005
6	2.082	0.563	-1.323	1.255	3.353	1.204	-1.059	2.095	1.973	1.756	-2.118	1.568	-0.099
7	1.149	-0.539	-0.019	2.204	0.044	2.199	-0.014	1.158	2.872	2.699	-0.028	2.387	-0.001
8	1.497	0.369	-0.082	1.996	0.159	1.968	-0.064	1.529	2.613	2.389	-0.128	2.217	-0.014
9	1.877	0.092	-0.228	1.633	0.876	1.623	-0.195	1.884	2.526	2.286	-0.390	2.155	-0.009
10	2.095	1.361	-0.303	1.886	0.808	1.869	-0.265	2.169	2.687	2.371	-0.530	2.400	-0.091
11	1.795	0.109	-0.099	2.158	0.216	2.146	-0.072	1.804	2.809	2.638	-0.143	2.320	-0.006
12	2.137	0.362	-1.421	1.176	4.566	1.212	-1.123	2.144	1.991	1.785	-2.246	1.568	-0.062
13	2.051	0.381	-0.541	1.574	1.498	1.591	-0.416	2.060	2.326	2.130	-0.832	1.886	-0.031
14	2.036	0.467	-0.268	1.987	0.560	1.964	-0.196	2.048	2.619	2.442	-0.392	2.143	-0.021
15	2.061	1.040	-0.330	1.869	0.777	1.869	-0.275	2.100	2.582	2.320	-0.550	2.238	-0.063
16	2.343	0.474	-0.815	1.602	2.753	1.580	-0.652	2.349	2.438	2.228	-1.303	2.021	-0.028
17	2.410	1.676	-0.627	1.886	1.671	1.869	-0.547	2.484	2.687	2.371	-1.095	2.400	-0.189
18	1.952	0.203	-0.128	2.164	0.307	2.155	-0.093	1.960	2.854	2.680	-0.187	2.371	-0.007
19	1.751	0.233	-0.618	1.243	1.611	1.204	-0.495	1.764	1.973	1.756	-0.989	1.568	-0.046
20	1.936	0.237	0.154	2.072	0.365	2.079	0.113	1.944	2.756	2.583	0.225	2.272	0.009
21	1.409	-0.260	0.043	2.149	0.091	2.158	0.031	1.419	2.781	2.616	0.062	2.281	0.003
22	1.629	0.386	0.164	1.580	0.560	1.568	0.153	1.653	2.438	2.143	0.306	2.130	0.018
23	1.926	1.399	0.365	1.857	0.586	1.881	0.272	2.039	2.477	2.190	0.544	2.161	0.173
24	1.687	0.527	0.193	1.869	0.329	1.903	0.141	1.717	2.431	2.238	0.281	1.987	0.035
25	2.065	-0.099	0.297	1.602	1.452	1.591	0.253	2.068	2.595	2.362	0.505	2.215	0.005
26	2.056	1.310	0.599	1.813	0.875	1.863	0.434	2.128	2.350	2.117	0.868	1.968	0.220
27	2.001	0.679	-0.375	1.690	1.022	1.699	-0.311	2.021	2.447	2.207	-0.622	2.076	-0.040
28	1.877	0.191	-0.119	2.164	0.258	2.146	-0.087	1.885	2.809	2.638	-0.173	2.320	-0.007
29	1.899	0.770	-0.207	1.996	0.400	1.964	-0.162	1.930	2.613	2.389	-0.323	2.217	-0.036
30	1.628	0.499	-0.221	1.690	0.433	1.681	-0.172	1.659	2.314	2.090	-0.345	1.919	-0.038
31	2.074	0.056	-0.231	1.881	0.780	1.875	-0.177	2.078	2.714	2.525	-0.354	2.262	-0.006
32	1.920	0.221	0.149	2.072	0.352	2.083	0.109	1.929	2.756	2.583	0.217	2.272	0.009
33	1.846	0.439	0.179	1.903	0.438	1.919	0.141	1.862	2.609	2.396	0.282	2.196	0.017
34	1.633	-0.195	0.143	1.699	0.430	1.681	0.110	1.640	2.486	2.290	0.220	2.045	0.006

Table 3.11: Using estimated coefficients for selecting the "best" regression equation

	q	s_1	u	r_3
H	7811.367	15.15738	92885.69	0.9608277
L	22655.21	25.81336	499697.7	0.9780739
α	1082.232	5.64184	11411.89	0.9557095
θ	101186.9	54.55351	203224.9	0.8170671
r	1193.874	5.925701	4044.362	0.8786835
μ	155.8594	2.141051	387.01	0.8443323

Through the stepwise regression and estimated coefficients (Table 3.11), we selected the most significant attributes. The final equations of regression obtained to estimate the depth, the dip extent, the dip angle, the strike angle, the radius of cylinder and the susceptibility, respectively are given. Namely, we obtain the system of regression for the magnetic anomaly interpretation.

$$H = 17.0251 * \beta_1 - 363.3289 * \beta_2 - 26.56787 * \beta_3 + 609.533 * \beta_4 + 578.9358 * \beta_6 + 344.1536 * \beta_8 + 7802.103 * \beta_9 - 6364.752 * \beta_{10} - 2471.2 * \beta_{12} - 2374.77$$

$$L = -1249.16 * \beta_1 + 432.4964 * \beta_2 - 399.2165 * \beta_4 + 28.97969 * \beta_5 - 1164.122 * \beta_6 + 767.3705 * \beta_8 - 13744.46 * \beta_9 + 10822.2 * \beta_{10} + 5145.374 * \beta_{12} + 2682.55$$

$$\alpha = 58.66501 * \beta_1 - 132.7803 * \beta_2 - 6.843981 * \beta_3 + 78.43094 * \beta_4 + 223.3361 * \beta_6 + 80.26672 * \beta_8 + 2061.873 * \beta_9 - 1680.958 * \beta_{10} - 675.9877 * \beta_{12} - 603.0068$$

$$\theta = -1207.091 * \beta_1 + 579.23 * \beta_2 + 221.94 * \beta_3 - 1965.463 * \beta_4 - 23.28669 * \beta_5 + 552.4362 * \beta_8 - 1629.684 * \beta_9 + 4353.063 * \beta_{10} - 947.8782 * \beta_{12} + 767.0967$$

$$r_{cylinder} = 158.0792 * \beta_1 - 41.57005 * \beta_2 + 165.7851 * \beta_4 + 5.707602 * \beta_5$$

$$
\begin{aligned}
&-17.38298*\beta_6-117.0736*\beta_8+242.4679*\beta_9\\
&-400.1155*\beta_{10}+74.04848*\beta_{12}-140.8824\\
k=&\,19.45921*\beta_1-13.97551*\beta_2+5.205135*\beta_4-1.820279*\beta_5\\
&+53.28494*\beta_6+5.480995*\beta_8+349.4315*\beta_9\\
&-279.7742*\beta_{10}-128.7827*\beta_{12}-103.3701
\end{aligned}
\tag{3-20}
$$

The predicted results are shown in Table 3.12. By comparing the predicted results and the initial model parameters, we can see that the system of regression for the determination of the magnetic susceptibility, the depth, the dip extent, the strike angle and the radius of cylinder yields reliable results.

Table 3.12: Prediction of cylinder's parameters from magnetic anomaly

No.	H	H'	Cr(%)	L	L'	Cr(%)	α	α'	Cr(%)	θ	θ'	Cr(%)	R	R'	Cr(%)	K	K'	Cr(%)
1	100	124.74	75.26	500	461.62	92.32	15	15.93	93.8	300	277.72	92.57	50	43.75	87.51	6.7	5.78	86.33
2	50	63.37	73.25	300	326.77	91.08	45	52.97	82.29	330	251.98	76.36	20	25.72	71.41	3	2.40	80.32
3	150	138.27	92.18	500	466.10	93.22	75	61.53	82.04	270	218.76	81.02	50	40.66	81.31	1.2	1.34	88.55
4	150	142.82	95.21	200	213.44	93.28	30	30.37	98.75	270	258.66	95.8	20	20.09	99.55	4	5.38	65.57
5	100	123.76	76.24	300	318.81	93.73	60	62.32	96.13	330	232.17	70.36	30	30.67	97.76	3.6	3.98	89.41
6	20	17.76	88.78	100	79.37	79.37	45	45.58	98.72	60	69.77	83.72	20	17.85	89.22	1	1.10	89.51
7	200	182.25	91.12	500	489.10	97.82	60	63.05	94.92	30	36.25	79.18	50	48.19	96.38	2	2.28	86.07
8	100	99.90	99.9	400	415.43	96.14	30	27.42	91.39	60	53.63	89.39	40	40.85	97.88	2.7	2.97	90.05
9	50	51.22	97.57	400	408.54	97.87	45	48.44	92.35	60	52.93	88.22	30	36.70	77.67	1.7	1.37	80.78
10	100	92.96	92.96	500	493.47	98.69	15	12.46	83.05	90	98.85	90.17	50	45.14	90.28	3	3.61	79.61
11	200	185.8	92.9	400	403.90	99.03	75	69.78	93.04	60	79.97	66.72	40	46.05	84.88	11	9.64	90.99
12	20	21.60	91.99	100	88.70	88.7	60	63.58	94.04	60	71.28	81.2	10	12.40	75.95	3.7	2.65	71.72
13	50	54.92	90.16	200	216.61	91.7	60	54.91	91.51	120	95.81	79.84	20	19.51	97.54	5	6.68	66.41
14	100	122.99	77.01	300	310.78	96.41	45	50.99	86.7	150	125.84	83.89	50	36.76	73.53	7	7.79	88.77
15	100	83.23	83.23	400	405.78	98.56	30	25.62	85.4	90	77.59	86.21	40	41.05	97.38	4.4	4.54	96.88
16	50	58.94	82.12	300	369.14	76.95	60	59.16	98.6	120	112.29	93.58	40	37.99	94.99	2.4	2.21	91.97
17	100	100.88	99.12	500	502.92	99.42	15	16.61	89.25	90	106.84	81.28	50	49.88	99.76	6.2	6.50	95.18
18	200	175.21	87.6	500	456.36	91.27	75	69.4	92.53	120	91.44	76.2	40	47.97	80.09	15	9.99	66.65
19	20	17.67	88.34	100	89.98	89.98	45	37.78	83.95	120	86.21	71.84	10	6.07	60.65	2	2.09	95.51
20	150	149.76	99.84	400	389.43	97.36	60	65.23	91.28	210	195.61	93.15	40	39.92	99.81	11	10.25	89.94
21	200	201.31	99.34	300	353.66	82.11	75	73.2	97.6	210	175.57	83.6	40	42.47	93.84	5.4	6.64	77.13
22	50	63.40	73.2	300	291.17	97.06	30	30.93	96.91	270	192.7	71.37	40	36.25	90.61	0.4	0.57	57.06
23	100	107.29	92.71	300	311.2	96.27	15	15.67	95.57	270	245.08	90.77	20	26.53	67.35	13	8.99	68.6
24	100	104.51	95.49	200	193.31	96.66	45	42.12	93.6	240	241.95	99.19	30	22.84	76.14	12	9.63	80.22
25	50	43.04	86.07	500	478.98	95.8	60	60.66	98.9	240	194.24	80.93	50	42.16	84.33	0.8	0.97	78.25
26	100	80.77	80.77	200	185.40	92.7	30	24.86	82.85	270	289.61	92.74	30	22.19	73.97	8.4	10.51	74.93
27	50	50.01	99.99	300	332.01	89.33	30	34.14	86.19	120	83.55	69.63	20	21.16	94.23	9.4	7.03	74.77
28	200	189.82	94.91	400	398.67	99.67	75	70.9	94.53	60	76.51	72.49	40	47.23	81.92	13	10.50	82.02
29	100	99.64	99.64	400	408.11	97.97	30	29.69	98.98	60	50.00	83.33	40	42.08	94.8	6.8	6.68	98.21
30	50	60.88	78.25	200	207.55	96.23	30	29.53	98.42	120	123.49	97.1	20	21.87	90.65	4.1	4.70	85.17
31	100	108.72	91.28	500	460.37	92.07	75	68.62	91.49	120	101.62	84.68	50	40.38	80.76	3	3.54	81.9
32	150	152.02	98.65	400	385.63	96.41	60	65.98	90.04	210	195.87	93.27	40	39.80	99.49	11	10.30	93.62
33	100	95.44	95.44	400	392.84	98.21	45	39.28	87.3	240	219.56	91.48	30	35.59	81.37	7	6.30	90.04
34	50	57.39	85.22	300	335.36	88.21	45	51.3	86.01	330	249.61	75.64	20	26.24	68.81	3.6	2.27	63.07

H : Top depth of the cylinder. L : Length of the cylinder. α : Dip angle. θ : Strike angle. R : Radius of cylinder. k : Magnetic susceptibility. $H^{'}$: Predicted H . $L^{'}$: Predicted L . $\alpha^{'}$: Predicted α . $\theta^{'}$: Predicted θ . $R^{'}$: Predicted R . $k^{'}$: Predicted k . Cr : Credibility.

3.3 Joint interpretations

3.3.1 Synthetic data tests

We developed individually a linear regression system for the gravity method (Equation 3-17) and for the magnetic method (Equation 3-20). In this section we present the utility of applying two systems of regression to constrain a same target in order to reduce the ambiguity. Ten arbitrary models are chosen (shown in Table 3.13). For the magnetic calculations, we considered that inclination of the magnetic inducing field is 75^0; its magnetic declination is 13^0, and the field strength is 57500nT.

Table3.13: Gravity and magnetic prediction estimates for the same target

	H (m)	L (m)	α (^{0})	θ (^{0})	$r_{cylinder}$ (m)	d (g/cm^3)	k (10^{-5}SI)
Model I							
True value	100	200	45	240	30	4	12
$Gra-p.v$	106.7850	233.0374	53.9548	236.5164	27.3104	4.8620	
$Gra-Cr$	93.21%	83.48%	80.10%	98.55%	91.03%	78.45%	
$Mag-p.v$	104.5064	193.3134	42.1179	241.9539	22.8421		9.6263
$Mag-Cr$	95.49%	96.66%	93.60%	99.19%	76.14%		80.22%
Model II							
True value	100	400	30	60	40	1	2.7
$Gra-p.v$	123.4142	372.2379	38.8871	67.7468	35.2366	1.2620	
$Gra-Cr$	76.59%	93.06%	70.38%	87.09%	88.09%	73.80%	
$Mag-p.v$	99.8957	415.4300	27.4183	53.6325	40.8477		2.9687
$Mag-Cr$	99.90%	96.14%	91.39%	89.39%	97.88%		90.05%
Model III							
True value	50	400	45	60	30	2	1.7
$Gra-p.v$	42.3558	455.3370	41.1474	46.7285	39.1110	1.8254	
$Gra-Cr$	84.71%	86.17%	91.44%	77.88%	69.63%	91.27%	
$Mag-p.v$	51.2153	408.5390	48.4420	52.9330	36.6993		1.3732
$Mag-Cr$	97.57%	97.87%	92.35%	88.22%	77.67%		80.78%
Model IV							
True value	200	400	75	60	40	5	10.6
$Gra-p.v$	165.6854	423.4855	65.0246	68.4269	43.8839	4.4837	

Gra – Cr	82.84%	94.13%	86.70%	85.96%	90.29%	89.67%	
Mag – p.v	185.7987	403.8961	69.7818	79.9693	46.0481		9.6447
Mag – Cr	92.90%	99.03%	93.04%	66.72%	84.88%		90.99%
Model V							
True value	100	300	60	330	30	4	3.6
Gra – p.v	111.7586	331.0072	60.9978	288.7686	35.8351	3.5633	
Gra – Cr	88.24%	89.66%	98.34%	87.51%	80.55%	89.08%	
Mag – p.v	123.7575	318.8138	62.3226	232.1728	30.6727		3.9814
Mag – Cr	76.24%	93.73%	96.13%	70.36%	97.76%		89.41%
Model VI							
True value	50	200	30	120	20	4.8	4.1
Gra – p.v	51.1362	185.0544	33.5436	119.4636	19.4408	4.7690	
Gra – Cr	97.73%	92.53%	88.19%	99.55%	97.20%	99.35%	
Mag – p.v	60.8750	207.5460	29.5257	123.4856	21.8701		4.7080
Mag – Cr	78.25%	96.23%	98.42%	97.10%	90.65%		85.17%
Model VII							
True value	20	100	45	120	10	3.4	2
Gra – p.v	23.9286	71.0096	30.6641	112.0873	9.1253	3.2912	
Gra – Cr	80.36%	71.01%	68.14%	93.41%	91.25%	96.80%	
Mag – p.v	17.6689	89.9829	37.7773	86.2105	6.0653		2.0898
Mag – Cr	88.34%	89.98%	83.95%	71.84%	60.65%		95.51%
Model VIII							
True value	100	300	45	150	50	1.7	7
Gra – p.v	122.8535	355.4255	59.6547	151.3700	37.7647	1.4694	
Gra – Cr	77.15%	81.52%	67.43%	99.09%	75.53%	86.43%	
Mag – p.v	122.9902	310.7753	50.9857	125.8362	36.7637		7.7860
Mag – Cr	77.01%	96.41%	86.70%	83.89%	73.53%		88.77%
Model IX							
True value	50	300	30	120	20	3.4	9.4
Gra – p.v	36.9812	336.4871	25.2906	111.6568	28.6363	3.2075	
Gra – Cr	73.96%	87.84%	84.30%	93.05%	56.82%	94.34%	
Mag – p.v	50.0073	332.0052	34.1437	83.5516	21.1550		7.0283
Mag – Cr	99.99%	89.33%	86.19%	69.63%	94.23%		74.77%
Model X							
True value	100	500	75	120	50	2.4	3
Gra – p.v	102.7812	442.0341	70.5918	131.6808	44.8402	3.0311	
Gra – Cr	97.22%	88.41%	94.12%	90.27%	89.68%	73.70%	
Mag – p.v	108.7222	460.3721	68.6191	101.6174	40.3776		3.5429
Mag – Cr	91.28%	92.07%	91.49%	84.68%	80.76%		81.90%

Note: $Gra-p.v$: the prediction from the gravity anomaly; $Mag-p.v$: the prediction from the magnetic anomaly; $Gra-Cr$: the credibility of prediction from the gravity anomaly; $Mag-Cr$: the credibility of prediction from magnetic anomaly.

From the Table 3.13, it can be seen that the most of the predicted values for density, magnetic susceptibility, depth, dip extent, strike angle and radius of cylinder are within an interval of confidence of 85% or higher on the estimations.

We can observe in Table 3.13 that dip angle predicted by the magnetic anomaly has better consistency with the original value for the most of the cylinder models than the one from the gravity anomaly, within the 90% confidence interval; however, it seems that the gravity data better predicts the strike direction than the magnetic data. In general, the prediction results from the magnetic anomaly are slightly better than for the gravity.

We chose randomly Model I and Model VI to compare the anomalies calculated by the predicted and original models. The anomalies are shown for Model I in Figure 3.9, and in Figure 3.10 for Model VI.

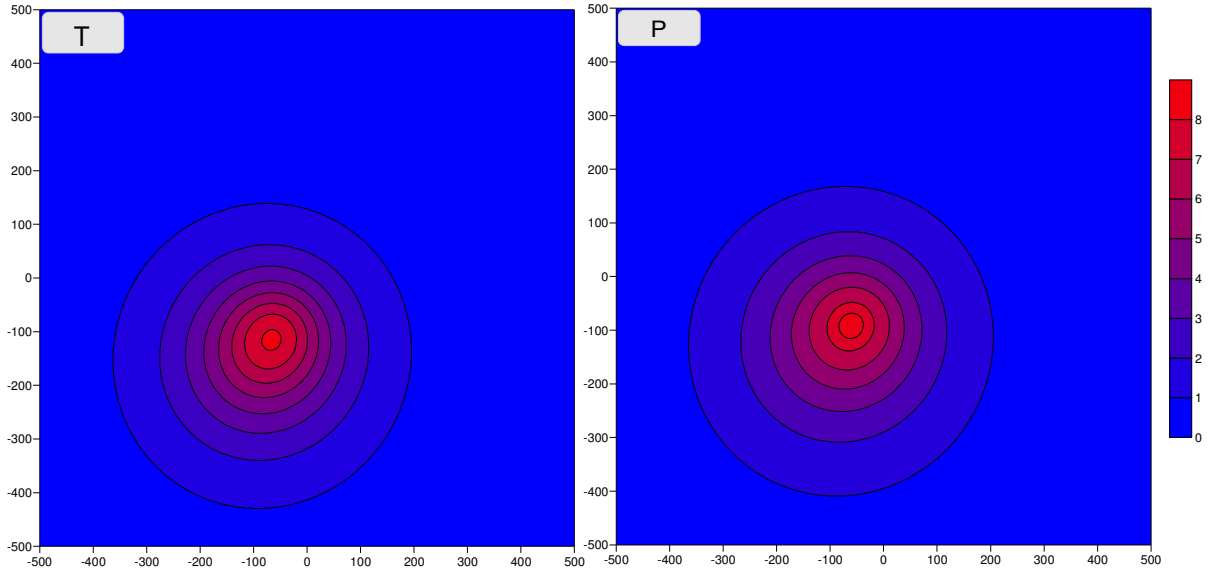

(a) Gravity anomaly of Model I. T is the theoretical anomaly, P is the predicted anomaly.

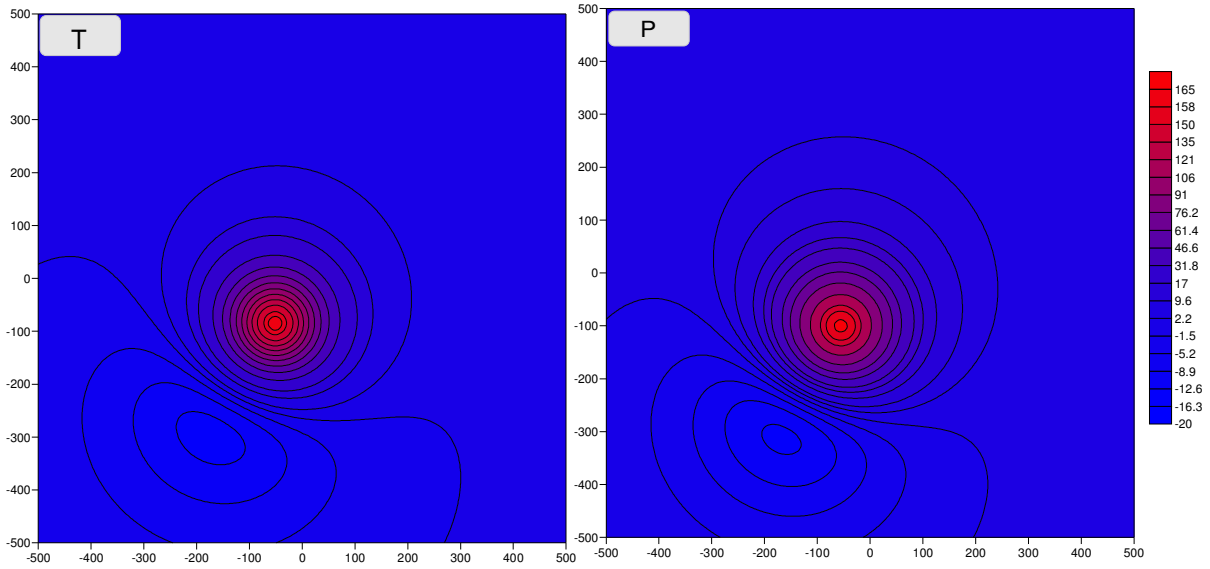

(b) Magnetic anomaly of Model I. T is the theoretical anomaly, P is the predicted anomaly.

Figure 3.9: Contour maps of gravity and magnetic anomalies for Model I.

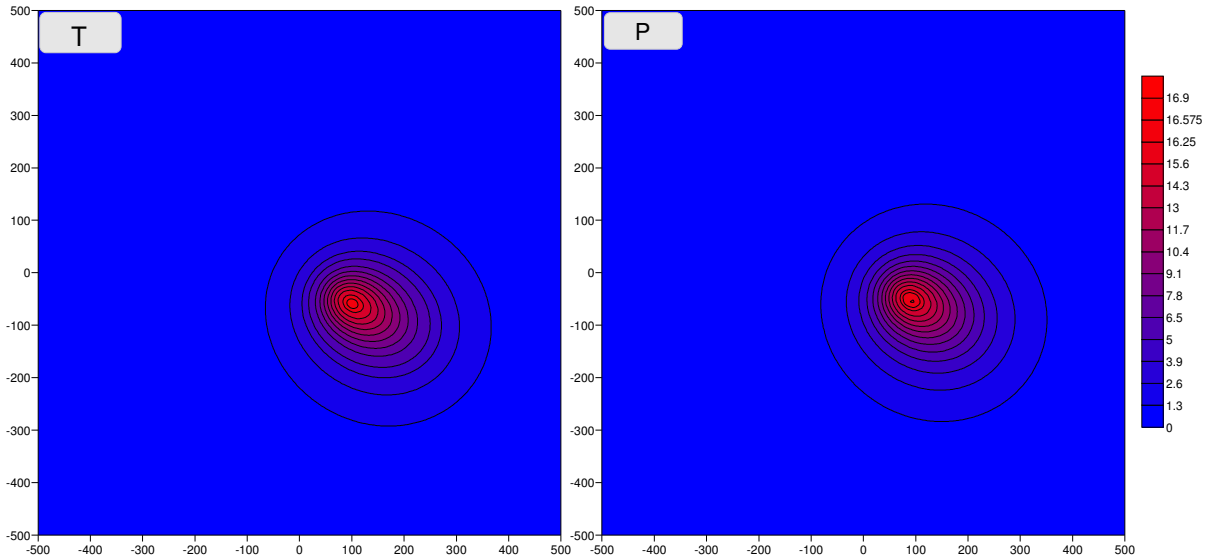

(a) Gravity anomaly of Model VI. T is the theoretical anomaly, P is the predicted anomaly.

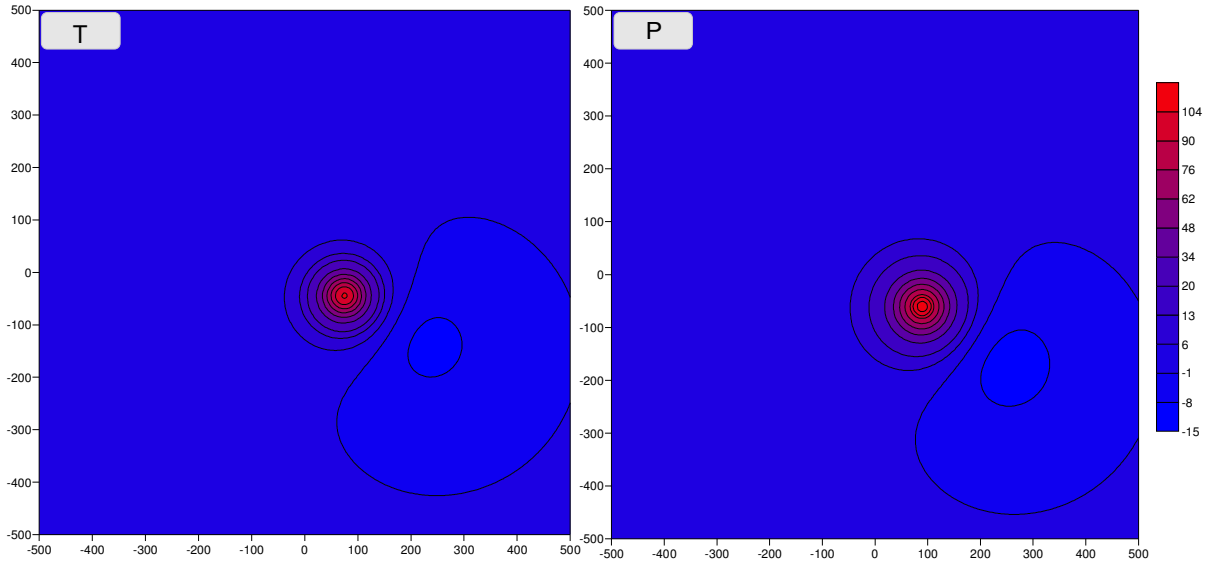

(b) Magnetic anomaly of Model VI. T is the theoretical anomaly, P is the predicted anomaly.

Figure 3.10: Contour maps of gravity and magnetic anomalies for Model VI.

For joint interpretations, we used two systems of multiple linear regressions simultaneously to estimate the cylinder's parameters, and then we average the value of each predicted parameter from gravity and magnetic anomalies. It seems that it reduced the error in the prediction (shown in Table 3.13).

3.3.2 Application to survey data

We applied the new approaches to an area located about 80 km north-west of Rouyn-Noranda in the Abitibi greenstone belt (Québec, Canada), where there are many syenitic intrusions. Gravity data are from a recent gravity survey (Jobin et al., 2008) where the average station spacing was 600 m. Magnetic data are from aeromagnetic surveys flown at a mean terrain clearance of 300 m along north-south lines at a spacing of 800 m from 1947 to 1981. The maps were digitized at the intersection of the flight lines and the magnetic contour lines to obtain a digital grid at a 200 m interval (Dion and Lefebvre, 2006). The location of the study region (coordinate system is UTM Zone 18) and the geology are shown on Figure 3.11. The background density is $2.75\ g/cm^3$ (presented in APPENDIX 9), and the blue lines outline the syenitic intrusion from geological observation on the outcrop.

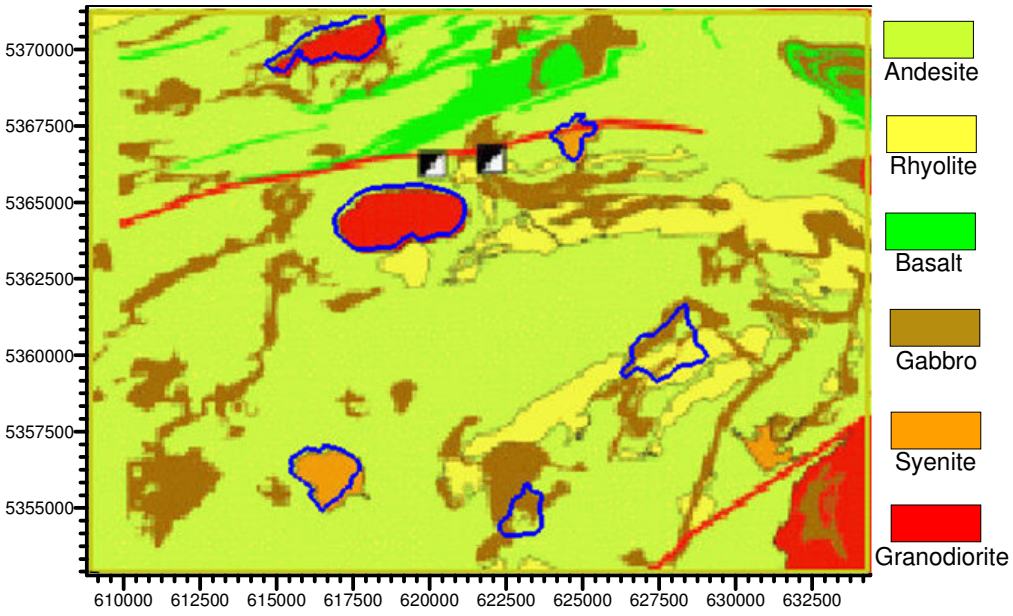

Figure 3.11: Geological map of the study area

The objective of the present study is to determine unknown parameters of intrusion from gravity and magnetic data. Since the intrusion is an individual and local geological feature, we therefore need to remove long wavelength anomaly variations from the data in order to get the residual anomaly that is possibly generated by the syenitic intrusion. By comparison with the surface geology and residual anomaly, the residual anomaly obtained once the second order trend surface is removed outlines better the intrusions. Their strong correlation with the known geological

bodies can be visualized in figures 3.11, 3.12 and 3.13. Then, we used this residual gravity and magnetic anomaly located directly over the syenitic intrusion to estimate their parameters.

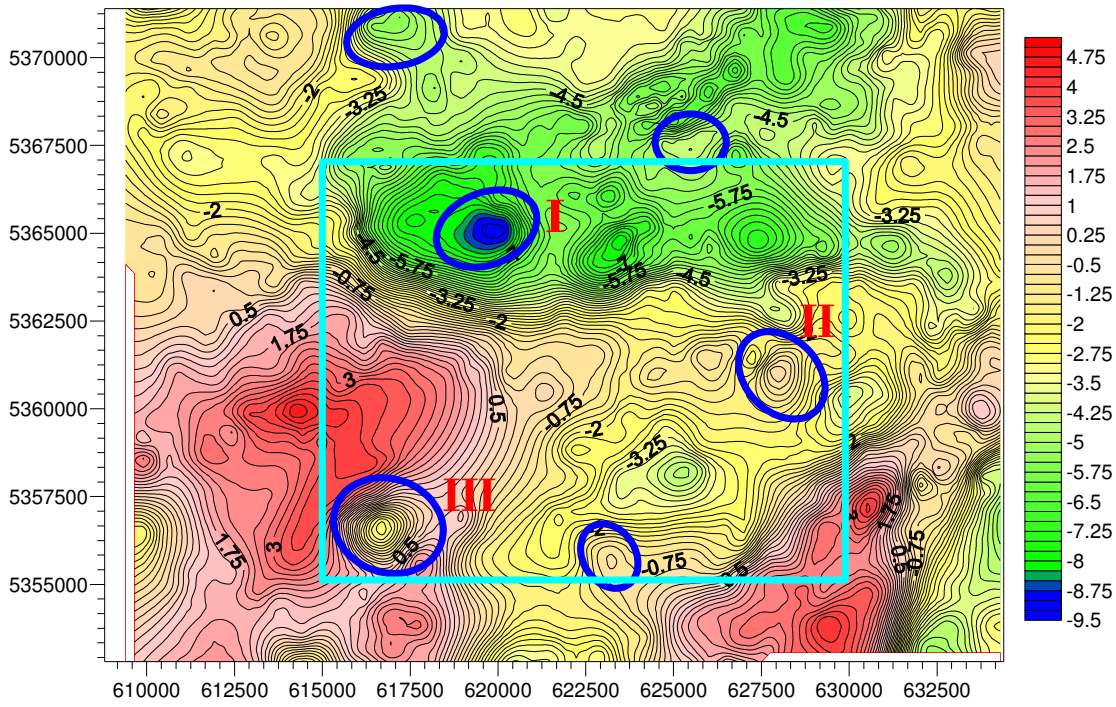

Figure 3.12: Corresponding gravity anomaly map in study area. Data units are mGal.

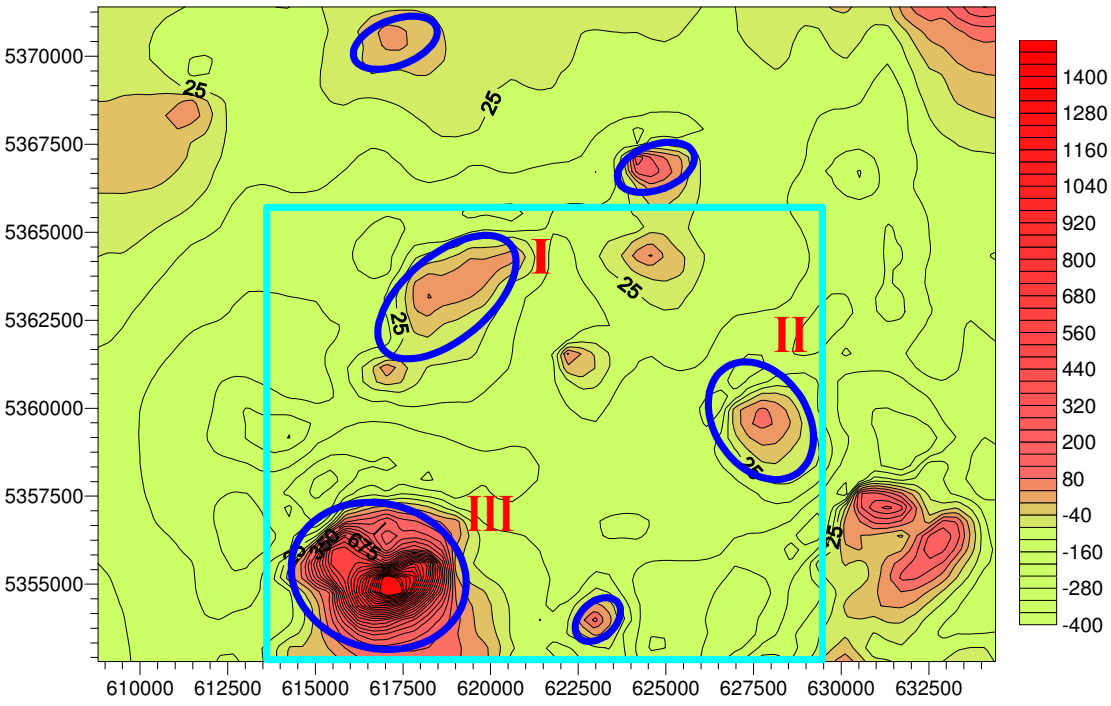

Figure 3.13: Corresponding magnetic anomaly map in study area. Data units are nT.

We chose the gravity and magnetic anomalies over geological bodies I, II and III from the central zone of the study area for the joint interpretation. The predicted parameters are shown in the Table 3.14. Please note that all radius of intrusion are in the order of 100 m while the depth to the top is about 6 m, which doesn't suit the assumption of a rod likely source (for the gravity) or a dipole (for the magnetic). What we show here is a rough interpretation, because the method developed in this thesis is mostly suitable for rod-like cylinder for which radius is much smaller than the distance to the observer.

Table 3.14: Predicted results from gravity and magnetic anomalies

Geologic body	**predicted results from gravity anomaly**					
	$r_{cylinder}$ **(m)**	$\theta(^0)$	$\alpha(^0)$	L **(m)**	H **(m)**	$\rho(g/cm^3)$
I	90.56	47.49	70.96	2305.18	8.56	2.57
II	64.65	232.52	42.93	1011.94	4.81	2.78
III	162.40	282.35	76.04	1187.0	7.44	2.74
Geologic body	**predicted results from magnetic anomaly**					
	$r_{cylinder}$ **(m)**	$\theta(^0)$	$\alpha(^0)$	L **(m)**	H **(m)**	$k(10^{-5}SI)$
I	108.45	34.88	56.44	2885.31	1.65	231.03
II	77.43	286.13	62.41	1156.47	8.34	168.47
III	209.72	265.63	88.39	917.37	5.19	312.19

The anomalies calculated from the predicted parameters (a) and real survey data (b) are shown in Figure 3.14 and Figure 3.15.

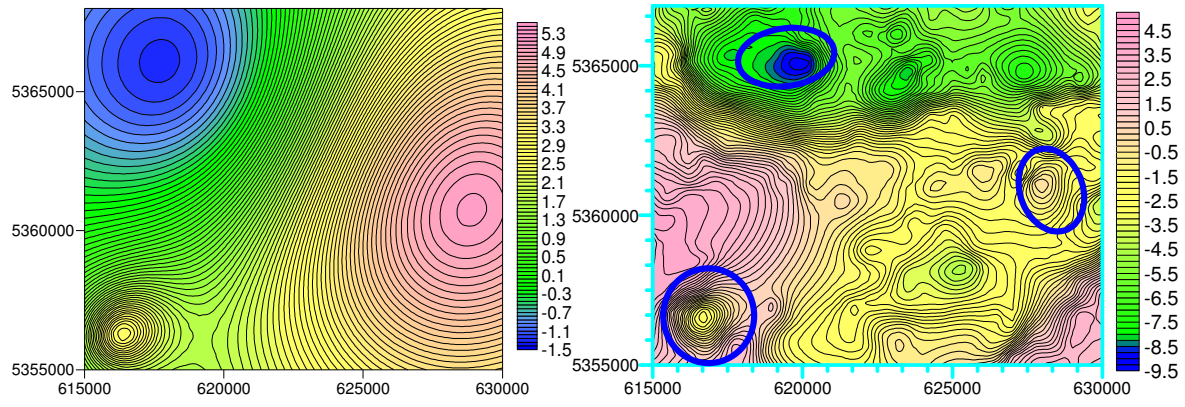

(a) (b)

Figure 3.14: Comparison between calculated gravity anomaly (a) and real survey data (b) for Model I, II, III.

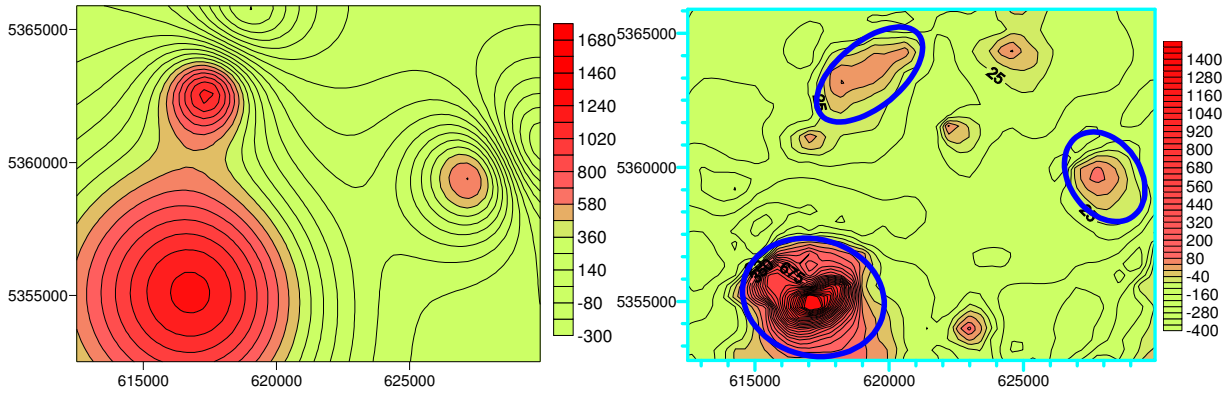

(a) (b)

Figure 3.15: Comparison between calculated magnetic anomaly (a) and real survey data (b) for Model I, II, III

From two systems prediction results (Table 3.14), we took the average of two predictions and estimated that parameters of syenitic intrusion I, II and III as follow:

Table 3.15: Predicted results from survey data

Geologic body	$r_{cylinder}$ **(m)**	θ (^{0})	α (^{0})	L **(m)**	H **(m)**	ρ (g/cm^3)	k (10^{-5} SI)
I	99.51	41.19	63.70	2595.25	5.11	2.57	231.03
II	71.04	259.33	52.67	1084.21	6.58	2.78	168.47
III	186.06	273.99	82.22	1052.18	6.32	2.74	312.19

According to our interpretation, intrusions I and III in the western part of study area are less dense than intrusion II in the eastern part. The dip extent of these two intrusions is 10 to 20 times larger than their radius and they are dipping bodies. They also contain more magnetic materials than intrusion II. Intrusion II seems of much smaller extent, the ratio of L/r is about 5, and it is sub-vertical. Among the three intrusions, intrusion I has the deepest root. Considering that the airborne magnetic survey was flown at a 300 m height, the assumption that the distance to the observer is larger than the radius is better achieved for magnetics and its interpretation is more acceptable in this case than for gravity.

CONCLUSIONS

We improved the method of calculation for gravity and magnetic field data interpretation based on a cylinder model freely oriented in space. Compared with the conventional method, our new development considers multiple factors that impact on geophysical observations.

Since the resolution of geophysical methods is influenceed by many factors, such as the source occurrence as well as its nature, we choose the multiple linear regression method to make links between the variations in gravity and magnetic field and the changes of source parameters. Starting from a series of forward models using the newly developed formulas, we have assessed the variability of gravity and magnetic anomalies as a function of the source occurrence. There are 6 most significant parameters for the gravity anomaly of a cylinder: density, depth to the top, dip extent, dip angle, strike angle and radius of the circular cross-section. For the magnetic method, there are 9 parameters: susceptibility, depth to the top, dip extent, dip angle, strike angle, radius, inclination, declination and strength of inducing (Earth's) magnetic field.

Two multiple linear regression systems (one for gravity and another for magnetism) have been developed in order to estimate the cylinder parameters from observed gravity and magnetic data. The formula developed in this thesis for direct calculation allows to make a quick estimation on the gravity and magnetic response for a cylindric geologic structure. The two linear regression systems allow the user to estimate the parameters of the cylinder model simultaneously under the constraint of two sets of geophysical data.

REFERENCES

Alheety, M.I., and Gore, S.D. (2008). A new estimator in multiple linear regression model. Model assisted statistics and application 3.187-200.

Aster, R.C., Borchers, B., and Thurber, C.H. (2005). Parameter estimation and inversion problems. Elsevier academic Press in Amsterdam, Boston, 1-16.

Chakravarthi, V., Raghuram, H.M., and Singh S.B. (2002). 3-D forward gravity modeling of basement interfaces above which the density contrast varies continuously with depth. Computers and Geosciences 28.53-57.

Chakravarthi, V., and Sundararajan, N. (2005). Invgrafalt-A fortran code for Marquardt inversion of gravity anomalies of faulted beds with varying density. Computers & Geosciences 31.1234-1240.

Chen, J.P. and Oldenburg, D.W. (2006). A new formula to compute apparent resistivities from marine magnetometric resistivity. Geophysics, VOL. 71, No.3; P.G73-G81.

Cheng, L.Z., Smith, R.S., Allard, M., Keating, P., Chouteau, M., et al. (2006). Geophysical case study of the Iso and new Insco deposits, Québec, Canada Part I: Data comparison and analysis, Exploration and Mining Geology, VOL.15, Nos.1-2, pp.53-63.

Cheng, L.Z., Smith, R.S., Allard, M., Keating, P., Chouteau, M., et al. (2006). Geophysical case study of the Iso and new Insco deposits, Québec, Canada Part II: Modeling and interpretation, Exploration and Mining Geology, VOL.15, Nos.1-2, pp.65-75.

Claprood, M., Chouteau, M. and Cheng, L.Z. (2008). Rapid detection and classification of airborne time-linear regression, Exploration Geophysics 39,1-17.

Dal Moro, G., and Pipan, M. (2007). Joint inversion of surface wave dispersion curves and reflection travel times via multi-objective evolutionary algorithms. Journal of Applied Geophysics 61.56-81.

Dion, D.J., and Lefebvre, D.L. (2006). Données numériques (profils) des leves aeromagnétiques du Québec. MRNF.DP-2006-07.

Dmitry, B.A. (2005). Three-Dimension electromagnetic modeling and inversion from theory to Application. Survey Geophysics.26:767-799.

Ellis, R.G., and Oldenburg, D.W. (1994). Applied geophysical inversion, Geophys. J. Int. 116, 5-11.

Fethi, A. (2001). New concepts for airborne gravity measurement, Aerosp. Sci.Technol. 5.413-424.

Gallardo, L.A., Marco, A.P.F., and Enrique, G.T. (2003). A versatile algorithm for joint 3D inversion of gravity and magnetic data. Geophysics. VOL. 68, No.3 (MAY-JUNE); P.949-959.

Gallardo, L.A. and Meju, M.A. (2003). Characterization of heterogeneous near-surface materials by joint 2D inversion of de resistivity and seismic data. Geophysics, Research letters. VOL.30, No.13, 1658, doi: 10.1029/2003GL017370.

Gallardo, L.A., and Meju, M.A., (2004). Joint two-dimensional DC resistivity and seismic travel

time inversion with cross-gradients constraints. Journal of Geophysical research, VOL. 109, B03311, doi: 10, 1029/2003 JB002716.

Guo, Z.H., Guan, Z.N., Xiong, S.Q. (2004). Cuboid ΔT and its gradient forward theoretical expressions without analytic odd points, Chinese journal of geophysics. Vol.47, No.6, Nov., 1131-1138.

Haber, E. and Oldenburg, D.W. (1997). Joint inversion: a structural approach, inverse problem. 13. 63-77, printed in the UK.

Hjelt, S.-E, (1972a). The gravity anomaly of a dipping prism. Geoexploration, Vol 12, p. 23-39.

Hjelt, S.-E, (1972b). Magnetostatic anomalies of dipping prisms. Geoexploration, Vol. 10, p. 239-254.

Jobin, D., Dion, C., and Keating, P. (2008). Geophysical series, NTS 32 D/6 and parts of 32 D/2, 32 D/3, 32 D/4, 32 D/5, 32 D/10, 32 D/11 and 32 D/12, gravity maps of the Blake River Group, Québec; Geological Survey of Canada, Open File 5981, 2 sheets.

Leite, L.W.B, and Leao, J.W.D. (1985). Ridge regression applied to the inversion of two-dimensional aeromagnetic anomalies. Geophysics, VOL. 50, No.8; P. 1294-1306.

Lelièvre, P.G., and Oldenburg, D.W. (2006). Magnetic forward modeling and inversion for material of high Susceptibility. Geophys. J. Int.166, 76-90.

Li X., Xue G.Q., Song J.P., Guo W.B. Wu J.J. and Shen M.F. (2005). Application of the adaptive Shrinkagge genetic algorithm in the feasible region to TEM conductive thin layer inversion.

Applied geophysics, Vol.2, No.4.

Li, Y.G., and Oldenburg, D.W. (1998). 3-D inversion of gravity data Geophysics. Vol.63. No.1, P.109-119.

Li, Y.G., and Oldenburg, D.W. (2000a). Joint inversion of surface and three-component borehole magnetic data. Geophysics, VOL.65, No.2 (MARCH-APRIL); P.540-552.

Li Y.G., and Oldenburg, D.W. (2000b). 3-D inversion of induced polarization data. Geophysics, VOL.65, No.6 (NOVEMBER-DECEMBER); P.1931-1945.

Lines L. (2005). Inversion 2005-yesterday, today, and tomorrow, 2005 CSEG National Convention-Evolving Geophysics through Innovation 251-252.

Luo, Y. (2007). Forward modeling of gravity, gravity gradients, and magnetic anomalies due to complex bodies. Journal of China University of Geosciences, Vol.18, No. 3, p280-286.

Meju, M.A. (1996). Joint inversion of TEM and distorted MT soundings: Some effective practical considerations. Geophysics, VOL. 61, No.1 (JANUARY-FEBRUARY); P. 56-65.

Nagy, D. (1966). The gravitational attraction of a right rectangular prism. Geophysics, Vol. 31, p. 362-371.

Oldenburg, D.W., and Li, Y.G. (1999). Estimating depth of investigation in DC resistivity and IP surveys. Geophysics, VOL.64, No.2 (MARCH-APRIL); P.403-416, 11 FIGS.

Oldenburg, D.W., Li, Y.G., and Lelièvre, P.G. (1997). Inversion of geophysical data over a copper gold porphyry deposit: A case history for Mt. M., Geophysics, VOL.62, No.5 (SEPTEMBER-OCTOBER); P.1419-1431, 15 FIGS.

Oldenburg, D.W., and Li, Y.G. (2003). On "3-D inversion of gravity and magnetic data with depth resolution (Maurizio Fedi and Antonio Rapolla)", Geophysics, Vol.68, No.1 (January-February); Doi 10. 1190/1.1552007 035301 GPY.

Rybakov, M., Goldshmidt, V., Fleischer, L., and Y. Ben-Gai (2000). 3-D gravity and magnetic interpretation for the Haifa Bay area (Iarael). Journal of Applied Geophysics 44. 353-367.

Santos, F. A. M., Sultan, S. A., Represas, P., & Sorady, A. L. (2006). Joint inversion of gravity and geoelectrical data for groundwater and structural investigation: application to the north western part of Sinai, Egypt, Geophys. J. Int. 165, 705-718.

Shi, G.R., Zhou, X.G., Zhang, G.Z., Shi, X.F. and Li, H.H. (2004). The use of artificial neural network analysis and multiple regression for trap quality evaluation: a case study of the Northern Kuqa Depression of Tarim Basin in western China, Marine and Petroleum 21, 411-420.

Shi, X.M., Wang, J.Y. (2007). Lecture on Non-linear inverse methods in geophysics (3), Simulated Annealing method, Chinese journal of engineering geophysics. Vol.4, No.3, Jun., 165-174.

Snopek, K., and Casten, U. (2006). 3GRAINS: 3D gravity interpretation software and its application to density modeling of the Hellenic subduction zone, Computers & Geosciences 32. 592-603.

Tan, H.Q. (1999). C Language Program Design, Tsinghua University press, 1999, 12.

Tan, H.Q., and Tian, S.Q. (1990). FORTRAN Language-fortran77 Structured Programming. Tsinghua University Press, 1990.3.

Tarantola, A. (2005). Inversion problem Theory and Methods for model Parameter Estimation. Institut de physique du Globe de Paris université de Paris 6, France.1-144.

Telford, W. M., Geldart, L. P., Sheriff, R. E., and Keys, D. A. (1976). Applied Geophysics. Cambridge University Press, 860 p.

Tian, J.T., Ren, Z.Y., and Hua, X.R. (2007). The forward modeling and inversion in geophysical electromagnetic field. Progress in geophysics, Vol.22 No.4, 1181-1194.

Treitel, S., and Lines, L.R. (1999). Past, present and future of geophysical inversion-a Y2K analysis. CREWES Research Report-Volume11.

Vozoff , K., and Jupp, D. L. B. (1975). Joint inversion of Geophysical Data, Geophys. J.R. astr. Soc. 42, 977-991.

Wang, F.Y., and Zhang, X.K. (2006). Genetic algorithm in seismic waveform inversion and it application in deep seismic sounding data interpretation. Acta seismological sinca, Vol.19 No.2 (163-172).

Wang, J.Y. (2007a). Lecture on Non-linear inverse methods in geophysics (1), Introduction to geophysical inverse problems, Chinese journal of engineering geophysics, Vol.4, No.1. 1-3.

Wang, J.Y. (2007b). Lecture on Non-linear inverse methods in geophysics (2), Monte Carlo method, Chinese journal of engineering geophysics, Vol.4, No.2, Apr.81-85.

Wang, X.B., Yu, H.J., and Luo, J.Q. (1997). Application of geophysical methods to guian GEO thermal field exploration. Journal of Chengdu University of technology, Vol.24, No. 3.

Wang, X.B., and Mao, L.F. (2004). Probability tomography of electromagnetic field-derivative method. Journal of Chengdu University of technology (Science and Technology Edition). Vol.31 No.6.

Wang, Z.G., He, Z.X., and Liu, H.Y. (2006). Three-dimensional inversion of borehole-surface electrical data based on quasi-analytical approximation. Applied Geophysics, Vol.3, No. P.141-147.

Xie, G.X., Li, J.H., Majer, E.L., Zuo, D.X. and Oristaglio, M.L. (2000). 3-D electromagnetic modeling and nonlinear inversion. Geophysics, Vol.65, No.3; P.804-822.

Yao, C.L., Hao, T.Y., et al. (2003). High-speed computation and efficient storage in 3-D gravity and magnetic inversion based on genetic algorithms. Chinese Journal of Geophysics, Vol.46, No.2.252-258.

Yao, Y. (2002). Basic Theory and Applied Methods of Geophysics. China University of Geosciences Press in China.2002, 1-12.

Young, H. S., Kwang, S.C. and Houze, X. (2006). Three-dimensional forward and inverse models for gravity fields based on the fast Fourier transform, Computers & Geosciences 32.727-738.

Zhang, S.Y. and Pan, Y.L. (2000). The principle of applied geophysics. China University of Geosciences Press in China.2000, 1-212.

APPENDICES

APPENDIX 1
VERTICAL PLATE ALGORITHM IN C LANGUAGE

```
#include <stdio.h>
#include <math.h>
#define  G  6.67e-011  //universal gravitation constant
#define  N  2001   //the number of survey points
/*********calculate the gravity anomaly of 2-D vertical plate *********/
void main()
{
        FILE *p; //file pointer
        int n; //circle variable
        double M1, M2, M3, M4;//middle variable
        double D, a, h, H, x, DG[N];//DG: the value of gravity anomaly
        D=3.0; // surplus density
        a=200.0;//the length of plate
        h=200.0;//the depth of top
        H=1200.0;//the depth of bottom

        if((p=fopen("gravity anomaly .dat", "w"))==NULL)
                printf("can not open for writing.\n");//open the file
        for(n=0; n<N; n++)
        {
                x=-N/2+n;// ground coordinate of measure points
```

```
        //the formula of 2-D erection plate forward:..
                M1=((x+a)*(x+a)+H*H)/((x+a)*(x+a)+h*h);
                M1=(x+a)*log(M1);
                M2=((x-a)*(x-a)+H*H)/((x-a)*(x-a)+h*h);
                M2=(x-a)*log(M2);
                M3=atan2(x+a,H)-atan2(x-a,H);
                M3=2.0*H*M3;
                M4=atan2(x+a,h)-atan2(x-a,h);
                M4=2.0*h*M4;
                DG[n]=G*D*(M1-M2+M3-M4);// the value of gravity anomaly
                fprintf(p, "%e %e\n", x, DG[n]);
                //output ground coordinate and corresponding value of gravity anomaly of measure
points;
                //and save the data in gravity anomaly.dat
        }

printf("the end of calculation of 2-D erection plate?\n");
        fclose(p);//close file
}
```

APPENDIX 2
THIN PLATE ALGORITHM IN C LANGUAGE

```
#include <stdio.h>
#include <math.h>
#define  PI  3.1415926535 //PI
#define  G  6.67e-011  //the universal gravitation constant
#define  N  10001   //the number of measuring points
#define  L  500  //the length of  2-D slope plate
////////////////////////////////////////////////////////////////////////////////////////////////////////////////////
/*    calculated idea: 2D slope plate gravity anomaly calculation can be      */
/*    viewed as the difference between the two level slope plate gravity      */
/*      anomaly. Separate calculation two level slope plate gravity anomalies, */
/*      and then correction coordinates and the corresponding position for      */
/*      getting the difference, namely, 2-D level slope gravity anomaly.        */
/*    Note: The calculation of the reference is the level slope gravity       */
/*       anomaly formula.                                                       */
////////////////////////////////////////////////////////////////////////////////////////////////////////////////////

/*************************************************/
/************** subroutine ********************/
/*************************************************/

void zlyc(double a, double x[], double DG3[])
{
```

```
int n;
double D, h, H;
double M1, M2, M3, M4, M5;
double m4, m44;//calculation M4 intermediate variables,
D=2.0;//surplus density
h=500.0;//the depth of top
H=1500.0;//the depth of bottom
a=a*PI/180.0;//Change the angle to radian angle
for(n=0; n<N; n++)
{
//M1, M2, M3, M4, M5 to the formula for calculating the brackets of five
        M1=PI*(H-h);
        M2=(x[n]+H*(cos(a)/sin(a)))/H;
        M2=2.0*H*atan(M2);
        M3=(x[n]+h*(cos(a)/sin(a)))/h;
        M3=2.0*h*atan(M3);
        m4=x[n]*sin(a)*cos(a);
        m44=x[n]*x[n]*pow(sin(a), 4.0);
        M4=(H+m4)*(H+m4)+m44;
        M4=M4/((h+m4)*(h+m4)+m44);
        M4=x[n]*sin(a)*sin(a)*log(M4);
        M5=x[n]*(H-h)*sin(a)*sin(a);
        M5=M5/(x[n]*x[n]*sin(a)*sin(a)+(H+h)*m4+H*h);
        M5=2.0*m4*atan(M5);
```

```
            DG3[n]=G*D*(M1+M2-M3+M4-M5);//gravity anomaly
        }
}

/***********************************************/
/*************** main program  ****************/
/***********************************************/
void main()
{
        FILE *q;
        int n;  //cycle variable
        double a, x, x1[N], x2[N], DG1[N], DG2[N], DG[N];
        //a:the angle of 2-D plate ; DG:gravity anomaly
        printf("please input the angel: a= ");
   scanf("%lf", &a);
        if((a>0.0 )&& (a<180.0))
        {
            for(n=0; n<N; n++)
            {
               x1[n]=-N/2+n;//long level slope measuring points coordinates
            }
            zlyc(a, x1, DG1);// call subroutine

      for(n=0; n<N; n++)
```

```
            {
               x2[n]=-N/2+n-L;
      //short level slope measuring points coordinates and unify coordinate
            }
      zlyc(a, x2, DG2);//call subroutine again
   }
   else printf("input a error.\n");
   //if the input angle is not in (0 , 180), the error of import

   if((q=fopen("the gravity anomaly of slope pale.dat", "w"))==NULL)
            printf("can not open for writing.\n");
   //open the file in order to write data

   for(n=0; n<N; n++)
   {
            x=-N/2+n;
            DG[n]=DG1[n]-DG2[n];
            //the difference between the two level slope plate gravity anomaly.
            //getting 2-D level slope gravity anomaly
      fprintf(q, "%f %e\n", x, DG[n]);
   }

   fclose(q);
printf("\n");
```

```
    printf("the end of calculation!\n");

    /** Note: 1. in accordance with the parameters necessary to do  **/
    /**  appropriate adjustment to meet the needs .2. The procedure  **/
    /**  can not be calculated level plate, that is a = 0 or a = 180.        **/

}
```

APPENDIX 3

GRAVITY AND MAGNETIC RESPONSE OF A PLATE

```
#include <stdio.h>
#include <math.h>
#define   PI  3.1415926535
#include "QATAN.c"
#define   N   201
#define   M   7
#define   DX  50.0
#define  PI  3.1415926535

double qatan(double B, double A)
{
        double FAI;
        if(fabs(A)>1.0e-15)
                if(B/A>0.0)
                        if(A>0.0 && B>0.0)
                                FAI=(atan2(B, A));
                        else FAI=(-PI-atan2(B, A));
                else FAI=(PI+atan2(B, A));
        else
                if(B<0.0)
                        FAI=(-PI/2.0);
                else FAI=(PI/2.0);
```

```
        return FAI;
}
void main()
{
        FILE *fp;
        int n;
        char  mod[20];
        double G, D, h, H;
        double xm[M], xk[N], zk[N], DG[N], DZ[N],DL[N];
        double r1, r2, r3, r4, fai1, fai2, fai3, fai4;
        double X1, X21, X22, Z1, Z2;
        double DG_1, DG_2, DG_3, DG_4, DG_5, DZ_1, DZ_2, DL_1, DL_2;

   printf("\n**********************************************\n");
        printf("***    gravity-magnetic abnomalty forward   ***\n");
        printf("**********************************************\n");

        printf("\nplease input parameter file: ");
        gets(mod);
        if((fp=fopen(mod,"r"))==NULL)
                printf("open model parameter file error.\n");

        printf("\nmodel paramters are:\n");
        for(n=0; n<M; n++)
```

```
        {
//READ PARAMETERS:
//x-coordinate of the center of the plate,z-coordinate of the center of the plate,
//the length of bottom 2B, the length of slope 2L, strike angle a,
//magnetic declination I, magnetic strength M.

                fscanf(fp, "%lf ", &xm[n]);
           printf("%f ", xm[n]);
        }
        fclose(fp);
        printf("\n");
        xm[4]=(xm[4]*PI/180.0);//transform angle
        xm[5]=(xm[5]*PI/180.0);//transform angle
        G=6.67; //zoom in
        D=1.0;
        h=(xm[1]-xm[3]*sin(xm[4])/2.0);
        H=(xm[1]+xm[3]*sin(xm[4])/2.0);
   printf("G, D, h, H :\n");
        printf("%f %f %f %f\n", G, D, h, H);
        for(n=0; n<N; n++)
        {
                xk[n]=-(N/2-n)*DX+0.1;
                zk[n]=0.0;
        }
```

```
for(n=0; n<N; n++)
{
        X1=xk[n]-xm[0];
        X21=(xm[2]/2+(xm[3]/2)*cos(xm[4]));
        X22=(xm[2]/2-(xm[3]/2)*cos(xm[4]));
        Z1=xm[1]-zk[n];
        Z2=((xm[3]/2)*sin(xm[4]));
        r1=((X1+X21)*(X1+X21)+(Z1-Z2)*(Z1-Z2));
        r1=(sqrt(r1));
        r2=((X1+X22)*(X1+X22)+(Z1+Z2)*(Z1+Z2));
        r2=(sqrt(r2));
        r3=((X1-X22)*(X1-X22)+(Z1-Z2)*(Z1-Z2));
        r3=(sqrt(r3));
        r4=((X1-X21)*(X1-X21)+(Z1+Z2)*(Z1+Z2));
        r4=(sqrt(r4));
        fai1=(PI-qatan(Z1-Z2, X1+X21));
        fai2=(PI-qatan(Z1+Z2, X1+X22));
        fai3=(PI-qatan(Z1-Z2, X1-X22));
        fai4=(PI-qatan(Z1+Z2, X1-X21));
////////////////////////////////////////////////////
        //DG_1----DG_5 gravity variable
        DG_1=(H*(fai2-fai4)-h*(fai1-fai3));
        DG_2=(sin(xm[4])*sin(xm[4])*log((r2*r3)/(r1*r4)));
        DG_3=(cos(xm[4])*sin(xm[4])*(fai1-fai2-fai3+fai4));
```

```
                DG_4=(sin(xm[4])*sin(xm[4])*log(r4/r3));
                DG_5=(cos(xm[4])*sin(xm[4])*(fai3-fai4));
                DG[n]=(DG_1+xk[n]*(DG_2+DG_3)+xm[2]*(DG_4+DG_5));
                DG[n]=(2.0*G*D*DG[n]/100.0);//zoom out
    //DZ_1, DZ_2 magnetic variable
    DZ_1=(sin(xm[4]-xm[5])*log((r2*r3)/(r1*r4)));
                DZ_2=(cos(xm[4]-xm[5])*(fai1-fai2-fai3+fai4));
    DZ[n]=(0.5*xm[6]*sin(xm[4])*(DZ_1+DZ_2));
                DZ[n]=(DZ[n]/PI);
                DL_1=(cos(xm[4]-xm[5])*log((r2*r3)/(r1*r4)));
                DL_2=(sin(xm[4]-xm[5])*(fai1-fai2-fai3+fai4));
    DL[n]=(0.5*xm[6]*sin(xm[4])*(DL_1-DL_2));
                DL[n]=(DL[n]/PI);
        }
        if((fp=fopen("gra-mag.dat", "wb"))==NULL)
                printf("can not open gra-mag.dat.\n");
        for(n=0; n<N; n++)
            fprintf(fp, "%f %f %f\n", xk[n], DL[n], DZ[n]);
   fclose(fp);
        printf("...calculating end.\n");
}
```

APPENDIX 4
GRAVITY ANOMALY PROFILE OF A CYLINDER

```
#include <stdio.h>
#include <math.h>
#define   PI  3.1415926535
#define   N   2001
#define   M   6
#define   DX 2.0

void main()
{
        FILE *fp;
   int n;
        char  mod[20];
        double par[M], xk[N],yk[N], GP[N];
   double x0,y0,z0;
        double CON;
        printf("\n please input parameter file: ");
        gets(mod);
        if((fp=fopen(mod,"r"))==NULL)
                printf("open model parameter file error.\n");
                 printf("\nmodel parameters are:\n");
           printf("Z0-position,L length,dip angle,strike angle,sylinder radius, density:\n");
     printf("\n");
```

```
        for(n=0; n<M; n++)
        {
                fscanf(fp, "%lf", &par[n]);
           printf("%f  ", par[n]);
        }
        fclose(fp);
        printf("\n");
        par[2]=(par[2]*PI/180.0);
        par[3]=(par[3]*PI/180.0);
       x0=par[0]/tan(par[2])*sin(par[3]);
        y0=par[0]/tan(par[2])*cos(par[3]);
z0=par[0];
        printf("\n");                printf("\n");
printf("the beginning position of the rod:\n");
printf("x0-position, y0-position, Z0-position, L length, dip angle, strike angle:\n");
        printf("\n");
printf("%f   %f   %f   %f   %f   %f\n ", x0,y0,z0,par[1],par[2]*180/PI,par[3]*180/PI);


        for(n=0; n<N; n++)
        {
          xk[n]=-((N-1)/2-n)*DX;
  yk[n]=0;
        }
CON=6.67e-02;
```

```
        for(n=0; n<N; n++)
        {
  //SI GP[N]=g.u
        GP[n]=CON*par[5]*PI*par[4]*par[4]*sin(par[2])*(-(sqrt((par[0]*par[0]-
cos(par[2])*sin(par[2])*par[0]*sin(par[3])*xk[n]-2*cos(par[2])*sin(par[2])*par[0]*cos(par[3])*
yk[n]+xk[n]*xk[n]*sin(par[2])*sin(par[2])+yk[n]*yk[n]*sin(par[2])*sin(par[2]))/sin(par[2])*sin(
par[2]))*cos(par[2])*par[0]*sin(par[3])*xk[n]+sqrt((par[0]*par[0]-*cos(par[2])*sin(par[2])*
par[0]*sin(par[3])*xk[n]-2*cos(par[2])*sin(par[2])*par[0]*cos(par[3])*yk[n]+xk[n]*xk[n]*
sin(par[2])*sin(par[2])+yk[n]*yk[n]*sin(par[2])*sin(par[2]))/sin(par[2])*sin(par[2]))*cos(par[2])
*par[0]*cos(par[3])*yk[n]+sqrt((par[0]*par[0]-2*cos(par[2])*sin(par[2])*par[0]*sin(par[3])
*xk[n]-*cos(par[2])*sin(par[2])*par[0]*cos(par[3])*yk[n]+xk[n]*xk[n]*sin(par[2])*
sin(par[2])+yk[n]*yk[n]*sin(par[2])*sin(par[2]))/sin(par[2])*sin(par[2]))*sin(par[2])*par[1]*cos(
par[2])*sin(par[3])*xk[n]+sqrt((par[0]*par[0]-2*cos(par[2])*sin(par[2])*par[0]*sin(par[3])
*xk[n]-2*cos(par[2])*sin(par[2])*par[0]*cos(par[3])*yk[n]+xk[n]*xk[n]*sin(par[2])*sin(par[2])
+yk[n]*yk[n]*sin(par[2])*sin(par[2]))/sin(par[2])*sin(par[2]))*sin(par[2])*par[1]*cos(par[2])*co
s(par[3])*yk[n]-sqrt((par[0]*par[0]-2*cos(par[2])*sin(par[2])*par[0]*sin(par[3])*xk[n]-
2*cos(par[2])*sin(par[2])*par[0]*cos(par[3])*yk[n]+xk[n]*xk[n]*sin(par[2])*sin(par[2])+yk[n]*
yk[n]*sin(par[2])*sin(par[2]))/sin(par[2])*sin(par[2]))*sin(par[2])*xk[n]*xk[n]-
sqrt((par[0]*par[0]-2*cos(par[2])*sin(par[2])*par[0]*sin(par[3])*xk[n]-2*cos(par[2])
*sin(par[2])*par[0]*cos(par[3])*yk[n]+xk[n]*xk[n]*sin(par[2])*sin(par[2])+yk[n]*yk[n]*sin(par
[2])*sin(par[2]))/sin(par[2])*sin(par[2]))*sin(par[2])*yk[n]*yk[n]-sqrt((par[1]*par[1]*
sin(par[2])*sin(par[2])+par[0]*par[0]-2*cos(par[2])*sin(par[2])*par[0]*sin(par[3])*xk[n]-
2*cos(par[2])*sin(par[2])*par[0]*cos(par[3])*yk[n]+xk[n]*xk[n]*sin(par[2])*sin(par[2])+yk[n]*
yk[n]*sin(par[2])*sin(par[2])+2*sin(par[2])*par[1]*par[0]-2*par[1]*cos(par[2])*
sin(par[2])*sin(par[2])*sin(par[3])*xk[n]-2*par[1]*cos(par[2])*sin(par[2])*sin(par[2])*
cos(par[3])*yk[n])/sin(par[2])*sin(par[2]))*cos(par[2])*par[0]*sin(par[3])*xk[n]-
```

```
sqrt((par[1]*par[1]*sin(par[2])*sin(par[2])+par[0]*par[0]-2*cos(par[2])*sin(par[2])*par[0]
*sin(par[3])*xk[n]-2*cos(par[2])*sin(par[2])*par[0]*cos(par[3])*yk[n]+xk[n]
*xk[n]*sin(par[2])*sin(par[2])+yk[n]*yk[n]*sin(par[2])*sin(par[2])+2*sin(par[2])*par[1]*par[0]
-2*par[1]*cos(par[2])*sin(par[2])*sin(par[2])*sin(par[3])*xk[n]-2*par[1]*cos(par[2])*sin(par[2])
*sin(par[2])*cos(par[3])*yk[n])/sin(par[2])*sin(par[2]))*cos(par[2])*par[0]*cos(par[3])*yk[n]+s
qrt((par[1]*par[1]*sin(par[2])*sin(par[2])+par[0]*par[0]-2*cos(par[2])*sin(par[2])*par[0]*
sin(par[3])*xk[n]-2*cos(par[2])*sin(par[2])*par[0]*cos(par[3])*yk[n]+xk[n]*xk[n]*sin(par[2])
*sin(par[2])+yk[n]*yk[n]*sin(par[2])*sin(par[2])+2*sin(par[2])*par[1]*par[0]-
2*par[1]*cos(par[2])*sin(par[2])*sin(par[2])*sin(par[3])*xk[n]-2*par[1]*cos(par[2])
*sin(par[2])*sin(par[2])*cos(par[3])*yk[n])/sin(par[2])*sin(par[2]))*sin(par[2])*xk[n]*xk[n]+sqr
t((par[1]*par[1]*sin(par[2])*sin(par[2])+par[0]*par[0]-2*cos(par[2])*sin(par[2])*par[0]
*sin(par[3])*xk[n]-2*cos(par[2])*sin(par[2])*par[0]*cos(par[3])*yk[n]+xk[n]*xk[n]
*sin(par[2])*sin(par[2])+yk[n]*yk[n]*sin(par[2])*sin(par[2])+2*sin(par[2])*par[1]*par[0]-
2*par[1]*cos(par[2])*sin(par[2])*sin(par[2])*sin(par[3])*xk[n]-2*par[1]*
cos(par[2])*sin(par[2])*sin(par[2])*cos(par[3])*yk[n])/sin(par[2])*sin(par[2]))*sin(par[2])*yk[n]
*yk[n])/sqrt((par[1]*par[1]*sin(par[2])*sin(par[2])+par[0]*par[0]-2*cos(par[2])*sin(par[2])*
par[0]*sin(par[3])*xk[n]-2*cos(par[2])*sin(par[2])*par[0]*cos(par[3])*yk[n]+xk[n]
*xk[n]*sin(par[2])*sin(par[2])+yk[n]*yk[n]*sin(par[2])*sin(par[2])+2*sin(par[2])*par[1]*par[0]
-2*par[1]*cos(par[2])*sin(par[2])*sin(par[2])*sin(par[3])*xk[n]-2*par[1]*cos(par[2])*
sin(par[2])*sin(par[2])*cos(par[3])*yk[n])/sin(par[2])*sin(par[2]))/(-xk[n]*xk[n]+xk[n]*xk[n]
*cos(par[2])*cos(par[2])*sin(par[3])*sin(par[3])+2*cos(par[2])*cos(par[2])*sin(par[3])*cos(par[
3])*yk[n]*xk[n]-yk[n]*yk[n]+cos(par[2])*cos(par[2])*cos(par[3])*cos(par[3])
*yk[n]*yk[n])/sin(par[2])/sqrt((par[0]*par[0]-2*cos(par[2])*sin(par[2])*par[0]*sin(par[3])
*xk[n]-2*cos(par[2])*sin(par[2])*par[0]*cos(par[3])*yk[n]+xk[n]*xk[n]*sin(par[2])*
sin(par[2])+yk[n]*yk[n]*sin(par[2])*sin(par[2]))/sin(par[2])*sin(par[2]))
    );
```

```
        }
        if((fp=fopen("GP.dat", "wb"))==NULL)
                printf("can not open GP.dat.\n");
        for(n=0; n<N; n++)
        {
           fprintf(fp, "%f %e\n", xk[n], GP[n]);
        }
   fclose(fp);
        printf("\n");
        printf("\n");              printf("\n");
        printf(".GRA-profile data..calculating end.\n");
}
```

APPENDIX 5

MAGNETIC ANOMALY PROFILE OF A CYLINDER

```
#include <stdio.h>
#include <math.h>
#define   PI  3.1415926535
#define   N   1501
#define   M   9
#define   DX  2.0
void main()
{
   FILE *fp;
   int n;
   char  mod[20];
   double par[M], xk[N],yk[N], Za[N],Hax[N],Hay[N],T[N], r1,r2,PD,PE,PF,PG;
   double x0,y0,z0;
   printf("\n input and output parameter file: ");
   gets(mod);
   if((fp=fopen(mod,"r"))==NULL)
            printf("open model parameter file error.\n");

     printf("\nmodel parameters are:\n");
     printf("\n");
```

```
printf("Z0-position,L length,dip angle,strike angle,sylinder radius,magnetic
susceptibility,inclination,declination,magnetic-field strength:\n");
printf("\n");
for(n=0; n<M; n++)
{
        fscanf(fp, "%lf ", &par[n]);
          printf("%f ", par[n]);
}
fclose(fp);
printf("\n");
par[2]=(par[2]*PI/180.0);
par[3]=(par[3]*PI/180.0);
par[6]=(par[6]*PI/180.0);
par[7]=(par[7]*PI/180.0);
x0=par[0]/tan(par[2])*sin(par[3]);
y0=par[0]/tan(par[2])*cos(par[3]);
z0=par[0];
printf("\n");          printf("\n");
printf("the beginning position of the rod:\n");
printf("x0-position, y0-position, Z0-position, L length, dip angle, strike angle:\n");
printf("\n");
printf("%f  %f  %f  %f  %f  %f\n ", x0,y0,z0,par[1],par[2]*180/PI,par[3]*180/PI);

for(n=0; n<N; n++)
{
```

```
        xk[n]=-((N-1)/2-n)*DX;
        yk[n]=0;
      }

    // calculate vertical component.
      for(n=0; n<N; n++)
      {
      r1=sqrt((xk[n]-(par[0]/tan(par[2]))*sin(par[3]))*(xk[n]-(par[0]/tan(par[2]))*
    sin(par[3]))+(yk[n]-(par[0]/tan(par[2]))*cos(par[3]))*(yk[n]-(par[0]/tan(par[2]))
    *cos(par[3]))+par[0]*par[0]);
      //r2=sqrt((xk[n]-(par[0]/sin(par[2])+par[1])*cos(par[2])*sin(par[3]))*(xk[n]-
    (par[0]/sin(par[2])+par[1])*cos(par[2])*sin(par[3]))+(yk[n]-(par[0]/sin
    (par[2])+par[1])*cos(par[2])*cos(par[3]))*(yk[n]-(par[0]/sin(par[2])
    +par[1])*cos(par[2])*cos(par[3]))+((par[0]/sin(par[2])+par[1])*sin(par[2]))
    *((par[0]/sin(par[2])+par[1])*sin(par[2])));
      r2=sqrt((xk[n]-(par[0]/sin(par[2])+par[1])*cos(par[2])*sin(par[3]))*(xk[n]-
(par[0]/sin(par[2])+par[1])*cos(par[2])*sin(par[3]))+(yk[n]-
(par[0]/sin(par[2])+par[1])*cos(par[2])*cos(par[3]))*(yk[n]-
(par[0]/sin(par[2])+par[1])*cos(par[2])*cos(par[3]))+(par[0]+par[1]*sin(par[2]))*(par[0]+par[1]*
sin(par[2])));
      Za[n]=0.001*(par[5]*par[8]*sin(par[6])*PI*par[4]*par[4]*(par[0]/(r1*r1*r1)-
(par[0]+par[1]*sin(par[2]))/(r2*r2*r2)));

      }
      /*
```

```
        if((fp=fopen("Za.dat", "wb"))==NULL)
                printf("can not open Za.dat.\n");
        for(n=0; n<N; n++)
        {
           fprintf(fp, "%f %f\n", xk[n], Za[n]);
        }
        fclose(fp);
      */
        printf("\n");
        printf("\n");              printf("\n");
        printf(".Za..calculating end.\n");
        printf("\n");
      // calculite horizontal-x component.
        for(n=0; n<N; n++)
        {
        r1=sqrt((xk[n]-(par[0]/tan(par[2]))*sin(par[3]))*(xk[n]-
(par[0]/tan(par[2]))*sin(par[3]))+(yk[n]-(par[0]/tan(par[2]))*cos(par[3]))*(yk[n]-
(par[0]/tan(par[2]))*cos(par[3]))+par[0]*par[0]);
        r2=sqrt((xk[n]-(par[0]/sin(par[2])+par[1])*cos(par[2])*sin(par[3]))*(xk[n]-
(par[0]/sin(par[2])+par[1])*cos(par[2])*sin(par[3]))+(yk[n]-
(par[0]/sin(par[2])+par[1])*cos(par[2])*cos(par[3]))*(yk[n]-
(par[0]/sin(par[2])+par[1])*cos(par[2])*cos(par[3]))+(par[0]+par[1]*sin(par[2]))*(par[0]+par[1]*
sin(par[2])));
       //   r2=sqrt((xk[n]-(par[0]/sin(par[2])+par[1])*cos(par[2])*sin(par[3]))*(xk[n]-
(par[0]/sin(par[2])+par[1])*cos(par[2])*sin(par[3]))+(yk[n]-
(par[0]/sin(par[2])+par[1])*cos(par[2])*cos(par[3]))*(yk[n]-
```

```
(par[0]/sin(par[2])+par[1])*cos(par[2])*cos(par[3]))+((par[0]/sin(par[2])+par[1])*sin(par[2]))*((
par[0]/sin(par[2])+par[1])*sin(par[2])));


        PD=(xk[n]-(par[0]/tan(par[2]))*sin(par[3]));
        PE=(xk[n]-(par[0]/sin(par[2])+par[1])*cos(par[2])*sin(par[3]));
        Hax[n]=0.001*par[5]*par[8]*cos(par[6])*sin(par[7])*PI*par[4]*par[4]*(PD/(r1*r1*r1)-
PE/(r2*r2*r2));
        }
      /*
        if((fp=fopen("Hax.dat", "wb"))==NULL)
                printf("can not open Hax.dat.\n");
        for(n=0; n<N; n++)
        {
           fprintf(fp, "%f %f\n", xk[n], Hax[n]);
        }
        fclose(fp);
        printf("\n");
      */
        printf(".Hax..calculating end.\n");
      // calculite horizontal-y component.
        for(n=0; n<N; n++)
        {
        r1=sqrt((xk[n]-(par[0]/tan(par[2]))*sin(par[3]))*(xk[n]-
(par[0]/tan(par[2]))*sin(par[3]))+(yk[n]-(par[0]/tan(par[2]))*cos(par[3]))*(yk[n]-
(par[0]/tan(par[2]))*cos(par[3]))+par[0]*par[0]);
```

```
        r2=sqrt((xk[n]-(par[0]/sin(par[2])+par[1])*cos(par[2])*sin(par[3]))*(xk[n]-
(par[0]/sin(par[2])+par[1])*cos(par[2])*sin(par[3]))+(yk[n]-
(par[0]/sin(par[2])+par[1])*cos(par[2])*cos(par[3]))*(yk[n]-
(par[0]/sin(par[2])+par[1])*cos(par[2])*cos(par[3]))+(par[0]+par[1]*sin(par[2]))*(par[0]+par[1]*
sin(par[2])));

      //   r2=sqrt((xk[n]-(par[0]/sin(par[2])+par[1])*cos(par[2])*sin(par[3]))*(xk[n]-
(par[0]/sin(par[2])+par[1])*cos(par[2])*sin(par[3]))+(yk[n]-
(par[0]/sin(par[2])+par[1])*cos(par[2])*cos(par[3]))*(yk[n]-
(par[0]/sin(par[2])+par[1])*cos(par[2])*cos(par[3]))+((par[0]/sin(par[2])+par[1])*sin(par[2]))*((
par[0]/sin(par[2])+par[1])*sin(par[2])));

        PF=((par[0]/tan(par[2]))*cos(par[3])-yk[n]);

        PG=((par[0]/sin(par[2])+par[1])*cos(par[2])*cos(par[3])-yk[n]);

        Hay[n]=0.001*par[5]*par[8]*cos(par[6])*cos(par[7])*PI*par[4]*par[4]*(PF/(r1*r1*r1)-
PG/(r2*r2*r2));

        }

     /*

        if((fp=fopen("Hay.dat", "wb"))==NULL)

                printf("can not open Hay.dat.\n");

        for(n=0; n<N; n++)

        {

           fprintf(fp, "%f %f\n", xk[n], Hay[n]);

        }


        fclose(fp);

     */

        printf("\n");
```

```
        printf(".Hay..calculating end.\n");


        if((fp=fopen("T.dat", "wb"))==NULL)
                printf("can not open T.\n");


        for(n=0; n<N; n++)
        {
        //T[n]=0.001*(Hax[n]*cos(par[6])*sin(par[7])+Hay[n]*cos(par[6])*cos(par[7])+Za[n]*si
n(par[6]));


        T[n]=(Hax[n]*cos(par[6])*sin(par[7])+Hay[n]*cos(par[6])*cos(par[7])+Za[n]*sin(par[6])
);
            fprintf(fp, "%f %f\n", xk[n],T[n] );
        }
        fclose(fp);
        printf("\n");
        printf(".T..calculating end.\n");printf("\n");printf("\n");printf("\n");
        printf(".MAG-profile data..calculating end.\n");
}
```

APPENDIX 6
GRAVITY ANOMALY MAP OF A CYLINDER

```
#include <stdio.h>
#include <math.h>
#define   PI  3.1415926535
#define   N   501
#define   M   6
#define   DX  2
#define   DY  2

void main()
{
        FILE *fp;
   int n,i;
        char  mod[20];
        double par[M], xk[N],yk[N], GM[N];
   double x0,y0,z0;
        double CON;
        printf("\n please input parameter file: ");
        gets(mod);
        if((fp=fopen(mod,"r"))==NULL)
                printf("open model parameter file error.\n");

          printf("\nmodel parameters are:\n");
```

```
        printf("Z0-position,L length,dip angle,strike angle,sylinder radius, density:\n");
  printf("\n");
      for(n=0; n<M; n++)
      {
            fscanf(fp, "%lf", &par[n]);
         printf("%f  ", par[n]);
      }
      fclose(fp);
      printf("\n");

      par[2]=(par[2]*PI/180.0);
      par[3]=(par[3]*PI/180.0);
      CON=6.67e-02;
x0=par[0]/tan(par[2])*sin(par[3]);
      y0=par[0]/tan(par[2])*cos(par[3]);
z0=par[0];
      printf("\n");              printf("\n");
printf("the beginning position of the rod:\n");
printf("x0-position, y0-position, Z0-position, L length, dip angle, strike angle:\n");
      printf("\n");
printf("%f  %f  %f  %f  %f  %f\n ", x0,y0,z0,par[1],par[2]*180/PI,par[3]*180/PI);
      if((fp=fopen("GM.dat", "wb"))==NULL)
            printf("can not open GM.dat.\n");
```

```
        for(i=0; i<N; i++)
        {
    yk[i]=-((N-1)/2-i)*DY;
        for(n=0; n<N; n++)
        {
    xk[n]=-((N-1)/2-n)*DX;
        GM[n]=CON*par[5]*PI*par[4]*par[4]*sin(par[2])*(-(sqrt((par[0]*par[0]-
2*cos(par[2])*sin(par[2])*par[0]*sin(par[3])*xk[n]-2*cos(par[2])*sin(par[2])*par[0]*
cos(par[3])*yk[i]+xk[n]*xk[n]*sin(par[2])*sin(par[2])+yk[i]*yk[i]*sin(par[2])*sin(par[2]))/sin(p
ar[2])*sin(par[2]))*cos(par[2])*par[0]*sin(par[3])*xk[n]+sqrt((par[0]*par[0]-
2*cos(par[2])*sin(par[2])
*par[0]*sin(par[3])*xk[n]-2*cos(par[2])*sin(par[2])*par[0]*cos(par[3])*yk[i]
+xk[n]*xk[n]*sin(par[2])*sin(par[2])+yk[i]*yk[i]*sin(par[2])*sin(par[2]))/sin(par[2])*sin(par[2])
)*cos(par[2])*par[0]*cos(par[3])*yk[i]+sqrt((par[0]*par[0]-2*cos(par[2])*sin(par[2])*par[0]*
sin(par[3])*xk[n]-2*cos(par[2])*sin(par[2])*par[0]*cos(par[3])*yk[i]+xk[n]*xk[n]
*sin(par[2])*sin(par[2])+yk[i]*yk[i]*sin(par[2])*sin(par[2]))/sin(par[2])*sin(par[2]))*sin(par[2])
*par[1]*cos(par[2])*sin(par[3])*xk[n]+sqrt((par[0]*par[0]-
2*cos(par[2])*sin(par[2])*par[0]*sin(par[3])
*xk[n]-2*cos(par[2])*sin(par[2])*par[0]*cos(par[3])*yk[i]+xk[n]*xk[n]*sin(par[2])
*sin(par[2])+yk[i]*yk[i]*sin(par[2])*sin(par[2]))/sin(par[2])*sin(par[2]))*sin(par[2])*par[1]*cos(
par[2])*cos(par[3])*yk[i]-sqrt((par[0]*par[0]-
2*cos(par[2])*sin(par[2])*par[0]*sin(par[3])*xk[n]-
2*cos(par[2])*sin(par[2])*par[0]*cos(par[3])*yk[i]+xk[n]*xk[n]*sin(par[2])*sin(par[2])+yk[i]*y
k[i]*sin(par[2])*sin(par[2]))/sin(par[2])*sin(par[2]))*sin(par[2])*xk[n]*xk[n]-
sqrt((par[0]*par[0]-2*cos(par[2])*sin(par[2])*par[0]*sin(par[3])*xk[n]-
2*cos(par[2])*sin(par[2])*par[0]*
cos(par[3])*yk[i]+xk[n]*xk[n]*sin(par[2])*sin(par[2])+yk[i]*yk[i]*sin(par[2])*sin(par[2]))/sin(p
```

ar[2])*sin(par[2]))*sin(par[2]) *yk[i]*yk[i]-sqrt((par[1]*par[1]*sin(par[2])*sin(par[2])

+par[0]*par[0]-2*cos(par[2])*sin(par[2])*par[0]*sin(par[3])*xk[n]-2*cos(par[2])*sin(par[2])

*par[0]*cos(par[3])*yk[i]+xk[n]*xk[n]*sin(par[2])*sin(par[2])+yk[i]*yk[i]*sin(par[2])*sin(par[2])+2*sin(par[2])*par[1]*par[0]-2*par[1]*cos(par[2])*sin(par[2])*sin(par[2])*sin(par[3])*xk[n]-2*par[1]*cos(par[2])*sin(par[2])*sin(par[2])*cos(par[3])*yk[i])/sin(par[2])*sin(par[2]))*cos(par[2])*par[0]*sin(par[3])*xk[n]-sqrt((par[1]*par[1]*sin(par[2])*sin(par[2])+par[0]*par[0]-2*cos(par[2])*sin(par[2])*par[0]*sin(par[3])*xk[n]-2*cos(par[2])*sin(par[2])*

par[0]*cos(par[3])*yk[i]+xk[n]*xk[n]*sin(par[2])*sin(par[2])+yk[i]*yk[i]*sin(par[2])*sin(par[2])+2*sin(par[2])*par[1]*par[0]-2*par[1]*cos(par[2])*sin(par[2])*sin(par[2])*sin(par[3])*xk[n]-2*par[1]*cos(par[2])*sin(par[2])*sin(par[2])*cos(par[3])*yk[i])/sin(par[2])*sin(par[2]))*cos(par[2])*par[0]*cos(par[3])*yk[i]+sqrt((par[1]*par[1]*sin(par[2])*sin(par[2])+par[0]*par[0]-2*cos(par[2])*sin(par[2])*par[0]*sin(par[3])*xk[n]-2*cos(par[2])*sin(par[2])*

par[0]*cos(par[3])*yk[i]+xk[n]*xk[n]*sin(par[2])*sin(par[2])+yk[i]*yk[i]*sin(par[2])*sin(par[2])+2*sin(par[2])*par[1]*par[0]-2*par[1]*cos(par[2])*sin(par[2])*sin(par[2])*sin(par[3])*xk[n]-2*par[1]*cos(par[2])*sin(par[2])*sin(par[2])*cos(par[3])*yk[i])/sin(par[2])*sin(par[2]))*sin(par[2])*xk[n]*xk[n]+sqrt((par[1]*par[1]*sin(par[2])*sin(par[2])+par[0]*par[0]-2*cos(par[2])
sin(par[2])

par[0]*sin(par[3])*xk[n]-2*cos(par[2])*sin(par[2])*par[0]*cos(par[3])*yk[i]+xk[n]*xk[n]*

sin(par[2])*sin(par[2])+yk[i]*yk[i]*sin(par[2])*sin(par[2])+2*sin(par[2])*par[1]*par[0]-2*par[1]*cos(par[2])*sin(par[2])*sin(par[2])*sin(par[3])*xk[n]-2*par[1]*cos(par[2])

*sin(par[2])*sin(par[2])*cos(par[3])*yk[i])/sin(par[2])*sin(par[2]))*sin(par[2])*yk[i]*yk[i])/sqrt((par[1]*par[1]*sin(par[2])*sin(par[2])+par[0]*par[0]-
2*cos(par[2])*sin(par[2])*par[0]*sin(par[3])*xk[n]-
2*cos(par[2])*sin(par[2])*par[0]*cos(par[3])*yk[i]+xk[n]*xk[n]*sin(par[2])*sin(par[2])+yk[i]*yk[i]*sin(par[2])*sin(par[2])+2*sin(par[2])*par[1]*par[0]-2*par[1]*cos(par[2])*sin(par[2])*

sin(par[2])*sin(par[3])*xk[n]-2*par[1]*cos(par[2])*sin(par[2])*sin(par[2])*cos(par[3])

*yk[i])/sin(par[2])*sin(par[2]))/(-xk[n]*xk[n]+xk[n]*xk[n]*cos(par[2])*cos(par[2])*sin(par[3])

*sin(par[3])+2*cos(par[2])*cos(par[2])*sin(par[3])*cos(par[3])*yk[i]*xk[n]-

```
yk[i]*yk[i]+cos(par[2])*cos(par[2])*cos(par[3])*cos(par[3])*yk[i]*yk[i])/sin(par[2])/sqrt((par[0]
*par[0]-2*cos(par[2])*sin(par[2])*par[0]*sin(par[3])*xk[n]-2*cos(par[2])*sin(par[2])
*par[0]*cos(par[3])*yk[i]+xk[n]*xk[n]*sin(par[2])*sin(par[2])+yk[i]*yk[i]*sin(par[2])*sin(par[2
]))/sin(par[2])*sin(par[2]))
        );
            fprintf(fp, "%f %f %e\n",  yk[i], xk[n], GM[n]);
          }
   }
          fclose(fp);
          printf("\n");
          printf("\n");                printf("\n");
          printf(".GRA-map data..calculating end.\n");
}
```

APPENDIX 7
MAGNETIC ANOMALY MAP OF A CYLINDER

```
#include <stdio.h>
#include <math.h>
#define   PI  3.1415926535
#define   N   501
#define   M   9
#define   DX  2.0
#define   DY  2.0

void main()
{
   FILE *fp;
   int n,i;
   char  mod[20];
   double par[M], xk[N],yk[N], Za[N],Hax[N],Hay[N],T[N], r1,r2,PD,PE,PF,PG;
   double x0,y0,z0;
   printf("\n input and output parameter file: ");
   gets(mod);
   if((fp=fopen(mod,"r"))==NULL)
            printf("open model parameter file error.\n");

     printf("\nmodel parameters are:\n");
     printf("\n");
```

```
        printf("Z0-position,L length,dip angle,strike angle,sylinder radius,magnetic
susceptibility,inclination,declination,magnetic-field strength:\n");
        printf("\n");
      for(n=0; n<M; n++)
      {
            fscanf(fp, "%lf ", &par[n]);
        printf("%f ", par[n]);
      }
      fclose(fp);
      printf("\n");
      par[2]=(par[2]*PI/180.0);
      par[3]=(par[3]*PI/180.0);
      par[6]=(par[6]*PI/180.0);
      par[7]=(par[7]*PI/180.0);
      x0=par[0]/tan(par[2])*sin(par[3]);
      y0=par[0]/tan(par[2])*cos(par[3]);
      z0=par[0];
      printf("\n");              printf("\n");
      printf("the beginning position of the rod:\n");
      printf("x0-position, y0-position, Z0-position, L length, dip angle, strike angle:\n");
      printf("\n");
      printf("%f  %f  %f  %f  %f  %f\n ", x0,y0,z0,par[1],par[2]*180/PI,par[3]*180/PI);

    // calculate vertical component.
      if((fp=fopen("Za.dat", "wb"))==NULL)
```

```
            printf("can not open Za.dat.\n");
        for(i=0; i<N; i++)
        {
              yk[i]=-((N-1)/2-i)*DY;
                 for(n=0; n<N; n++)
         {
           xk[n]=-((N-1)/2-n)*DX;
        r1=sqrt((xk[n]-(par[0]/tan(par[2]))*sin(par[3]))*(xk[n]-
(par[0]/tan(par[2]))*sin(par[3]))+(yk[i]-(par[0]/tan(par[2]))*cos(par[3]))*(yk[i]-
(par[0]/tan(par[2]))*cos(par[3]))+par[0]*par[0]);
        r2=sqrt((xk[n]-(par[0]/sin(par[2])+par[1])*cos(par[2])*sin(par[3]))*(xk[n]-
(par[0]/sin(par[2])+par[1])*cos(par[2])*sin(par[3]))+(yk[i]-
(par[0]/sin(par[2])+par[1])*cos(par[2])*cos(par[3]))*(yk[i]-
(par[0]/sin(par[2])+par[1])*cos(par[2])*cos(par[3]))+(par[0]+par[1]*sin(par[2]))*(par[0]+par[1]*
sin(par[2])));
        Za[n]=0.001*par[5]*par[8]*sin(par[6])*PI*par[4]*par[4]*(par[0]/(r1*r1*r1)-
(par[0]+par[1]*sin(par[2]))/(r2*r2*r2));
            fprintf(fp, "%f %f %f\n", yk[i], xk[n], Za[n]);
                  }
        }
        fclose(fp);
        printf("\n");
        printf("\n");              printf("\n");
        printf(".Za..calculating end.\n");
        / calculite horizontal-x component.
                  if((fp=fopen("Hax.dat", "wb"))==NULL)
```

```
            printf("can not open Hax.dat.\n");
        for(i=0; i<N; i++)
        {
          yk[i]=-((N-1)/2-i)*DY;
         for(n=0; n<N; n++)
         {
           xk[n]=-((N-1)/2-n)*DX;
           r1=sqrt((xk[n]-(par[0]/tan(par[2]))*sin(par[3]))*(xk[n]-
(par[0]/tan(par[2]))*sin(par[3]))+(yk[i]-(par[0]/tan(par[2]))*cos(par[3]))*(yk[i]-
(par[0]/tan(par[2]))*cos(par[3]))+par[0]*par[0]);
        r2=sqrt((xk[n]-(par[0]/sin(par[2])+par[1])*cos(par[2])*sin(par[3]))*(xk[n]-
(par[0]/sin(par[2])+par[1])*cos(par[2])*sin(par[3]))+(yk[i]-
(par[0]/sin(par[2])+par[1])*cos(par[2])*cos(par[3]))*(yk[i]-
(par[0]/sin(par[2])+par[1])*cos(par[2])*cos(par[3]))+(par[0]+par[1]*sin(par[2]))*(par[0]+par[1]*
sin(par[2])));
        PD=(xk[n]-(par[0]/tan(par[2]))*sin(par[3]));
        PE=(xk[n]-(par[0]/sin(par[2])+par[1])*cos(par[2])*sin(par[3]));
        Hax[n]=0.001*par[5]*par[8]*cos(par[6])*sin(par[7])*PI*par[4]*par[4]*(PD/(r1*r1*r1)-
PE/(r2*r2*r2));
        fprintf(fp, "%f %f %f\n", yk[i], xk[n], Hax[n]);


         }
        }
        fclose(fp);
        printf("\n");
        printf(".Hax..calculating end.\n");
```

```
// calculite horizontal-y component.
    if((fp=fopen("Hay.dat", "wb"))==NULL)
            printf("can not open Hay.dat.\n");
    for(i=0; i<N; i++)
    {
      yk[i]=-((N-1)/2-i)*DY;

     for(n=0; n<N; n++)
     {
       xk[n]=-((N-1)/2-n)*DX;
    r1=sqrt((xk[n]-(par[0]/tan(par[2]))*sin(par[3]))*(xk[n]-
(par[0]/tan(par[2]))*sin(par[3]))+(yk[i]-(par[0]/tan(par[2]))*cos(par[3]))*(yk[i]-
(par[0]/tan(par[2]))*cos(par[3]))+par[0]*par[0]);
    r2=sqrt((xk[n]-(par[0]/sin(par[2])+par[1])*cos(par[2])*sin(par[3]))*(xk[n]-
(par[0]/sin(par[2])+par[1])*cos(par[2])*sin(par[3]))+(yk[i]-
(par[0]/sin(par[2])+par[1])*cos(par[2])*cos(par[3]))*(yk[i]-
(par[0]/sin(par[2])+par[1])*cos(par[2])*cos(par[3]))+(par[0]+par[1]*sin(par[2]))*(par[0]+par[1]*
sin(par[2])));
    PF=(yk[i]-(par[0]/tan(par[2]))*cos(par[3]));
    PG=(yk[i]-(par[0]/sin(par[2])+par[1])*cos(par[2])*cos(par[3]));
    Hay[n]=0.001*par[5]*par[8]*cos(par[6])*cos(par[7])*PI*par[4]*par[4]*(PF/(r1*r1*r1)-
PG/(r2*r2*r2));
            fprintf(fp, "%f %f %f\n", yk[i], xk[n], Hay[n]);
      }
    }
    fclose(fp);
```

```
printf("\n");
printf(".Hay..calculating end.\n");

if((fp=fopen("T.dat", "wb"))==NULL)
        printf("can not open T.\n");
for(i=0; i<N; i++)
{
  yk[i]=-((N-1)/2-i)*DY
 for(n=0; n<N; n++)
 {
r1=sqrt((xk[n]-(par[0]/tan(par[2]))*sin(par[3]))*(xk[n]-
(par[0]/tan(par[2]))*sin(par[3]))+(yk[i]-(par[0]/tan(par[2]))*cos(par[3]))*(yk[i]-
(par[0]/tan(par[2]))*cos(par[3]))+par[0]*par[0]);
r2=sqrt((xk[n]-(par[0]/sin(par[2])+par[1])*cos(par[2])*sin(par[3]))*(xk[n]-
(par[0]/sin(par[2])+par[1])*cos(par[2])*sin(par[3]))+(yk[i]-
(par[0]/sin(par[2])+par[1])*cos(par[2])*cos(par[3]))*(yk[i]-
(par[0]/sin(par[2])+par[1])*cos(par[2])*cos(par[3]))+(par[0]+par[1]*sin(par[2]))*(par[0]+par[1]*
sin(par[2])));
PD=(xk[n]-(par[0]/tan(par[2]))*sin(par[3]));
PE=(xk[n]-(par[0]/sin(par[2])+par[1])*cos(par[2])*sin(par[3]));
PF=((par[0]/tan(par[2]))*cos(par[3])-yk[i]);
PG=((par[0]/sin(par[2])+par[1])*cos(par[2])*cos(par[3])-yk[i]);

Hay[n]=0.001*par[5]*par[8]*cos(par[6])*cos(par[7])*PI*par[4]*par[4]*(PF/(r1*r1*r1)-
PG/(r2*r2*r2));
```

```
        Hax[n]=0.001*par[5]*par[8]*cos(par[6])*sin(par[7])*PI*par[4]*par[4]*(PD/(r1*r1*r1)-
PE/(r2*r2*r2));

        Za[n]=0.001*par[5]*par[8]*sin(par[6])*PI*par[4]*par[4]*(par[0]/(r1*r1*r1)-
(par[0]+par[1]*sin(par[2]))/(r2*r2*r2));

        T[n]=Hax[n]*cos(par[6])*sin(par[7])+Hay[n]*cos(par[6])*cos(par[7])+Za[n]*sin(par[6]);

          fprintf(fp, "%f %f %f\n", yk[i], xk[n], T[n]);

         }

        }

        fclose(fp);

        printf("\n");

        printf(".T..calculating end.\n");printf("\n");printf("\n");

        printf(".MAG-profile data..calculating end.\n");

    }
```

APPENDIX 8

THE MULTIPLE LINEAR REGRESSION

(Debugged successfully the algorithm and it is from mutual algorithms)

```
#include "stdio.h"
#include "FUNCTION.C"
 main()
   { int i;
    double a[7],v[6],dt[4];
          static double x[6][34]={ data };
          static double y[34]={data };
          sqt2(x,y,6,34,a,dt,v);
         printf("\n");
        //for (i=0; i<=3; i++)//=3 a0, a1, a2, a3
         for (i=0; i<=6; i++)
          printf("a(%2d)=%e\n",i,a[i]);
         printf("\n");
         printf("q=%e  s=%e  r=%e\n",dt[0],dt[1],dt[2]);
         printf("\n");
         //for (i=0; i<=2; i++)//=2,
         for (i=0; i<=5; i++)
          printf("v(%2d)=%e\n",i,v[i]);
         printf("\n");
         printf("u=%e\n",dt[3]);
         printf("\n");
```

```
  }


#include "math.h"
#include "stdlib.h"
#include "CHOLESKY.C"
  void sqt2(x,y,m,n,a,dt,v)
  int m,n;
  double x[],y[],a[],dt[],v[];
  { int i,j,k,l,mm;
    double q,e,u,p,yy,s,r,pp,*b;
    b=malloc((m+1)*(m+1)*sizeof(double));
    mm=m+1;
    b[mm*mm-1]=n;
    for (j=0; j<=m-1; j++)
      { p=0.0;
        for (i=0; i<=n-1; i++)
          p=p+x[j*n+i];
        b[m*mm+j]=p;
        b[j*mm+m]=p;
      }
    for (i=0; i<=m-1; i++)
      for (j=i; j<=m-1; j++)
        { p=0.0;
          for (k=0; k<=n-1; k++)
```

```
        p=p+x[i*n+k]*x[j*n+k];
      b[j*mm+i]=p;
      b[i*mm+j]=p;
    }
a[m]=0.0;
for (i=0; i<=n-1; i++)
  a[m]=a[m]+y[i];
for (i=0; i<=m-1; i++)
  { a[i]=0.0;
    for (j=0; j<=n-1; j++)
      a[i]=a[i]+x[i*n+j]*y[j];
  }
chlk(b,mm,1,a);
yy=0.0;
for (i=0; i<=n-1; i++)
  yy=yy+y[i]/n;
q=0.0; e=0.0; u=0.0;
for (i=0; i<=n-1; i++)
  { p=a[m];
    for (j=0; j<=m-1; j++)
      p=p+a[j]*x[j*n+i];
    q=q+(y[i]-p)*(y[i]-p);
    e=e+(y[i]-yy)*(y[i]-yy);
    u=u+(yy-p)*(yy-p);
```

```
    }
  s=sqrt(q/n);
  r=sqrt(1.0-q/e);
  for (j=0; j<=m-1; j++)
    { p=0.0;
      for (i=0; i<=n-1; i++)
        { pp=a[m];
          for (k=0; k<=m-1; k++)
            if (k!=j) pp=pp+a[k]*x[k*n+i];
          p=p+(y[i]-pp)*(y[i]-pp);
        }
      v[j]=sqrt(1.0-q/p);
    }
  dt[0]=q; dt[1]=s; dt[2]=r; dt[3]=u;
  free(b); return;
}

#include "math.h"
#include "stdio.h"
int chlk(a,n,m,d)
int n,m;
double a[],d[];
{ int i,j,k,u,v;
  if ((a[0]+1.0==1.0)||(a[0]<0.0))
```

```
  { printf("fail\n"); return(-2);}
a[0]=sqrt(a[0]);
for (j=1; j<=n-1; j++) a[j]=a[j]/a[0];
for (i=1; i<=n-1; i++)
  { u=i*n+i;
    for (j=1; j<=i; j++)
      { v=(j-1)*n+i;
        a[u]=a[u]-a[v]*a[v];
      }
    if ((a[u]+1.0==1.0)||(a[u]<0.0))
      { printf("fail\n"); return(-2);}
    a[u]=sqrt(a[u]);
    if (i!=(n-1))
      { for (j=i+1; j<=n-1; j++)
          { v=i*n+j;
            for (k=1; k<=i; k++)
              a[v]=a[v]-a[(k-1)*n+i]*a[(k-1)*n+j];
            a[v]=a[v]/a[u];
          }
      }
  }
for (j=0; j<=m-1; j++)
  { d[j]=d[j]/a[0];
    for (i=1; i<=n-1; i++)
```

```
      { u=i*n+i; v=i*m+j;
        for (k=1; k<=i; k++)
          d[v]=d[v]-a[(k-1)*n+i]*d[(k-1)*m+j];
        d[v]=d[v]/a[u];
      }
   }
  for (j=0; j<=m-1; j++)
   { u=(n-1)*m+j;
     d[u]=d[u]/a[n*n-1];
     for (k=n-1; k>=1; k--)
       { u=(k-1)*m+j;
         for (i=k; i<=n-1; i++)
           { v=(k-1)*n+i;
             d[u]=d[u]-a[v]*d[i*m+j];
           }
         v=(k-1)*n+k-1;
         d[u]=d[u]/a[v];
       }
   }
  return(2);
}
```

APPENDIX 9

BACKGROUND DENSITY OF THE STUDY AREA

Densities of igneous rocks in the Abitibi-Témiscamingue

Rock type	**Range (g/cm^3)**	**Average (g/cm^3)**	**Total average (g/cm^3)**
Andesite	2.40~2.80	2.61	2.753
Rhyolite	2.30~2.70	2.5	
Basalt	2.70~3.30	2.93	
Gabbro	2.70~3.50	3.03	
Syenite	2.60 ~ 2.95	2.75	
Granodiorite	2. 4~3.0	2.70	